

Nuclear Energy Research Initiative # 01-022

Particle-Bed Gas-Cooled Fast Reactor (PB-GCFR) Design

Project Final Technical Report (Sept 2001 – Aug 2003)

POC:

**Temitope A. Taiwo
Argonne National Laboratory
9700 South Cass Avenue
Argonne, Illinois 60439**

Phone: (630) 252-1387

FAX: (630) 252-4500

E-mail: Taiwo@anl.gov

Contributors:

**T. A. Taiwo, T. Y. C. Wei, E. E. Feldman, E. A. Hoffman, M. Fatone,
J. W. Holland, I. G. Prokofiev, W. S. Yang, G. Palmiotti, R. N. Hill (ANL)**

M. Todosow (BNL)

M. Salvatores (CEA, France)

A. Gandini (University of Rome, Italy)

September 24, 2003

Disclaimer: Any opinions, findings, and conclusions or recommendations expressed in this material are those of the authors and do not necessarily reflect the views of the Department of Energy

TABLE OF CONTENTS

	<i>Page</i>
Executive Summary	5
Task 1: Neutronics Analyses	9
Task 2: Thermal-Hydraulic (T-H) and Safety Evaluations.....	41
Task 3: Mechanical Design.....	94
Task 4: Fuel/Structural Material Irradiation Performance	110
Task 5: Engineering Assessment of Selected Core Design.....	113
Publication List and Presentations	131
Acknowledgment.....	134

Executive Summary

Particle-Bed Gas-Cooled Fast Reactor (PB-GCFR) Design

PI:	Temitope A. Taiwo, Argonne National Laboratory
Collaborators:	Brookhaven National Laboratory; Commissariat a l'Energie Atomique (CEA), France; University of Rome, Italy
Project Start Date:	September 2001
Projected End Date:	August 2003
Project Number:	01-022

Research Objectives

The objective of this project is to develop a conceptual design of a particle-bed, gas-cooled fast reactor (PB-GCFR) core that meets the advanced reactor concept and enhanced proliferation-resistant goals of the U.S. Department of Energy's NERI program. The key innovation of this project is the application of a fast neutron spectrum environment to enhance both the passive safety and transmutation characteristics of the advanced particle-bed and pebble-bed reactor designs. The PB-GCFR design is expected to produce a high-efficiency system with a low unit cost. It is anticipated that the fast neutron spectrum would permit small-sized units (~150 MWe) that can be built quickly and packaged into modular units, and whose production can be readily expanded as the demand grows. Such a system could be deployed globally. The goals of this two-year project are as follows:

- (1) Design a reactor core that meets the future needs of the nuclear industry, by being passively safe with reduced need for engineered safety systems. This will entail an innovative core design incorporating new fuel form and type;
- (2) Employ a proliferation-resistant fuel design and fuel cycle. This will be supported by a long-life core design that is refueled infrequently, and hence, reduces the potential for fuel diversion;
- (3) Incorporate design features that permit use of the system as an efficient transmuter that could be employed for burning separated plutonium fuel or recycled LWR transuranic fuel, should the need arise; and
- (4) Evaluate the fuel cycle for waste minimization and for the possibility of direct fuel disposal. The application of particle-bed fuel provides the promise of extremely high burnup and fission-product protection barriers that may permit direct disposal.

Research Progress

In the first year of the project, physics calculations in support of a reference compact fast-spectrum core based on the pebble-bed design were performed. The results provided indications that mixed uranium and transuranics (TRU) carbide and nitride fuel forms are attractive for meeting the goals of a long-life core and high temperature operation. Potential matrix materials (titanium nitride (TiN),

zirconium carbide (ZrC), and silicon carbide (SiC)) were identified for these fuel forms. The physics studies also showed that the goal of a long-life core (with conversion ratio greater than one) requires a fuel volume fraction greater than employed in current High Temperature Reactor (HTR) designs. A high core fuel-volume fraction (~30%) or large core size (power density less than 25 W/cc) is required to reach the desired sustainable design with a high conversion ratio. It was indicated that achieving a high fuel volume fraction would require a redesign of the typical coated fuel particles, as it implies the minimization of the volume occupied by the non-fuel components of the matrix. Using this design knowledge, core physics studies were done in the earlier part of the second year in support of a core design using the promising cold finger device for passive safety. Additionally, a study investigating waste amounts in the PB-GCFR fuel cycle was performed. The impact of the fuel management scheme on transuranics (TRU) waste minimization was evaluated, using the lifetime TRU material processed as the figure of merit. A thirty-year period was used in the study. Because of the requirement that all the cores have the same power density (50 W/cc) and the constraint on the maximum TRU enrichment (20%), the long-life core was found to be the preferable design; it resulted in the lowest amount of radiotoxic transuranics to be processed and hence sent to the repository.

Those earlier studies were for TRU breakeven cores, which are consistent with Generation IV nuclear system sustainability goals. It is however conceivable that Generation IV reactor systems might be deployed early in their lifetimes for the burning of the TRU contained in spent nuclear fuel that are currently accumulating in spent fuel pools and dry storage at power plants. For this reason, the feasibility of configuring the PB-GCFR as a TRU burner was evaluated during the second year. The performance of a non-fertile fuel core was also investigated. The findings of this study formed the basis of a deliverable report.

It is known that the safety case for fast spectrum reactors employing gas as coolant is complicated by the poor heat transfer properties and low thermal inertia of the gas coolant. The ability of this reactor type to survive a scrammed depressurization accident with a concurrent loss of electrical power, without undue hazard to the public, is clearly an attractive feature of an advanced GCFR of the Generation IV class. This NERI project has explored a number of concepts that could potentially provide this safety feature through passive means. A fundamental assessment of heat transfer modes and the implications of the decay heat curve was first performed. Scoping thermal calculations were carried out. The study revealed that natural convection at one atmosphere cannot be relied upon for the available selection of primary coolant gases, and that radiation through the core would dominate above 1,000°C. Below this temperature, providing conduction pathways may be the better alternative. For the period immediately following scram, however, substantial core thermal inertia is needed, as heat transfer on this timescale is not adequate for the core materials of the near future. In addition, the results indicated that to improve the feasibility of the passive core concept, it would be prudent to reduce the reactor power envelope to below 300 MWt. Three types of basic core elements were investigated which could possibly provide core configurations with the desired passive core safety feature: (1) block/plate, (2) pin/tube, and (3) pebble/particle. After the initial investigation, it was decided that the major focus of the work would be on the pebble/particle fuel element and, in particular, on the pebble-bed core configuration.

In the first year, various concepts to promote passive safety in a 300 MWt PB-GCFR core were investigated. A unique concept to increase the heat storage capacity of the fuel pebble was introduced. This concept uses fuel spheres in which the center is filled with a material that does not contain fuel and which can melt and absorb heat as latent heat of fusion. While workable temperatures (maximum fuel temperature less than 1630°C) during normal operation and transient (severe depressurization accident) conditions were obtained, the permissible core power density of

23 W/cc was deemed low and uneconomical for a fast reactor. Other concepts for passive decay heat removal in the event of a severe depressurization were therefore investigated. These included: (1) prompt unloading of the pebble fuel, (2) extended flow coastdown, and (3) tube reactor with a tank. These approaches were primarily using heat removal by passive conduction or radiation heat transfer. It was found that these individual approaches could not adequately remove the heat for the relatively high power density of interest in the project. Consequently, the cold finger concept, that combined two heat removal approaches, was conceived and developed.

The cold fingers served dual purposes, both as reactivity-control devices as well as passive decay-heat removal mechanism during severe depressurization. In addition to core physics, thermal-hydraulic and safety assessments, mechanical design issues (flow instability and flow induced vibration) were investigated. The results for core designs using cold fingers indicated that they provide a potential solution to passive decay heat removal. Their application will however require that a significant portion of the core volume be occupied by them, thus, leading to core designs with relatively low power density (~ 25 W/cc). Additionally, the mechanical design and structural integrity of the cold fingers could be a major issue. Finding materials that could withstand the fluence, temperatures, temperature gradients, and pressure-induced stresses that the cold finger could be subjected to is a serious challenge. Alternatives to these devices were therefore investigated. The idea is that if a low power density is the maximum that can be tolerated from a passive safety viewpoint, then it might be possible to come up with a design that is less demanding.

The alternate designs explored two new approaches for decay heat removal. These are autonomous systems and natural convection in a pebble bed core. For direct-cycle plants, both concepts require one or more additional primary flow loops. These loops would contain heat exchangers that either power the autonomous systems or merely dump decay heat, in the case of natural convection. These extra loops require check valves to help prevent reverse flow that could cause a significant portion of the main coolant flow to bypass the reactor core. It was found that using natural convection at the low power density as the primary means for decay heat removal might work in a helium-cooled PB-GCFR, provided a coolant pressure greater than 10 atm is maintained following severe depressurization. Approaches for ensuring this pressure level were investigated. A leading approach is to provide a pressurized guard containment around the reactor vessel. The aforementioned semi-passive autonomous approach for passive decay heat removal was also investigated. Such systems use the decay heat from the shutdown reactor core to provide the pumping power that forces the flow for decay heat removal. Results using these two devices were positive. However, additional investigations are required before conclusive statements about them can be made. It is conceivable that a combination of two systems might be needed. The resolution of these items would require more refined models (than used for these conceptualization studies) and balance of plant considerations that were beyond the scope of this work.

A literature review was performed to identify candidate fuels and materials for the development of a GCFR that meets Generation IV system criteria. Much of the effort was devoted to identifying sources of pertinent information, collecting material properties and reviewing current gas-cooled reactor fuel designs, as well as evaluating space-reactor development efforts of the 1960s. The review evaluated fuel and material compatibility issues, high-temperature mechanical and thermal properties, and performance issues expected by operation in a fast neutron spectrum ($E > 0.1$ MeV). The study recommended mixed carbide and nitride fuels as preferred fuels for the PB-GCFR. Titanium nitride (TiN), silicon carbide (SiC), and zirconium carbide (ZrC) were identified as

possible matrix materials. More conclusive selection of the PB-GCFR materials requires additional investigation.

In a similar manner, property data for industrially available structural materials with well-established manufacturing technologies were collected and assessed to identify candidate materials for various key components of the PB-GCFR. Since detailed design information about these components do not presently exist, materials and materials production systems that were evaluated in other reactor development projects were considered first. Based on this evaluation, recommendations for structural materials have been made for structures in the vicinity of the fuel zone (ceramics such as SiC, SiC/SiC composites, ZrC, TiC, MgO, Zr(Y)O₂, TiN, Si₃N₄); for the pressure vessel (2 ¼ Cr-1Mo and 9-12Cr steel); cooling system components (Inconel 718, Inconel 800 and Hastelloy X); shielding and thermal barriers (borated Type 304 and 316 stainless steel, ferritic HT9 and various vanadium alloys); and the reflector zone (uranium, tungsten, iron, stainless steel, Nb-1Zr, Zr₃Si₂).

The project has also remained cognizant of fuel and material activities under the GFR INERI project led by ANL and French CEA, and pertinent activities under the Generation IV and AFCI programs.

Planned Activities

This two-year project was completed in August 2003. The project has accomplished its objectives by investigating fuel cycle and safety issues for a pebble-bed gas-cooled fast reactor core:

- Core designs with passive/semi-passive safety features have been conceived and analyzed
- Preliminary literature review of materials for use in high temperature and fluence environment has been performed
- Considerations have been given to proliferation resistant fuel/core designs (systems with no blanket and long-life core designs)
- Assessment of systems for waste minimization and for TRU burning has been done, by considering long-life core designs, feasibility of non-fertile fuel, and utilization of coated fuel particles.

The project has also developed a core group of experts in gas-cooled fast reactor issues and has incorporated a post-graduate student and a fresh Ph.D. holder in the efforts. In addition, the project has been able to leverage its activities with those of the USDOE-CEA INERI project on the gas-cooled fast reactor (GFR). The expertise developed in both the NERI and INERI activities has also contributed significantly to the progress of the Generation IV GFR system design, including development of international and U.S. program plans. Finally, the GFR being considered in the project or its variant could be utilized for the Advanced Fuel Cycle Initiative (AFCI) mission of burning transuranics and providing benefits to the geologic repository.

Task 1: Neutronics Analyses

The following are highlights of activities conducted in the physics area, during the two years of the project.

1.1 Fuel Pebble Design and Dimensions (T. A. Taiwo, G. Palmiotti)

The pebble fuel type typically consists of a spherical container (pebble) made of matrix material that contains a central zone of coated or particulate fuel dispersed in the matrix material. Since the graphite used as matrix material in the PBMR design might not be appropriate for the fast concept, because of its strong neutron moderating properties, alternative matrix materials were used for most of our study. The requirements for high operating temperatures that give a high thermal efficiency (45-50%) necessitated the use of refractory metals and high melting point materials having favorable fast neutron properties (e.g., low absorption cross section). Matrix materials that have been considered in this study include vanadium (V), titanium (Ti), titanium-nitride (TiN) enriched to 99.9% in N-15, silicon carbide (SiC), niobium-1% zirconium (Nb-1Zr), and zirconium carbide (ZrC).

Physics studies have been performed for two different particulate fuel designs. The first design uses coated fuel particles dispersed in a matrix. This design has a central fuel kernel and two coating layers typical of one of the fuel types employed in gas-cooled thermal systems. The first layer, called the buffer, is made of low-density graphite, and performs two vital functions. This layer protects the outer layer against fission product recoil bombardment effects. It also provides a free volume through its internal porosity and, by irradiation-induced shrinkage, permits kernel swelling and minimizes fission gas pressure. The outer layer is made of SiC. This layer functions as the pressure vessel and acts as barrier for solid fission product diffusion. Most of the physics calculations in the first year were done with a fuel kernel diameter of 800 μm , a buffer thickness of 30 μm and a SiC layer thickness of 70 μm . These low layer thicknesses were used to obtain a higher fuel kernel volume fraction in the particle, compared to PBMR designs. For this case, the fuel volume fraction in a given particle is ~ 0.5 . Optimization of the coated particle dimensions will depend on fuel performance and should be investigated. The other design is for a fuel particle with same matrix and coating material (or uncoated). This design permits a core fuel volume fraction of up to $\sim 30\%$, which ensures a sustained critical mode operation for a 15-30 years fuel irradiation cycle. Currently we have used potentially compatible fuel and matrix forms for this fuel type, e.g., carbide fuel in a zirconium carbide matrix and nitride fuel in a titanium nitride matrix. Additional fuels material work is however required to ensure that these are feasible fuel-matrix forms in the irradiation and temperature fields of the PB-GCFR.

The pebble employed in most of the physics study has an outer radius of 6 cm. A dispersion fuel zone diameter of 5.5 cm was used in the study (compare to 5 cm for PBMR), in order to increase the fuel loading in the pebble. The pebbles are packed into a cylindrical core and are assumed to occupy 61% of the volume. Helium gas flows through the pebble-bed to remove the heat generated by the fission process. The helium coolant, being neutronically benign (i.e., low neutron absorption), does not adversely affect the fraction of neutrons available for converting fertile nuclides to fissile nuclides. Thus, reactivity losses can be effectively compensated by the inclusion of fertile material, which tends to reduce the enrichment and excess reactivity requirements of long-lived systems. Other pebble designs and dimensions are emerging, based on core passive safety considerations. These dimensions are discussed in the presentations on the cold finger concept for passive decay heat removal (under Task 2).

The requirement of a long life design necessitates a fuel converter core in which sufficient fissile material is charged and produced for the duration of the long cycle, in order to reduce the cycle excess reactivity requirements. A uranium-transuranics (U-TRU) based fissile fuel system was considered in the current study. Depleted or natural uranium fertile constituent is also employed. In this fuel form, the fertile U-238 is converted to fissile material that is used to sustain the long life core. Additionally, for comparison, uranium-plutonium (U-Pu) fuel was also considered with the Pu being reactor-grade or weapons-grade. Because of the fast spectrum, it is anticipated that the discharge isotopic vector would be similar to the charge vector, and so the irradiated fuel could be reprocessed to recover the TRU that could additionally be used in other fuel irradiation cycles, hence sustaining the nuclear fuel cycle.

The fuel forms considered in our study included mixed transuranics (TRU) and uranium oxide [(U,TRU)O_{1.7}], carbide [(U,TRU)C, UC, TRUC, PuC] and nitride [(U,TRU)N, (U,Pu)N] fuels, with different TRU isotopics (LWR-discharge and weapons-grade). The weapons-grade constituents and carbide or nitride fuel forms were employed to boost the core neutron multiplication factor (K_{eff}). Previous work has shown that carbide fuels offer significant economic and doubling time advantages over oxide fuel, because of its better neutron economy. The carbide fuel also has a superior thermal conductivity than oxide fuel and hence allows operation at a higher linear power. The fuel also has a significant economic advantage over nitride fuel because of its better neutron economy. The behavior of carbides under fast neutron fluence can be problematic, however. Nitride fuels have several advantages such as heavy metal density (larger than oxides) and a better thermal conductivity. However, there is only a limited knowledge about their properties, in particular regarding their stability at high temperatures. Moreover, the production of the radioactive isotope C-14 (unless enrichment in N-15 is performed) is another negative feature. The advantages of oxide fuel are that they are very well known and have a good tolerance to radiation and fission, and also a good capacity for relatively high burnup and temperature.

1.2 Reactor Physics Analysis Methodology (T. A. Taiwo, M. Fatone, G. Palmiotti, E. A. Hoffman)

The bulk of the reactor physics calculations performed in the first year were done with the ERANOS (European Reactor Analysis and Operation System) code. The ECCO module is used for generating 33-broad group cross-section data for actual material composition and temperature. The multigroup cross-section library contained in the ECCO code is based on the JEF2.2 nuclear data library. The 33-group cross sections are used in a finite-difference transport and diffusion theory module (BISTRO) for core calculations.

Traditionally, the REBUS-3 code has been used for fuel cycle analysis of fast reactor systems at Argonne. A REBUS-3 model for a 300 MWt PB-GCFR was created in the latter part of FY2002. (This and other similar models have been used for the balance of the project.) The core k_{eff} values calculated with the model were compared with those from ERANOS calculations. The 50 W/cc PB-GCFR core that was used in the study utilizes (15% TRU, U)C fuel, a ZrC matrix, and a SS-316 reflector. The core consists of a single fuel batch that was depleted for 10,000 days. For the purpose of the preliminary comparisons, the REBUS-3 and ERANOS codes used the same core calculation methodology (diffusion theory).

The BOC k_{eff} predicted by REBUS-3/DIF3D with 33 neutron energy groups was 0.5% lower than the ERANOS value. The time dependence was somewhat different with REBUS-3 predicting a larger peak k_{eff} and a longer core lifetime. The k_{eff} at 10,000 days predicted by REBUS-3 was 1.2% higher than ERANOS. The instantaneous conversion rate showed a similar time behavior with REBUS-3

predicting a 0.5% lower conversion rate at BOC and the difference increased slowly over the cycle. The difference was 2.6% at the EOC. The cause of the differences has not yet been explored, but overall REBUS-3 will give similar conclusion for the PB-GCFR using the same input.

k_{eff} as a function of time was compared for the neutronics calculations performed using the TWODANT (transport theory) and DIF3D (diffusion theory) modules of REBUS-3. A 33-group cross section library and a 230-group cross section library were generated using MC²-2 for the BOC fuel. The fuel zone was divided into 5 radial regions of equal fuel volume and 5 axial regions of uniform height above the symmetric core midplane for a total of 50 (5r x 10z) depletion zones in the core. The calculations were performed using TWODANT (33-group library) and DIF3D (33 & 230 group libraries). The three calculations showed the same time dependence with a maximum difference in k_{eff} of 0.46%. Figure 1 shows the results.

The calculations were repeated with one large fuel or depletion zone and 160 (10r x 16z) fuel zones and compared with the 50-fuel zone case. The calculations were performed with the DIF3D/ 33-group neutronics model. The one fuel zone model was found to overpredict significantly the core lifetime. The 160-fuel zone case predicts very similar values to the 50-fuel zone case.

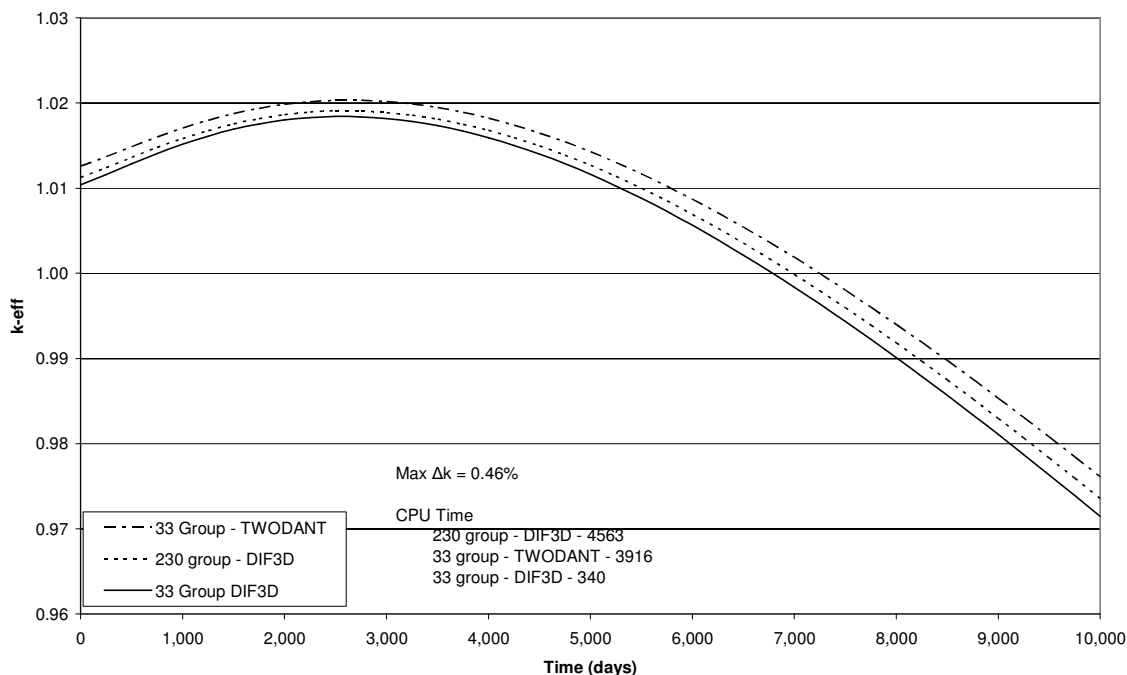


Figure 1. Comparison of Neutronics Methods for Depletion of PB-GCFR.

The current model for the coated fuel particles in a matrix assumes that the fuel pebble can be homogenized into a single region. Previous calculations performed for the thermal PBMR and GT-MHR systems suggest that a rigorous and explicit treatment of the double heterogeneity be performed to get an accurate multiplication factor (k_{inf}) for each of the systems. Those calculations indicated that simply homogenizing pebble regions results in an underprediction of the k_{inf} by as much as 8-14%. These mispredictions arise because the smeared models inadequately represent the resonance self-shielding of the fuel kernel, and result in higher resonance cross sections (primarily U-238) compared to explicit models. From physics considerations, it is expected that such simple homogenization models should be able to treat adequately the double

heterogeneity effect in the fast system that is of interest in this project. This is because the resonance region's (4 to 9000 eV) contribution to the k-inf is small in such systems. Preliminary evaluation of this effect seems to confirm this trend. MCNP calculations performed by the BNL project participant (M. Todosow) show that the homogeneous model is quite accurate for this phase of the project. The code results have been obtained using explicit representation of the coated fuel particles in pebbles and the pebbles in a core, and using the homogeneous smeared model (see next section).

1.3 Investigation of Heterogeneous Core Model (M. Todosow, BNL)

BNL's role in support of this NERI project on gas-cooled fast reactors is to develop detailed MCNP/MONTEBURNS (MCNP + ORIGEN) models of selected core configurations to validate core performance predictions from more approximate computational models.

The key concern was that the neglect of the multiple heterogeneous nature of a pebble-bed core, which is not reflected in standard reactor design codes, would introduce a significant error in the core eigenvalue. For example, earlier studies for an HTGR had observed differences of up to 14%Δk depending on whether the discrete structure of the particle fuel was accounted for. For the configurations considered here, a considerably smaller effect was expected due to the fast neutron spectrum versus the thermal spectrum in an HTGR. Consequently, there were two MCNP models for each configuration considered as shown in Figs. 1 and 2: one where the core is homogenized and one where the discrete character of the particles and pebbles was represented explicitly. The heterogeneous model utilized the lattice feature available in MCNP assuming that the particles and pebbles are arranged in a "body-centered cubic" array; this is the representation used by General Atomics in their detailed modeling of HTGR fuel. The lattice dimensions were determined so as to match the desired particle fraction in the pebbles, and pebble fraction in the core. The core k_{eff} was determined based on room temperature ENDF/B-VI cross sections. Results for different PB-GCFR cores are summarized in Table 1.

These results demonstrate that there is a reduction in k_{eff} when the detailed heterogeneous pebble-particle geometry is included. However, since these are fast spectrum systems, the effect is relatively modest. It should be noted that the approach selected for the heterogeneous representation may also be a contributor to the observed differences. As noted above, the assumption of a "body-centered cubic" array for the particles and pebbles was based on previous work by General Atomics. As a result, streaming paths are introduced which would not be present in the true random arrays of particles/pebbles.

Table 1. Core k_{eff} .

Case	Homogeneous	Heterogeneous
Compact Carbide Core	1.0361±0.0013	1.0299±0.0014
Annular Carbide Core	0.9994±0.0015	0.9989±0.0012
Compact Nitride Core	1.0904±0.0014	1.0827±0.0014

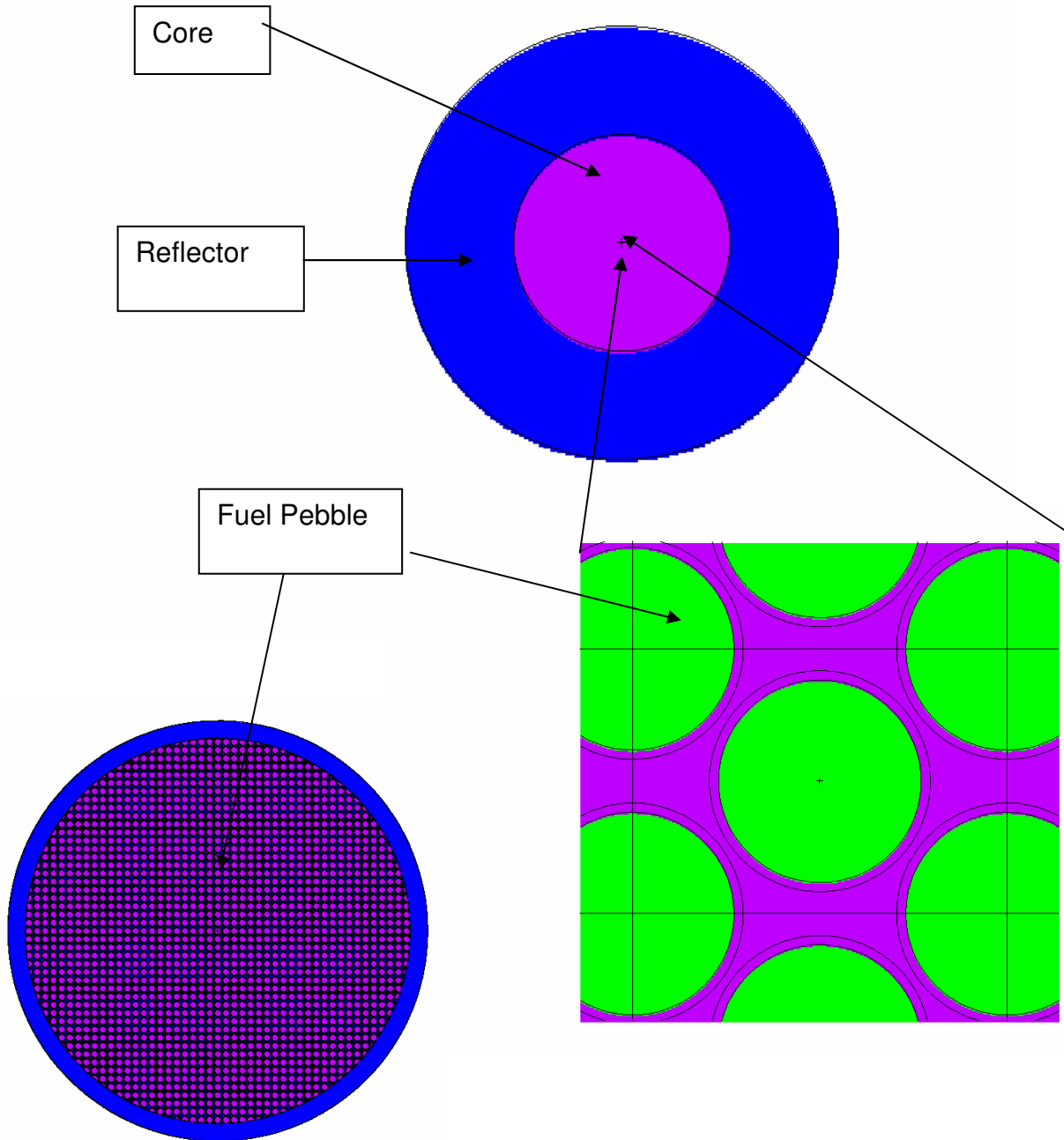


Fig. 1. MCNP Geometry for Homogeneous and Heterogeneous Representations.

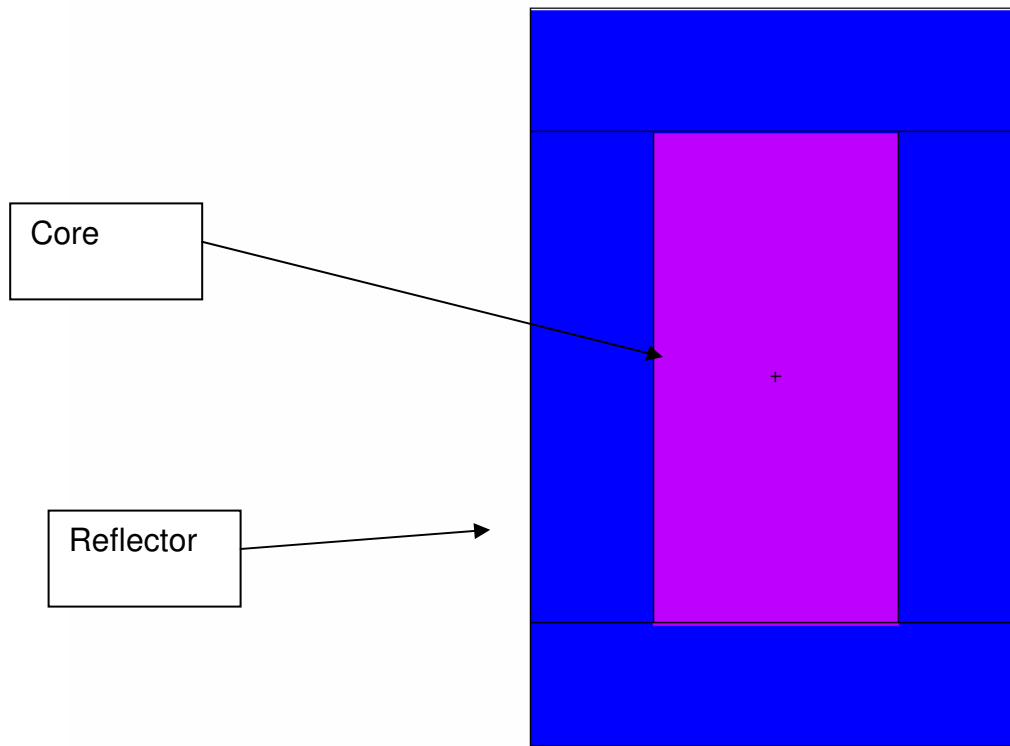


Fig. 2. Axial MCNP Geometry.

1.4 Results of Unit Pebble and Preliminary Whole-Core Parametric Studies (M. Fatone, T. A. Taiwo, G. Palmiotti)

Preliminary calculations have been performed to provide an indication of the impact of pebble packing fraction on the multiplication factor (k_{inf}). This issue is considered important because in the thermal PBMR system, the k_{inf} does not vary linearly with fuel particle packing fraction in the nominal range. Two core depletion cases using pebble packing fractions of 0.70 and 0.61, respectively, have been performed for the PB-GCFR design. Typically, observed values for the packing fraction of fuel pebbles in a pebble-bed reactor are about 0.60-0.65. A decrease in the pebble packing fraction from 0.7 to 0.61 results in a decrease of 2% Δk in the multiplication factor of the initial state. Additional calculations utilizing lower pebble packing fractions similarly show monotonically lower multiplication factors. Parametric studies on material temperature indicated that the PB-GCFR would have a negative temperature coefficient. Material temperatures of 800 and 1000 K were used in the study. The temperature value of 1000 K is used to represent the average fuel and matrix temperature being proposed for the PBMR (~1040 K for fuel and ~970 K for graphite).

The impact of power density on the core physics performance was also evaluated. Passive safety is usually enhanced by low power density, since a large surface area is available for heat removal. The low power density of the PBMR core is one of its advantages in achieving a passively safe system. However, the anticipated "exotic" materials and high heavy-metal loading required for fast-spectrum designs necessitate a reduced core volume. A reduced core volume would also give

economic benefits, provided it does not adversely affect the system pumping requirements and the passive safety in design that could result in the need for expensive backup/redundant systems. For these reasons, the targeted power density of the PB-GCRF is about 50 W/cc, which would be about one order of magnitude greater than that in thermal gas cooled-systems and a factor of two lower than that for thermal LWRs. For an ortho-cylindrical core and total power of 300 MWt, this power density implies an active core height and diameter of ~2 meters. If system-cooling costs/penalties become prohibitive, this power density would be reduced. As would be expected however, for a given irradiation time, a higher power density implies a higher flux level and material depletion (burnup). This results in a lower k_{inf} value at the end of irradiation, compared to a lower power density case that gives a longer cycle length at a sustained critical core operation. Additionally, a low power density results in a large core size (which reduces the core neutron leakage), a high total material loading, and a flat reactivity letdown with burnup. The system cost, which increases with core size, could limit the core size. The trade-off of rated power density on system passive safety, feasibility of a long-lived core, and system cost, is yet to be evaluated.

Parametric studies have been done to investigate the impacts of fuel, matrix and reflector materials on the potential for obtaining a sustainable critical core for a long life design. The results have provided indications that titanium is desirable as matrix material because of its low absorption of neutrons. The lower melting temperature of titanium, compared to TiN and ZrC might negate this advantage however. The performance behaviors with vanadium and zirconium-carbide as matrix materials are fairly similar. Application of TiN-15 results in the highest matrix absorption; when compared to Ti, TiN-15 has a higher material density. The desirable fuel material is [TRU,U]N because it results in the highest multiplication factor and gives a slightly better conversion ratio than carbide fuel. Enrichment considerations might however make carbide fuel the preferred choice. The application of both enriched uranium and weapons grade constituents of the fuel has been discarded in our current outlook, because of the potential proliferation issues that could arise by the use of these fuel forms and because they generally result in a higher reactivity swing than TRU fuel. Reflector studies indicated that for the same reflector thickness, graphite reflector competes favorably with beryllium and beryllium-oxide, nickel, and stainless steel (SS-316). Additionally it appears that graphite is also acceptable because the resulting core-average neutron spectrum is still a fast spectrum (median energy greater than 125 KeV). Graphite however has the disadvantage that it results in undesirable power peaking at the core reflector interface, and has a negative impact on the conversion ratio when compared to SS-316 and other reflector materials.

The preliminary assessment of a PB-GCFR core indicated that the goal of a long-life core (with conversion ratio greater than one) requires a fuel volume fraction higher than employed in present High Temperature Reactor (HTR) designs. The original coated fuel particle in pebble design used in this study results in a core fuel volume fraction of 15%. Preliminary investigations indicated that a higher core fuel volume fraction (~30%) or core size (power density less than 25 W/cc) is required to get the desired sustainable design with a high conversion factor. Achieving a high fuel volume fraction would require a redesign of the coated fuel particles, as it implies that the low-density carbon buffer and SiC zones be replaced with fuel to get the higher fuel volume fraction. Calculations made under this assumption, using [TRU,U]N in TiN-15 matrix or [TRU,U]C in ZrC matrix, indicated that a high conversion ratio (greater than 1.2) can be obtained with low reactivity losses over the 15 to 30 years of irradiation with a capacity factor of 0.91. These findings therefore suggest that the development of materials in layers, or possibly in compacts, must trend toward a minimization of their volume without losing their ability for high temperature confinement.

1.5 Evaluation of Graphite as Matrix Material (M. Fatone, T. A. Taiwo)

Matrix materials like ZrC and TiN have been used in previous studies for the PB-GCFR core because of their high melting points and their attractive neutron cross sections (not high in the spectrum of interest.) These studies have generally precluded the use of graphite, because of the expected degradation of the neutron flux. Because large database is available on graphite performance by virtue of its use in gas-cooled thermal systems, an evaluation of its applicability to the PB-GCFR core design has been done. Calculations were performed to assess the spectra, the multiplication factor (K_{eff}), and the conversion ratio, for different matrix volume fractions. Additionally, the graphite case has been compared with earlier cases, which use different materials for the matrix. The reference core system used in the study has the following features:

- Core fuel and matrix volume fraction, 61%; coolant volume fraction, 39%.
- Fuel type, (TRU, U)C or (TRU, U)N; TRU fraction, 15%; depleted uranium.
- Reflector material, SS-316.
- Power density, 50 W/cc; power level, 300 MWt.

The results for the cases using graphite matrix volume fractions of 30.5%, 22%, and 15%, indicated a fast neutron spectrum for the three cases. The volume fraction of the fuel is quite high in all the cases, compared to typical gas-cooled thermal reactors in which it is less than 1%. A case was also analyzed using a fuel volume fraction of 0.5% and increasing the graphite matrix volume fraction in the core to 60.5%. The spectrum for this latter case was found to be much softer than those for the three cases above. The calculations were performed using the deterministic ERANOS code (ECCO and BISTRO modules). As a consequence, a verification of the results was done by comparing the results to those obtained using the MCNP code. Results of the comparison show that the two codes give very similar spectra for the PB-GCFR core (Figure 1).

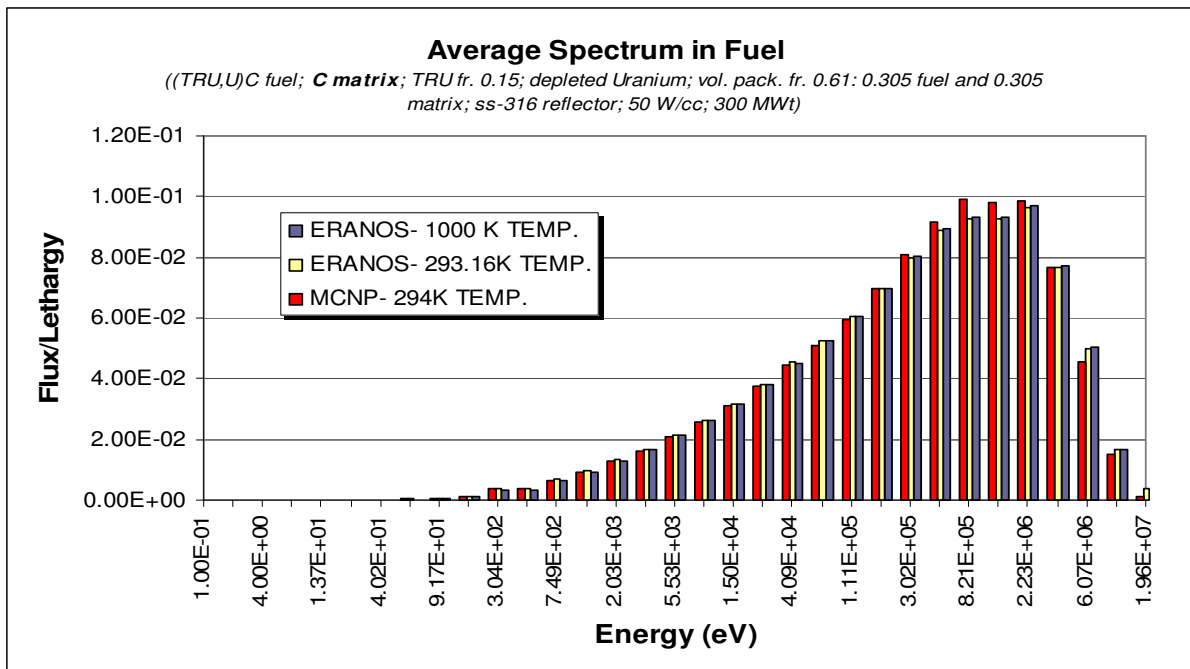


Figure 1. Comparison of Core Average Spectra Calculated by MCNP and ERANOS.

The multiplication factors at time zero for the thermal spectrum and fast spectrum cases are presented in Table 1. ERANOS results using both transport and diffusion theory approximations are provided in the Table, in addition to MCNP results.

There is a difference of about 1% in the k_{eff} results obtained with MCNP and ERANOS for the fast spectrum case. The difference is quite large for the thermal case. While additional analysis of the 1% difference (fast spectrum case) might be worthwhile, it is however within the range that has been observed between calculations using ENDF/B-VI (MCNP) and JEF2.2 (ERANOS) for this fuel form containing minor actinides. The results presented in Table 1 were obtained from 33-group ERANOS calculations. The ERANOS code system was however developed primarily for fast reactor analysis. Refinement of the number of groups from 33 groups to 172 groups results in more accurate evaluation of the k_{eff} for the thermal spectrum case. With 172 groups, the difference in k_{eff} between ERANOS and MCNP calculations for the thermal case is about 0.4%. The ERANOS results for the fast spectrum case are however insensitive to the variation in the number of groups (33 to 172 groups), since the 172-energy group structure has relatively more group size refinement in the epithermal and thermal energy zones than in the fast one.

Depletion calculations were done for the core with a fuel volume fraction of 30.5%. The results for this case were compared to earlier ones using TiN, ZrC, and SiC. Figure 2 contains a comparison of the k_{eff} as a function of depletion time for the cases. It is observed that the case using graphite matrix gives the lowest k_{eff} values over the irradiation period. This is due to the softer spectrum for this case, compared to those for the others.

The results presented in this section indicate that the use of graphite as matrix material for the PB-GCFR is neutronically feasible. The high fluence (irradiation damage) and temperature in the system might however preclude its use.

Table 1. Comparison of k_{eff} Values from MCNP and ERANOS Calculations.

Case	MCNP (294 K)	ERANOS- Diffusion (293.2 K)	ERANOS- Transport (293.2 K)	ERANOS- Diffusion (1000 K)	ERANOS- Transport (1000 K)
Thermal Spectrum	1.026	1.060	1.065	0.992	0.997
Fast Spectrum (PB-GCFR)	1.047	1.038	1.038	1.010	1.010

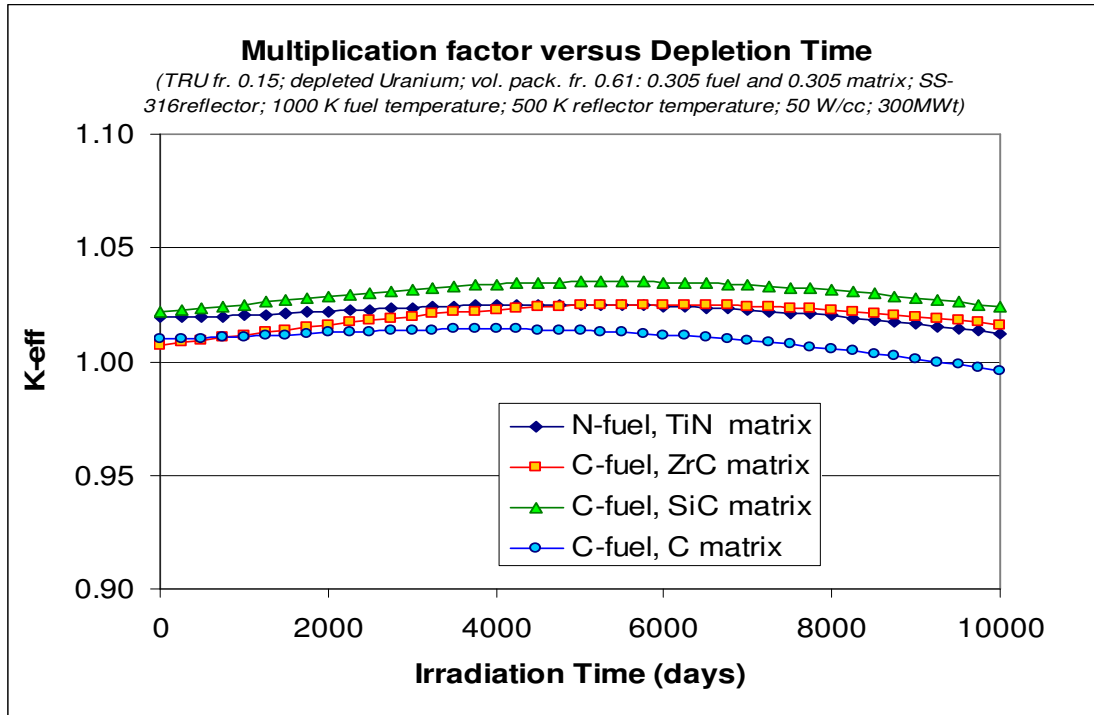


Figure 2. Time-Dependent Multiplication Factors for PB-GCFR Cores with Different Matrix Materials.

1.6 Physics Study of PB-GCFR Core with Cold Finger Design for Passive Safety (M. Fatone)

To achieve passive safety goals, a new concept for the decay heat removal system, called "Cold Finger," has been proposed and its safety implications have been analyzed. (See Task 2 below for more information on cold fingers.) A certain number of these cold fingers are required in the core. For a power rating of 300 MWt, the required number of cold fingers was initially estimated as 12. The cold fingers have an additional function besides serving as passive decay heat removal devices. They also provide core locations for control rods used for reactivity control.

Physics calculations have been done to evaluate the k_{eff} and conversion ratio for the Pebble-Bed Gas Cooled Fast Reactor (PB-GCFR) design using the cold finger concept as passive decay heat removal system. Sensitivity calculations have been performed using two different pebble designs and different materials for a reactor with a power rating of 300 MWt and a power density of 50 W/cc.

For the given power requirements, a core diameter of 2.119 m and a height of 2.00 m have been used to accommodate the 12 cold fingers recommended from safety/T-H considerations. The 12 cold fingers occupy 15% of the core volume and are symmetrically distributed in the core. Eight of the fingers are equally spaced with their centers on an imaginary circle of 1.507 m diameter. The other four fingers are equidistant from the center of the core and centered on the edges of an imaginary square with a side length of 0.424 m. Each cold finger has a diameter of 0.236 m and a height of 2 m, in the core region.

In these physics studies, two different materials were considered for the finger walls. These are INCONEL-625 CLF, commercial grade and INCONEL-690, nuclear grade.

To meet thermal constraints, pebbles with a smaller diameter than the 6 cm that has been used in previous studies have been considered. Two different concepts for the PB-GCFR fuel pebble have been proposed, and their impacts on core physics performance have been evaluated. The designs are:

1. Hollow Spherical (HS) pebble fuel, with a diameter of 5 cm;
2. Solid Spherical (SS) pebble fuel, with a diameter of 4 cm.

The HS design (see Figure 1) has a hollow (non-fuel) zone at the center of the pebble, surrounded by the fuel zone and an outer cladding zone. Based on the requirement for a high fuel fraction in the pebble ($\sim 50\%$) and assuming a cladding thickness of 0.15 cm, a hollow zone diameter of 3.46 cm is obtained.

The materials used for the HS pebble are:

- Porous graphite or SiC (80% theoretical density) as "hollow" zone material; besides thermal issues, the non-fuel zone is designed to also provide a space for the fission gases;
- (Pu, U)C for the solid fuel; 90% theoretical density, in order to contain the fission gases;
- different materials have been considered for the fuel cladding:
 - ◆ Ti6Al4V: a Titanium alloy containing 6% of Al, 4% of V and 2% of Sn; this alloy has a high melting point, but unfortunately a low thermal conductivity (see Table 1);
 - ◆ Nb-1%Zr; this would be the best material based on thermal and physical characteristics only (high melting point and high thermal conductivity). However, Niobium has a high capture cross-section;
 - ◆ Vanadium (V) is a material with properties in between the two listed above; it has a good thermal conductivity and relatively high melting point.

The SS pebble has a fuel zone of 3.6 cm diameter and an outer non-fuel zone that has a thickness of 0.2 cm. The materials considered for the SS design are:

- (Pu, U)C fuel kernels dispersed in a graphite matrix (80% theoretical density);
- Graphite as material for the non-fuel outer zone.

The core performance of the PB-GCFR with the cold fingers has been analyzed with the ERANOS core model. The ECCO module of the code was used for generating 33-group neutron cross sections for all core regions, including the SS-316 reflector (50 cm thick) and the surrounding B₄C shield region (thickness of 14 cm). The cross sections were used in the BISTRO transport/diffusion theory module of the code. The R-Z geometry option of BISTRO is utilized. This core model has five homogeneous zones (as shown in Figure 2).

The zones correspond to:

- Zone 1: all fuel;
- Zone 2: 4 fingers plus fuel;
- Zone 3: all fuel;
- Zone 4: 8 fingers plus fuel;
- Zone 5: all fuel.

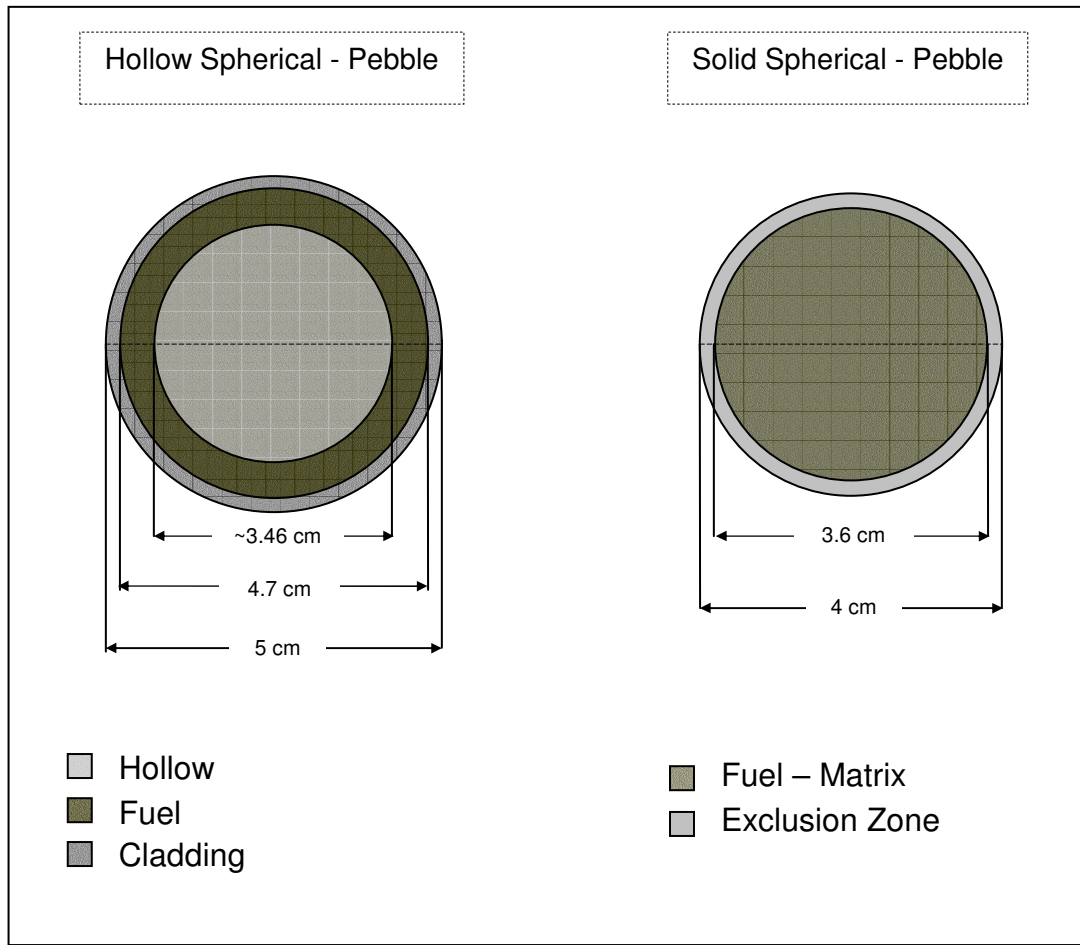


Figure 1. Pebble designs.

Table 1. Cladding Materials.

Materials	Density (g/cc)	Tensile Strength, Ultimate (MPa)	Thermal Conductivity (W/m-K)	Melting Point (°C)
Ti6A6V2E	4.54	1100	6.6	Min 1627
Nb-1Zr	8.59	241	41.9	Max 2407
Vanadium	6.11	911- 472 ¹	31	1735

¹ Depends on the manufacturing technique.

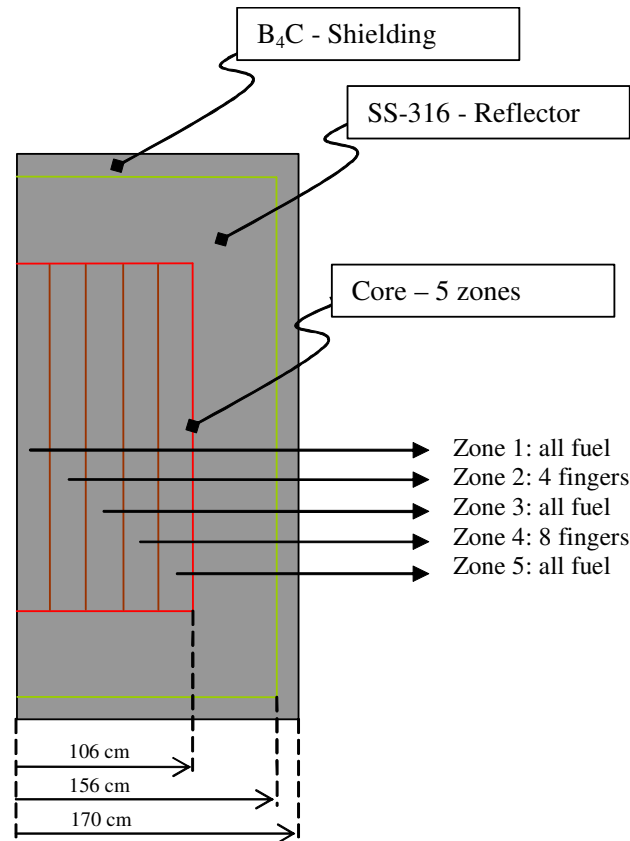


Figure 2. Core homogeneous zones; 300 MWt; 50 W/cc.

In each zone, the fuel pebbles and finger regions are homogenized by calculating the fuel and finger volume fractions and considering that a fraction (39%) of the fueled-zone is coolant. Based on these smeared zone models and the fuel designs, the *average total fuel volume fraction in the core* using the HS pebble design is about 26.2%, and that in the core using the SS pebble design is about 24.5%. In the three zones containing only fuel, the temperature assumed for the neutron cross-section calculation (ECCO code) is 1000 K. In the two zones with fingers, it has been assumed that during normal operation almost 1% of the heat is removed by the fingers. Therefore, a material temperature of 990 K has been used for generating the cross sections for these zones.

In Figure 3 is displayed the k_{eff} versus depletion time for four different cases using INCONEL 625 as material for the cold fingers. Three cases are for the HS pebble designs using the different cladding materials mentioned above. The last one considers the SS fuel pebble design. The results show that using Nb-1%Zr as cladding for the HS design is unacceptable, since its high capture cross-section results in a low core k_{eff} . It was found that the best result is obtained for the HS fuel when Titanium alloy is used as the cladding material. The Vanadium case lies in the middle of the results for Titanium and Niobium as cladding materials, but is closer to the Titanium case.

Using the SS pebble configuration, a k_{eff} value comparable to that of the HS-Titanium cladding case has been obtained. Though the average total volume fraction of the fuel in the core for the SS design (24.5%) is smaller than the fraction used in the HS configuration (26.2%), the k_{eff} values are similar because of the lower absorption cross-section of graphite, relative to Titanium.

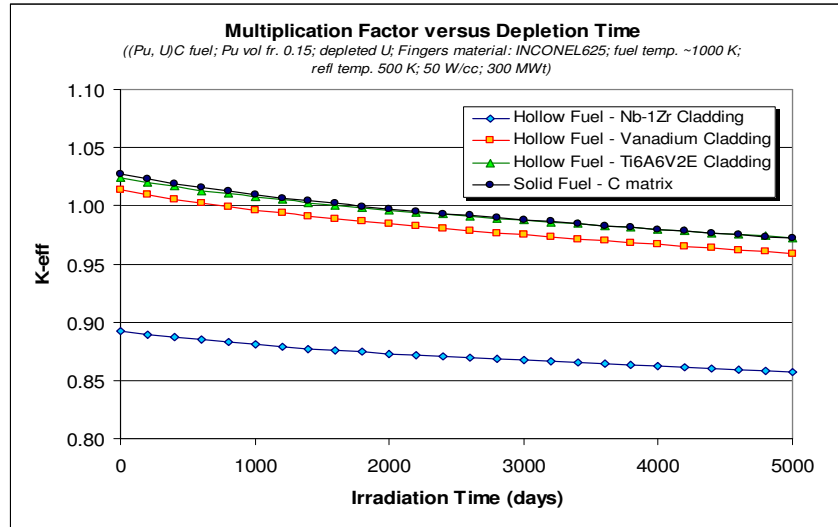


Figure 3. k_{eff} as Function of Irradiation Time.

It is evident in Figure 3 that a k_{eff} value of one or higher is not sustained for the entire life of the core (5,000 days at full power). The targeted long-life core can be obtained by reducing the power density. It is also possible to reduce the reactivity swing (Δk_{eff}) between the beginning and end of cycle by increasing the U-238 content to increase the conversion ratio.

In Figure 4 is displayed the preliminary result obtained using the SS pebble configuration and INCONEL 690 (reactor grade) as material for the cold finger tubes, in a reduced power density core. Reducing the power density to a value of about 22 W/cc and the Pu content to a value of 14.2%, it has been possible to obtain a sustained cycle length of 5,000 days at full power. The burnup reactivity swing is relatively high (~5%) with this design and should be optimized in the future. (The primary purpose of the current study is to evaluate the feasibility of a sustained k_{eff} value.) Therefore, a low reactivity swing could therefore be obtained by reducing the Pu weight fraction and by reducing the power density (bigger core minimizes leakage and improves the conversion ratio).

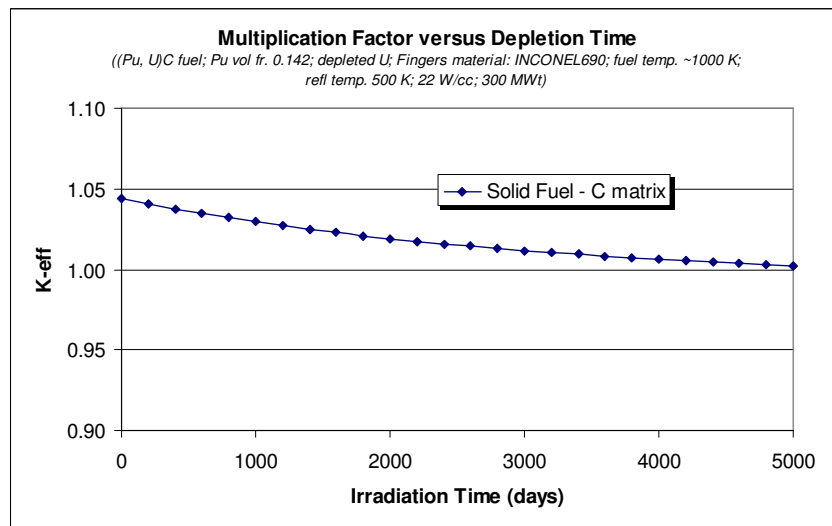


Figure 4. k_{eff} for the Reduced Power Density Core with Cold Fingers.

1.7 Parametric Studies for TRU Breakeven Cores (E. A. Hoffman, T. A. Taiwo, W. S. Yang)

Because the long-life core appears to be attractive from the waste minimization viewpoint, we have additionally performed parametric studies of this fuel management scheme for TRU breakeven cores, using different uranium feed, TRU feed, fuel form, and matrix and reflector materials. The description for each case is provided in Table 1. The maximum cycle length that achieves TRU breakeven for each design option was determined for a fixed fuel volume fraction (30.5%). Two different uranium feeds were considered. These are natural uranium (NU) and depleted uranium (DU). The TRU feed options include that coming from the LWR spent nuclear fuel and another coming from recycled fuel. The (U,TRU)C and (U,TRU)N fuel forms were included in the study. For the nitride fuel, it is assumed that the nitride is enriched to 99.9% ^{15}N . When the nitride fuel is used, only the TiN (enriched in ^{15}N) matrix type is considered. With the carbide fuel, cases using zirconium carbide (ZrC), titanium (Ti), vanadium (V), and graphite (C) as matrix were evaluated. The reflectors considered are SS-316, graphite, beryllium (Be) and its oxide (BeO), nickel (Ni), lead (Pb), tungsten (W).

From a waste management point of view, it might be desirable to have initially a net TRU destruction rate to reduce the legacy (accumulated) TRU inventory. Eventually, the equilibrium system would need to operate on a TRU breakeven system or slightly positive TRU production to feed a growing nuclear fleet. To first order, the relative TRU waste merits of a TRU breakeven fuel cycle are proportional to the TRU processing rate on a per unit electrical energy basis. Assuming the same processing systems, the amount of TRU lost to the waste stream is proportional to the rate of processing. For fuel cycles that either produce or consume TRU, other figures of merit need to be evaluated to account for the net change in the TRU inventory.

As can be seen in Table 2, the TRU breakeven cores range from 20 years (W reflector) to 30 years (Pb reflector) with the reference (SS-316 reflector) design being in the middle of this range. The thermalization of neutrons in the light element reflectors (C, Be, BeO) resulted in very large power peaking factors near the periphery of the core. This seems to be sufficiently problematic to preclude the use of the very light elements in the reflector. In addition, the light element reflectors give slightly larger reactivity swings than SS-316 reflector. Along with the Pb results, it appears that the reflector material should be made of the heaviest elements possible to obtain a low reactivity swing. Lead (Pb) has a low melting point and may not be acceptable, however, as reflector for the PB-GCFR. Other heavy elements with higher melting points will be evaluated.

The reactivity swing for all of these designs is very large, with the lowest having a BOC k_{eff} of 1.064; for all the cases the end of cycle k_{eff} is 1.0.

The rate of TRU discharge and consequently recycle is proportional to the TRU charge enrichment and inversely proportional to the cycle length. The long cycle length of the Pb reflector leads to the lowest TRU recycle rate of 0.44 MT per $\text{GW}_{\text{th}}\text{-yr}$ of energy generation.

The recycle of TRU, instead of using LWR spent nuclear TRU feed, has a small effect on the performance of the reactor as shown by the equilibrium cycle results.

Table 1. Case Descriptions.

Case	U Feed	TRU Feed	Fuel Form	Matrix	Reflector
Reference	DU	LWR	C	ZrC	SS-316
NU Feed	NU	LWR	C	ZrC	SS-316
Ti Matrix	DU	LWR	C	Ti	SS-316
V Matrix	DU	LWR	C	V	SS-316
Graphite Matrix	DU	LWR	C	C	SS-316
Nitride Fuel	DU	LWR	¹⁵ N	Ti ¹⁵ N	SS-316
Graphite Reflector	DU	LWR	C	ZrC	C
Be Reflector	DU	LWR	C	ZrC	Be
BeO Reflector	DU	LWR	C	ZrC	BeO
Ni Reflector	DU	LWR	C	ZrC	Ni
Pb Reflector	DU	LWR	C	ZrC	Pb
V Reflector	DU	LWR	C	ZrC	V
W Reflector	NU	LWR	C	ZrC	W
Equilibrium (DU)	DU	Recycle	C	ZrC	SS-316
Equilibrium (NU)	NU	Recycle	C	ZrC	SS-316

Table 2. TRU Breakeven Cycle Behavior.

Case	Cycle Length (FPY)	BOC k_{eff}	TRU Charge Enrichment	Discharge Burnup (GW _{th} d/MTHM)	TRU Discharge Rate (MT/GW _{th} -yr)
Reference	24.9	1.082	17.1%	115	0.54
NU Feed	25.1	1.091	16.8%	116	0.53
Ti Matrix	23.8	1.064	15.3%	110	0.51
V Matrix	23.2	1.069	16.1%	108	0.55
Graphite Matrix	22.7	1.100	17.8%	105	0.62
Nitride Fuel	21.9	1.082	17.3%	97	0.65
Graphite Reflector	25.8	1.090	15.9%	119	0.49
Be Reflector	23.8	1.096	15.7%	110	0.52
BeO Reflector	26.1	1.104	15.8%	121	0.48
Ni Reflector	24.1	1.075	16.8%	111	0.55
Pb Reflector	29.7	1.084	16.8%	138	0.44
V Reflector	22.2	1.069	16.8%	103	0.60
W Reflector	20.3	1.069	17.0%	94	0.66
Equilibrium (DU)	23.7	1.057	16.9%	119	0.52
Equilibrium (NU)	23.7	1.061	16.9%	120	0.51

1.8 Investigation of Long-Life Transuranics Breakeven and Burner Cores for PB-GCFR (E. A. Hoffman, T. A. Taiwo, W. S. Yang)

Abstract – *Transuranics (TRU) breakeven and burner core designs have been studied for the Particle-Bed Gas-Cooled Fast Reactor (PB-GCFR) being developed under the U.S. Department of Energy Nuclear Energy Research Initiative (USDOE NERI) Program. The issues of minimizing waste production, fuel cost, and burnup reactivity swing, and maximizing TRU burning have been investigated.*

For TRU breakeven cores, it was found that for the given core power (300 MWt) and power density (50 W/cc), the lowest amount of radiotoxic transuranics to be processed is obtained for a long-life (single-batch) core. Minimizing the TRU processed results in a minimization of the TRU losses that ultimately will have to be entombed in a geologic repository. The long-life core has a higher upfront fuel cost than multi-batch cores. However, the overall fuel cost could be lower for the long-life core because of additional fuel costs incurred during the operational lifetime of a multi-batch core.

The results confirmed that the PB-GCFR could be designed to operate over a wide range of cycle lengths and fuel loadings. By modifying the TRU feed to have a higher minor actinides (MA) fraction than contained in LWR spent fuel, the burnup reactivity swing for the long-life core can be reduced significantly. With this approach, it is also possible to configure the long-life PB-GCFR core as a TRU burner using non-fertile fuel. A non-fertile fuel PB-GCFR with 24% plutonium and 76% MA can operate for 17 full power years and achieve 25% burnup with a reactivity swing of 3%Δk. Detailed considerations have not been given to fuel fabrication and handling issues in the fuel cycle. It is however noted that remote handling will be required for the manufacturing of such a fuel.

I. INTRODUCTION

A solution must be found for LWR spent nuclear fuel (SNF) that is accumulating in spent-fuel ponds and dry-storage sites, if nuclear is to play a prominent role in future energy generation in the U.S. Indeed, nuclear waste minimization is a key attribute for advanced nuclear fuel cycles. An approach to accomplish this is to recycle and incinerate the radiotoxic transuranics (TRU) in nuclear power reactor systems.

The issue of nuclear waste minimization is being investigated under a USDOE-sponsored NERI project on the Particle-Bed Gas-Cooled Fast Reactor (PB-GCFR) design that is evaluating the impact of different fuel forms and types on core performance. In addition, the other advanced nuclear systems goals of improved safety, enhanced proliferation resistance, and reduced system cost are being pursued in the study. The key requirement for the project is the application of a fast neutron spectrum environment to enhance both the passive safety and transmutation characteristics of advanced pebble-bed reactor designs.

A healthy future nuclear enterprise in a sustainable environment requires that fuel material be effectively utilized. In this regard, the PB-GCFR study has focused on reactor designs with a high TRU conversion ratio. The intent is to design a TRU self-sufficient core in which for a given initial core load, the continuous recycle and application of the fuel would be obtained without need for external TRU makeup material. As a basis for trade-off studies, a reference compact fast-spectrum core based on the pebble-bed system has been developed. This core is designed for a power rating of 300 MWt (with about 50 W/cc power density) and has no blanket zone, to preclude the production of

high-purity fissile material. It was additionally imposed on this design that the TRU component of SNF extracted by a separation process be used as fuel, in order to minimize the TRU sent to the repository. This fuel type would enhance proliferation resistance because the TRU would be unavailable in a repository that could become a plutonium mine.

The relatively low power and power density of the PB-GCFR design are due to the requirements that the system be passively safe and be optionally exportable to international markets having little or no nuclear infrastructure. On this basis, the TRU content of the heavy metal in the fuel has been limited to 20%, in support of non-proliferation goals of the U.S. government. Additionally, intrinsic proliferation protection is provided by the pebble fuel form. Because the system is for foreign export, it is currently planned that the core would be loaded offshore and following long-life irradiation (10 to 30 years), the core would be removed and discharged offshore. If fuel reprocessing is required, this too would be done offshore.

The inventory of TRU may initially far exceed that needed to produce nuclear fuel to maintain the fleet of nuclear reactors in a sustainable manner. Therefore, it may be desirable for the PB-GCFR to destroy a large fraction of the TRU. The fertile fuel PB-GCFR, particularly if constrained to low TRU enrichment for non-proliferation reasons, will not be capable of significant TRU destruction. To maximize TRU destruction, a non-fertile (no uranium) system will be desirable. A PB-GCFR design that utilizes non-fertile fuel for deep TRU burning has therefore been evaluated. This design might not be suitable for export because of proliferation concerns. If the non-fertile fuel has a relatively high content of minor-actinides (MA), however, this proliferation concern may be diminished because material theft (handling) is made difficult by the inherently high radiation intensity. In this case, fuel manufacturing would probably have to be done remotely and fuel transport would require heavy shielding, both resulting in added cost.

With TRU recycle, reprocessing losses only would be sent to the repository. In this case, the amount of TRU lost to the repository is determined by the amount of TRU to be processed and the recovery factor in recycle. Therefore, in order to minimize the TRU sent to the repository in a sustainable system, it is desirable to design a reactor fueled with TRU in such a way that the total amount of TRU fuel required to operate the reactor for its lifetime is minimized. This implies that the initial TRU inventory and TRU mass flow for the core lifetime should be minimized. On the contrary, for the non-sustainable TRU burner systems, the TRU lost in reprocessing is minimized when the fractional TRU burnup in each pass through the reactor is maximized. Various trade-studies have been performed to investigate the impact of typical fuel management schemes on fuel waste minimization. Based on the finding of this work, additional studies have been done to optimize the long-life core, by investigating the impact of fuel materials on the core physics performance.

In Section II, the reference core design and analysis approach used for the study are discussed. This design is for a long-life (single-batch) core, which intuitively should result in the minimum amount of TRU being sent to the repository, compared to multi-batch cores, for a given core size. The results of the sensitivity study on various fuel management schemes are presented in Section III. Typical schemes such as three-batch schemes with various cycle lengths (1, 3, 10 years), and semi-continuous schemes were evaluated, along with the single-batch scheme. Preliminary estimates of the relative fuel cost for the various schemes are also provided. In Section IV, the design envelop for a PB-GCFR using carbide fuel, SiC matrix and Zr_3Si_2 reflector is presented. The capability for deep TRU burning using non-fertile fuel in the PB-GCFR is reported in Section V. The conclusions from the work are presented in Section VI.

II. DESCRIPTION OF METHODS AND MODELS

II.A. Reference Design

A reference compact fast-spectrum core¹ based on the pebble-bed system has been developed. This core is designed for a power rating of ~ 300 MWt (50 W/cc power density) and uses the pebble fuel type. Each spherical pebble consists of a central zone of coated or particulate fuel dispersed in a matrix material and an outer zone of matrix material only. Since the graphite used as matrix material in the Pebble-Bed Modular Reactor (PBMR) design might not be appropriate for the fast-spectrum concept, because of its strong neutron moderating properties, other matrix materials have been evaluated. The requirements for high operating temperatures that give a high thermal efficiency (45-50%) necessitated the use of refractory metals and high melting point materials having favorable fast neutron properties (e.g., low absorption cross section).

The pebble employed in this study has an outer radius of 6 cm. A dispersion fuel-zone diameter of 5.5 cm was used in the study, in order to increase the fuel loading in the pebble. The pebbles are packed into a cylindrical core and are assumed to occupy 61% of the volume. The use of dispersion (or coated) fuel particles in a pebble imposes a physical limit on the maximum fuel volume fraction ($\sim 31\%$). The practical limit could be less due to material performance considerations.

Helium gas flows through the pebble-bed to remove the heat generated by the fission process. The helium coolant, being neutronically benign (i.e., low macroscopic absorption cross section), does not adversely affect the fraction of neutrons available for converting fertile nuclides to fissile nuclides. Thus, reactivity losses can be effectively compensated by the inclusion of fertile material, which tends to reduce the enrichment and excess reactivity requirements of long-life systems. For the reference design, depleted uranium is employed as the fertile material.

In order to limit the solution search space for this study, the core geometry was fixed with a height-to-diameter ratio of one. The fuel volume fraction and enrichment were searched to satisfy the design requirements and the criticality condition during the cycle. The core power density for all the cases is 50 W/cc, which is much lower than that employed for typical fast reactor systems, but higher by a factor of ~ 8 than the value for the PBMR. Passive safety requirements might change the final value of this core parameter.

The fuel pebble design used for this study utilizes the same matrix and coating material (or uncoated). This design permits a core-fuel volume fraction of up to $\sim 30\%$ that ensures a sustained critical mode operation for a 15-30 years fuel irradiation cycle. Currently, we have used potentially compatible fuel and matrix forms for this fuel type. Specifically, mixed uranium-transuranics carbide [(U,TRU)C] fuel dispersed in a zirconium carbide (ZrC) or silicon carbide (SiC) matrix. The reference core volume fractions are 30.5% fuel, 30.5% matrix, and 39% helium (He) coolant. A 50-cm reflector (20% He coolant) of either SS-316 or Zr_3Si_2 is assumed. Additional fuels material study is required, however, to ascertain that these are applicable fuel-matrix forms in the irradiation and temperature fields of the PB-GCFR.

II.B. Analysis Method

Full-core equilibrium and non-equilibrium cycle calculations have been performed using the REBUS-3 fuel-cycle analysis code.² Region-dependent 33-group cross sections were generated with the MC²-2 code³ based on ENDF/B-V nuclear data. Beginning of cycle material compositions and temperatures were used in the MC²-2 calculations. An R-Z computational model with homogenized pebbles has been developed for the PB-GCFR core. The flux distributions were obtained using the

finite-difference diffusion theory option of the DIF3D code,⁴ based on the observation that it gives similar results as S_n transport calculations for the homogenized core model.

Physics considerations suggest that such simple homogenization models should be able to treat adequately the double heterogeneity effect of fuel particles in pebbles, in the fast-spectrum system of interest in this study. This is because the low-energy resonance region contribution to the multiplication factor is small in such systems. Preliminary evaluations of this effect, using higher fidelity (deterministic transport and Monte Carlo) codes, confirm this trend. However, it is additionally planned to perform a more rigorous investigation of this issue in the future using an MCNP model as reference.

For the fertile fuel systems, equilibrium-cycle enrichment searches were performed using the REBUS-3 code. Here, the enrichment is defined as the TRU fraction of heavy metal. TRU from LWR SNF and depleted uranium were used as the feed materials. For the multi-batch cores, a scatter loading was also assumed. The equilibrium fuel-cycle calculation assumed the fuel is not recycled in determining the initial core loading of the long-life (single-batch) core. Equilibrium calculations with recycle give quite similar results. For the non-fertile system, a non-equilibrium fuel-cycle calculation was performed. This is a simple core depletion calculation in which the core model employs radial and axial fuel depletion zones to account for non-uniform fuel depletion.

III. IMPACT OF FUEL MANAGEMENT SCHEME ON TRU WASTE MINIMIZATION

The advanced nuclear systems goals of waste minimization and effective fuel utilization (sustainability) can be met by designing a TRU breakeven core. For such a core, the total amount of TRU required to operate a reactor for its lifetime was estimated for various fuel management schemes, in order to determine the favorable approach for waste minimization. A thirty-year core lifetime was used as basis for comparison of the various cases. This implies that the core would be initially loaded, periodically reloaded (depending on the fuel management scheme), and ultimately offloaded at the end of the thirty years.

Multi-batch fuel management requires fuel batches to startup the initial core and at least one additional fuel batch manufactured from outside sources of TRU in order to operate the reactor until reprocessed TRU is available. The PB-GCFR fuel will be homogeneously recycled (uranium and TRU together), with depleted uranium (DU) used as external feed to makeup the material consumed. For the TRU breakeven cycle, the only external TRU needed is for the initial fuel batches prior to recycle. In this regard, it is assumed that there is an interval of five years between fuel discharge and recycle back into the core following fuel separation and fabrication. In order to operate the reactor until reprocessed fuel is available, the initial core and one additional batch of fuel manufactured from external sources of TRU will be required if the fuel-cycle length is greater than 2.5 years. For cycles less the 2.5 years, multiple additional batches will be required to operate the reactor until reprocessed fuel is available.

For the initial fuel batches, it is assumed that LWR SNF can be separated to (1) obtain high purity uranium, (2) recover the TRU, and (3) partition the fission products. The TRU will be blended with DU to produce the initial fuel batches. The uranium would be stored for future use (preferred) or buried in a low-level disposal site. PB-GCFR fuel is assumed to be reprocessed and the uranium and TRU recycled with DU used as the makeup material for subsequent batches of fuel. Fission products and TRU losses from the separation stages would be packaged into waste forms and buried at the repository after cooling and packaging.

The results for the single-batch and multi-batch cases are summarized in Table I. The *lifetime TRU processed* is the figure of merit used to evaluate the relative TRU losses. The amount of TRU ultimately reaching the repository has an effect on the amount of nuclear waste that can be contained in the repository, as this material constitutes the primary long-term hazard. The TRU losses will be proportional to the TRU processed. In this study, the loss rates for the processing of LWR SNF and PB-GCFR SNF are assumed the same. Waste minimization and the ability to package the material into effective waste forms is dependent on the lifetime TRU processed.

In Table I, it is seen that the TRU discharge rate (in MT/GWt-yr) is dependent on the burnup. Maximizing the burnup reduces the TRU discharge rate and hence the required processing. For a fixed fuel residence time (30 years), the initial TRU inventory increases slightly with the cycle length and hence the TRU discharge burnup decreases slightly. As a result, longer cycle length increases the TRU processing per cycle. However, because of less frequent recycling, the lifetime TRU processed decreases considerably with the cycle length.

TABLE I.
Impact of Fuel Management Scheme on Lifetime TRU Processing.

Fuel Management Scheme		1-batch; 30-yr cycle	3-batch; 10-yr cycle	3-batch; 3-yr cycle	3-batch; 1-yr cycle	30-batch; 1-yr cycle	60-batch; ½-yr cycle
Fuel Volume Fraction (%)		32.0	28.1	23.5	22.5	26.9	26.9
Core TRU Inventory (MT)		4.09	3.69	3.46	3.44	3.58	3.58
Charge	HM Mass/Cycle (MT)	24.82	7.26	6.08	5.82	0.70	0.35
	TRU Enrichment (%)	16.5	17.0	19.0	19.7	17.2	17.2
Discharge	Max. HM Burnup (GWd/MT)	132.4	150.9	54.0	18.8	157.6	157.7
	Ave. HM Burnup (GWd/MT)	132.4	90.6	45.1	17.7	79.6	79.6
	TRU Rate (MT/GW-yr)	0.45	0.41	1.28	3.83	0.40	0.40
Lifetime TRU Processed	Legacy LWR TRU (MT)	4.09	4.93	4.61	9.18	4.18	4.17
	Recycled TRU (MT)	0.00	1.23	9.23	27.55	2.87	2.92
	Total TRU (MT)	4.09	6.16	13.84	36.73	7.04	7.10

NOTES:

- (1) HM means heavy metal.
- (2) Legacy LWR TRU is the amount of LWR TRU required to startup the system, including initial reloads.
- (3) ZrC matrix and SS-316 reflector are used in the calculations.

For a fixed number of batches, the discharge burnup can be increased by maximizing the cycle length or the specific power under the material irradiation and safety constraints. As discussed above, the passive safety requirements limit the specific power significantly, in the PB-GCFR design. Therefore, in order to increase the discharge burnup and hence to reduce the amount of TRU to be processed, it is desirable to increase the cycle length. This can be confirmed by comparing the results for 3-batch fuel management schemes with different cycle lengths shown in Table I. Finally, the single-batch core results in the lowest TRU procurement requirement and lowest lifetime TRU processed.

These results indicate that the fuel management scheme will have an impact on fuel cost. An evaluation of this impact has been done by assuming that the fuel cost is proportional to the TRU content of the fuel. If partially burned fuel can be used in subsequent reactors, the equilibrium cycle fuel cost will be determined primarily by the TRU discharge rate. The current analysis is for the first reactor and therefore accounts for the fact the entire first core must be manufactured. Additionally, the residual partially burned fuel is assumed to be of no value at the end of the first reactor life. This assumption would be true for a scenario in which the fuel would be discharged and reprocessed into new fuel form, prior to insertion into a subsequent second reactor. The thirty-year or so lifetime of the core makes this a possibility, since new advancements in reactor design might eliminate the option of direct utilization of partially burned assembly in the second reactor. Finally, in the calculation, the entire fuel cost for a batch was assumed to be incurred at the beginning of the year the fuel is loaded into the reactor, without considering the lead-time.

The fuel cost will be an expense that can be deducted from revenue to reduce the tax liability. The accounting rules may be particularly important for treatment of the fuel cost. If the fuel is considered a capital cost, which seems likely for the long-life core, it will be subject to depreciation rules. Therefore, the cost will have to be deducted over time, which reduces the value of the deduction. A fuel-costing scenario that is adverse to the long-life core is utilized. The scenario assumes a uniform depreciation over the useful life of the fuel. The useful lifetime corresponds to the time of fuel discharge from the core or the end of plant life, whichever is shorter. For evaluating the value of the deductions, a high marginal tax rate of 50% was assumed. The net cost is then given by the present value of the fuel cost minus the present value of the reduced tax liability.

The net fuel cost for each fuel management scheme is shown in Fig. 1. The results indicate that adverse tax treatment of the long-life core could negate the advantage of smaller fuel requirements over the life of the plant. Adverse tax treatment would significantly increase the likelihood that smaller upfront capital costs will dominate the decision making process.

For a low rate of return and immediate deduction of the fuel costs, the long-life core has a distinct fuel cost advantage. For high rates of return, long depreciation times, and high marginal tax rates, there is a significant advantage to pushing costs into the future. The reduced cost of the initial core load for the multi-batch cores may offset the higher fuel costs in the future under these conditions. To accommodate a multi-batch core, a more complex design that incorporates on-site fuel handling equipment would be required, however. This should be more expensive than the long-life core that is fueled once and only unloaded after the plant is shutdown. Even though scenarios may exist that could result in lower fuel cost for the multi-batch cores, these seem to be rather extreme conditions and the long-life core still seems a better choice than the multi-batch core for these low power density systems.

The long-life core will also have a significant proliferation resistance advantage over the multi-batch cores. The primary advantage of the long-life core is that at no point is nuclear fuel outside of the reactor after startup of the plant. For the multi-batch core, fresh fuel will be on-site prior to reload and irradiated fuel will be stored at the site until it has cooled sufficiently for shipment to the reprocessing facility, which might be co-located or off-site. The first batch of irradiated fuel will have a very low burnup, particularly for the short cycle length designs. In addition, far more fuel will need to be processed for the multi-batch core. This not only increases fuel costs and TRU in the waste stream, but also increases the opportunity for diversion.

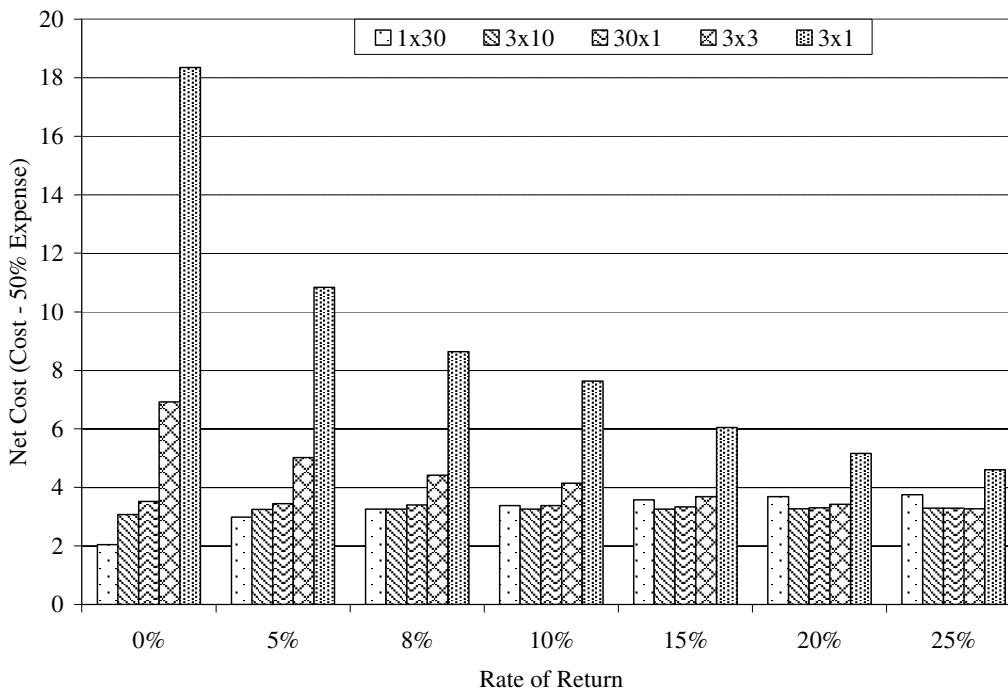


Fig. 1. Present-Value Net Fuel Costs for a Long Depreciation and a High Marginal Tax Rate.

IV. DESIGN ENVELOP FOR CARBIDE-FUEL, SiC-MATRIX, Zr₃Si₂-REFLECTED PB-GCFR

More detailed analysis of the PB-GCFR core has been done to determine the applicable design envelop based on an initial set of design criteria. The results for a core using carbide fuel, SiC matrix and Zr₃Si₂ reflector is presented in this section. These material choices have been found to be favorable neutronically from sensitivity studies that have been performed for the long-life PB-GCFR core. The combination results in the longest TRU breakeven cycle length and lowest TRU discharge rate, but has nearly the highest burnup reactivity swing because of the long cycle length. These materials appear superior to the ZrC matrix and SS-316 reflector, respectively, and do not have melting or power peaking concerns arising from the use of other materials having similarly good neutronic performance.¹ The ZrC matrix, however, might be able to withstand higher operating temperatures, which could prove to be a significant safety advantage.

Five different constraints were imposed on the PB-GCFR. A constraint on the maximum fuel volume fraction has not been imposed on the design, but could prove to be limiting, depending on the core power rating. The constraints are:

1. Design for a long-life (single-batch) core with a core life greater than 10 full-power years of operation. This makes the PB-GCFR attractive for export to countries with less developed nuclear infrastructure.
2. Ensure fuel integrity during operation by limiting the maximum fluence (burnup) to which the fuel can be exposed. This limit is undetermined at this time and will most likely be a function of the fuel volume fraction. An optimistic limit of 15% burnup is imposed for this analysis.
3. The reactor must be critical at all times during the cycle.
4. Limit the TRU enrichment to 20 w/o for non-proliferation reasons.

5. Constrain the PB-GCFR to be a TRU breakeven or burner core.

The region of interest meeting these criteria has been evaluated for the PB-GCFR using TRU from LWR spent fuel (90% Pu, 10% MA; Pu-239 is 52% of TRU). This was done by performing enrichment searches for specific cycle lengths and fuel/matrix volume ratios.

The five criteria are met by the region enclosed by the solid line in Fig. 2. We note that the beginning of life (BOL) critical curve (line 3) corresponds to a breeder design for which the unpoisoned BOL and end of life (EOL) k_{eff} are equal to 1.0. Above this curve, the breeder design would have an unpoisoned k_{eff} less than 1.0, for a fixed EOL k_{eff} of 1.0. This curve is well above the TRU breakeven line (line 5) and therefore is not limiting. The analysis revealed that over this region, the BOL k_{eff} ranges from approximately 1.05 to 1.15 (~\$15 to \$50) with the lowest value corresponding to the case with the shortest cycle length. This signifies relatively large excess reactivity. The permissible excess reactivity is however set by the control requirements, which is intimately connected to reactor safety. While a limit has not been set for the excess reactivity, lower values are desirable.

The PB-GCFR could burn nearly 10% of the initial TRU inventory, but this would result in a design with a high burnup reactivity swing. Achieving a low reactivity swing with the current fuel form would require a TRU breeder design. A degraded TRU vector could be used to reduce the reactivity swing without the core being a TRU breeder. An appropriately chosen vector would allow internal TRU "breeding" (e.g., conversion of Np-237 to Pu-238) without net TRU production. In one concept, the PB-GCFR could be operated as a Tier 2 reactor in a multi-tier transmutation concept⁵, in order to obtain the appropriate MA content from a Tier 1 system that burns the plutonium from LWR SNF. For the current evaluation, a vector utilizing half the plutonium and all of the minor actinides from LWR

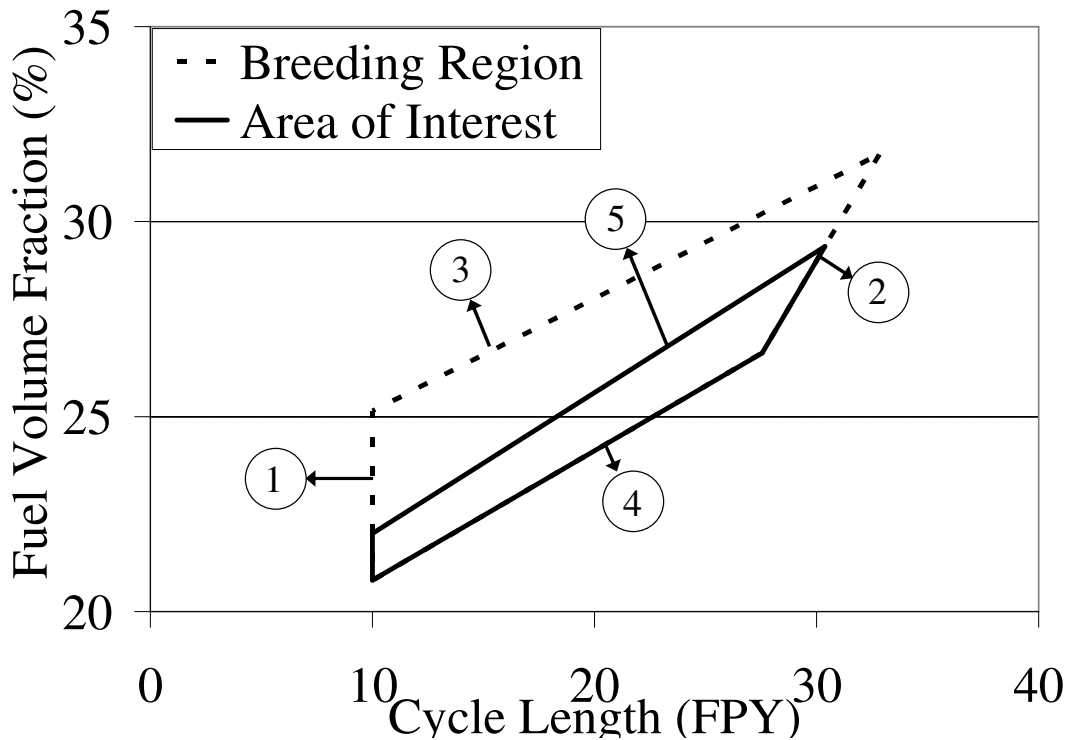


Fig. 2. Design envelop for long-lived PB-GCFR using LWR TRU Feed. 1) Cycle length < 10 FPY; 2) Burnup > 15%; 3) BOL k_{eff} < 1 (Not Limiting); 4) TRU Enrichment > 20%; 5) $\Delta_{TRU} > 0$.

SNF was chosen as the TRU feed for the long-life PB-GCFR. The remaining plutonium could be recycled as either MOX fuel in advanced LWRs or in multi-batch fast reactors. The main purpose of the evaluation is to determine if a long-life PB-GCFR with relatively low reactivity swing could be designed. How this reactor fits into an integrated system would need further consideration.

A higher TRU enrichment is required for the degraded TRU because of its lower fissile content. The fissile and plutonium fractions of this TRU form would increase over the cycle. The degraded TRU vector gives a large decrease in the Np-237 concentration over the cycle, which results in a significant reactivity addition. The peak k_{eff} for the degraded TRU feed is 5 to 6% Δk lower for the same fuel loading and cycle length than for the LWR TRU feed. This suggests there may be an advantage to using a high MA feed material, but other considerations such as reduced β_{eff} (impact on reactor safety) and difficulty of manufacturing the fuel need to be considered.

Figure 3 displays the region that meets the design criteria for the degraded TRU feed. The BOL critical curve ($k_{eff} = 1.0$) has been shifted, and has become constraining, in contrast to LWR TRU case. Also, the reactor using degraded TRU fuel will not be critical at BOL with 20% TRU enrichment and a fuel volume fraction of less than 23.2%.

By degrading the TRU vector, the reactivity of the fuel is reduced to the point where initial breeding will increase the reactivity of the core. Therefore, the reactivity swing will be the maximum unpoisoned k_{eff} of the system (no longer at BOL) minus the minimum unpoisoned k_{eff} (1.0 at EOL). It seems possible to design a PB-GCFR with a cycle length of 15 FPY and a reactivity swing of approximately 2% Δk or nearly 30 FPY and a reactivity swing of approximately 5% Δk . Further design optimization could probably reduce these values.

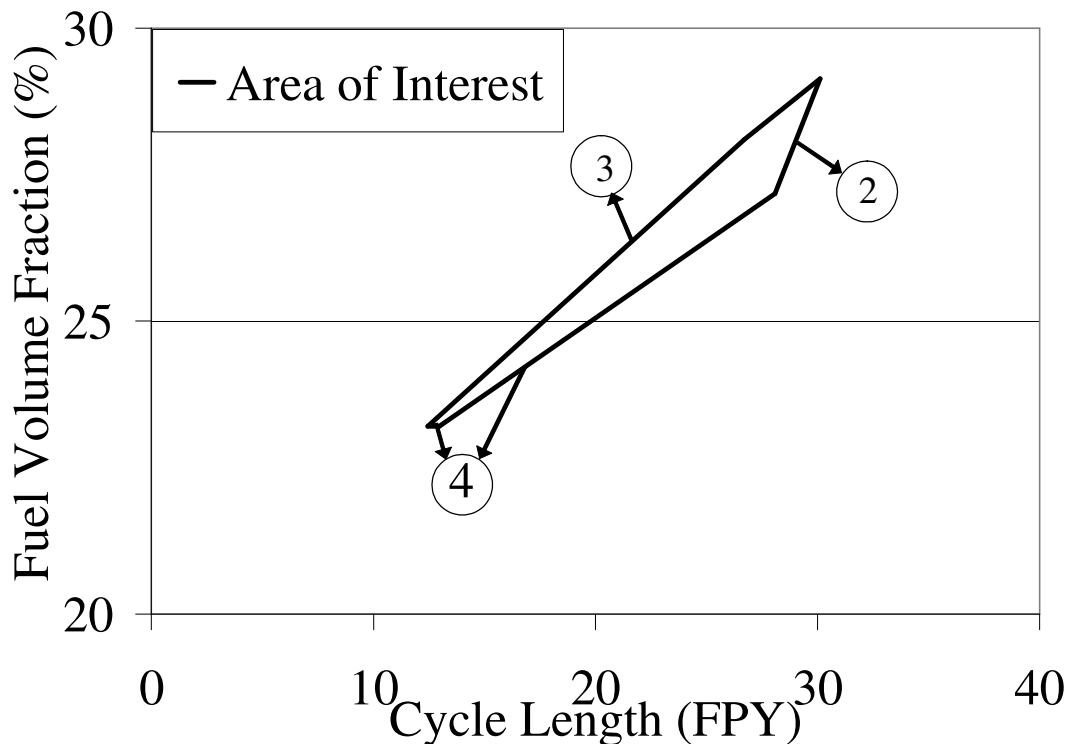


Fig. 3. Reactivity swing for PB-GCFR with degraded TRU feed stream. 1) Cycle length < 10 FPY (Not Limiting); 2) Burnup > 15%; 3) BOL $k_{eff} < 1$; 4) TRU Enrichment > 20% (Not critical at BOL for FVF < 23.2); 5) $\Delta_{TRU} > 0$ (Not Limiting).

The PB-GCFR fueled with the degraded TRU vector will be a slight TRU burner. The maximum TRU destruction is slightly over 5%. With the degraded TRU vector, the PB-GCFR will be capable of destroying (fission and capture) over 45% of the MA content. The plutonium inventory will increase by 5% to 15%. The increased plutonium inventory will complicate homogeneous recycle of fuel since the recycled feed will be more reactive even if only minor actinides are used as makeup.

The results presented in this section indicate that a long-life (single-batch) PB-GCFR core can be designed. The long-life core will have a high reactivity swing if all of the transuranics from LWR SNF are used. To reduce the reactivity swing, a degraded (high MA content) TRU vector must be utilized. As a result, the long-life PB-GCFR can only be a component of a strategy designed for destroying all transuranics, since the plutonium fraction of the fuel has to be reduced (burned elsewhere). For a small long-life PB-GCFR, the 20% TRU enrichment limit intended to reduce proliferation risks will limit the TRU burning capability of the PB-GCFR. It is noted, however, that if a high TRU enrichment fuel with a high MA fraction is loaded into a long-life nuclear battery (e.g., PB-GCFR), the proliferation risk might not necessarily increase. The radiation field resulting from the use of the material might make it unattractive for theft and effective weapons utilization.

V. NON-FERTILE FUEL PB-GCFR DESIGN

In the previous section, the TRU enrichment was limited to 20%. This limit will allow the design of TRU breakeven cores and possibly slight TRU burners. To achieve more effective burner designs, a higher TRU content is needed. Assuming a non-fertile fuel could be utilized, the performance of a non-fertile PB-GCFR design using the same carbide fuel, SiC matrix and Zr_3Si_2 reflector employed for the TRU breakeven core has been evaluated.

The non-fertile PB-GCFR fueled with TRU feed from LWR SNF would have a very large reactivity swing ($>40\% \Delta k$ for a 10 FPY cycle), which is unacceptable. To reduce the reactivity swing, the approach utilized for the fertile fuel design was used. The TRU vector must be degraded by reducing the fraction of plutonium in the fuel. This yields a non-fertile fuel with a relatively high content of minor actinides for the single-batch long-life core of interest in this work. Practically, the plutonium that is not being used in the PB-GCFR could be utilized either in advanced LWRs using MOX fuel or in other fast spectrum systems, but this would require Pu separation and raise the associated proliferation concerns. A sensitivity study investigating the impact of the initial Pu fraction on the core reactivity swing has been done.

The time evolution of the multiplication factor (k_{eff}) for four different non-fertile feed streams with relatively high MA contents are displayed in Fig. 4. All designs were for a fuel loading of 9.1 MT-TRU. Lowering the plutonium fraction will reduce the reactivity of the fuel to the point where TRU breeding will initially increase the k_{eff} . The reduction of the plutonium fraction will also lower the multiplication factor; large reduction of the plutonium content can result in a sub-critical state at BOL. BOL criticality will therefore determine the smallest TRU loading (i.e., fuel volume fraction) for a given TRU vector.

More representative calculations have been done for core loadings that ensure a critical state for the duration of the core life. Figure 5 is a comparison of the time-dependent k_{eff} for different degraded TRU vectors. A lower plutonium fraction in the TRU vector requires a larger TRU loading for the system to be critical. This shortens the cycle length, but indicates there is an optimum TRU vector for a given cycle length. The non-fertile PB-GCFR has not been optimized and many issues relating to the use of fuel containing high MA content have not been evaluated. Nevertheless, it appears that it is possible to design a long-life, non-fertile fuel PB-GCFR with a relatively small reactivity swing.

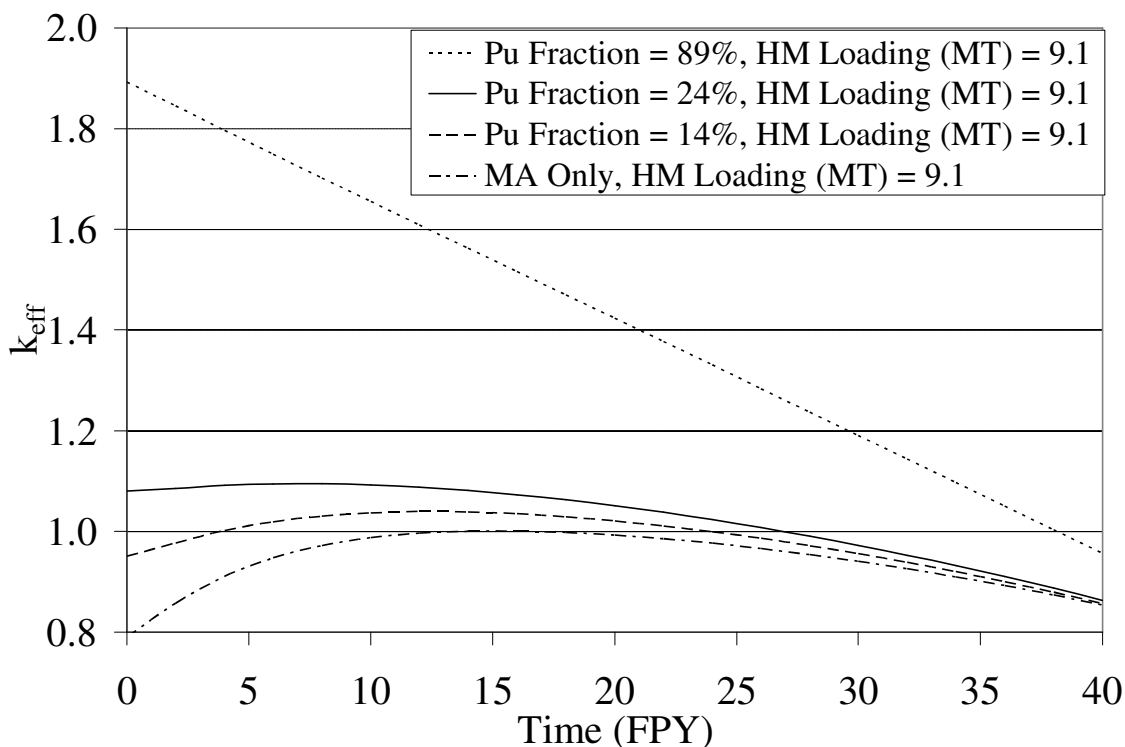


Fig. 4. Non-fertile PB-GCFR with a 12% fuel volume fraction

A PB-GCFR core using MA-only fuel would need approximately 14 MT of fuel. This would necessitate the processing of 14,000 MTU of LWR SNF to recover the required minor actinides. The MA fueled PB-GCFR would be capable of operating in excess of 40 FPY. With this cycle length, more than 30% of the original minor actinides would be fissioned. About 20% of the original minor actinides would be transmuted to plutonium (~70% ^{238}Pu). The peak k_{eff} will be slightly higher than 1.15.

The TRU vector containing 14% plutonium and 86% MA will remain critical in excess of 30 FPY. Approximately 10 MT of TRU will be required for the PB-GCFR to be critical. The peak k_{eff} is still high at 1.077 and only a small fraction of the plutonium is being recycled in the PB-GCFR. Nearly 35% of the original TRU will be fissioned with over 60% of the minor actinides being destroyed and the total plutonium content is more than doubled because of a large increase in the ^{238}Pu inventory.

With a Pu/MA ratio of 24/76 in the non-fertile TRU fuel, the PB-GCFR would remain critical for approximately 17 FPY. Less than 8 MT-TRU would be required. The peak k_{eff} would be 1.031. A large quantity of LWR SNF (~ 6,000 MTU) would still be required because only a small fraction of the plutonium (~3%) is being recycled in the PB-GCFR. Approximately 25% of the original TRU will be fissioned, with over 45% of the minor actinides being destroyed. This is accompanied with a 36% increase in the total plutonium content, because of an increase in the ^{238}Pu inventory.

These results indicate that a single-batch long-life core (> 10 FPY) can be designed with non-fertile fuel. To reduce the reactivity swing, a low concentration of plutonium and high concentration of minor actinides will be required. The fuel volume fraction in the core could be as low as 10%, which is less demanding on the fuel design than the 25-30% required for a TRU breakeven core. Other issues associated with the use of non-fertile and high MA content fuel (e.g., low β_{eff} , fuel

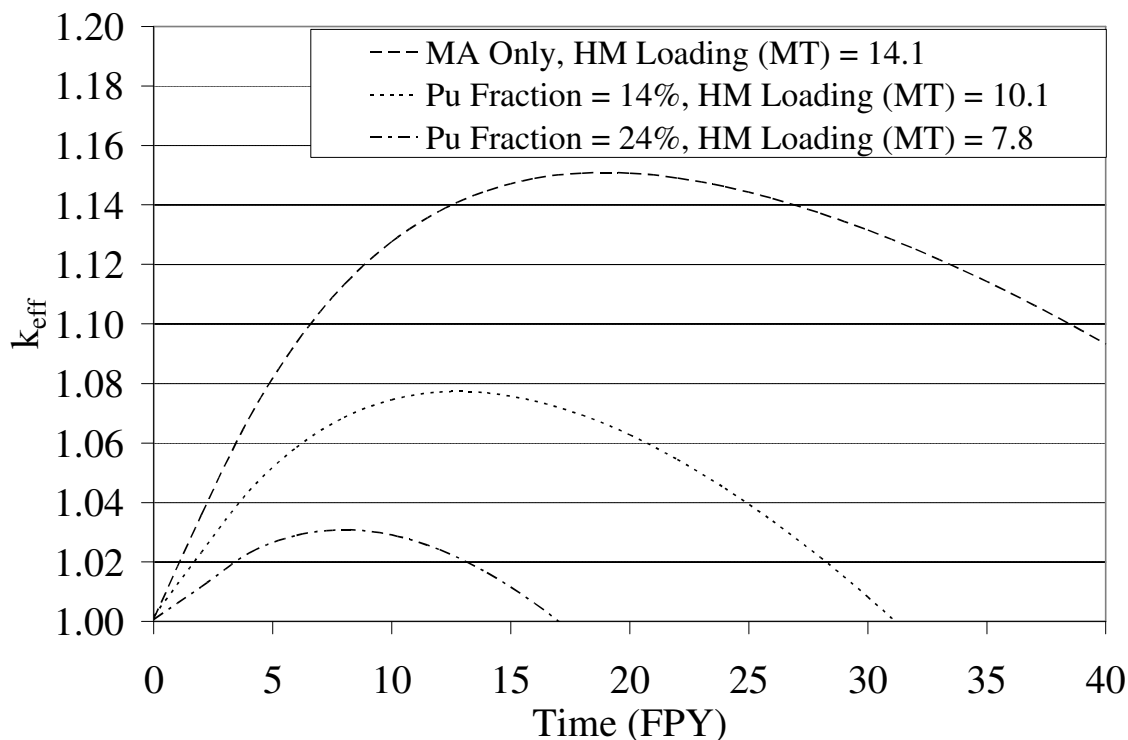


Fig. 5. Non-fertile PB-GCFR fueled with degraded TRU vector (BOL $k_{\text{eff}} = 1.0$).

handling and manufacturing difficulties, and increased helium production in the fuel) are yet to be evaluated.

VI. CONCLUSIONS

Transuranics (TRU) breakeven and burner core designs have been studied for the PB-GCFR, focusing on the issues of minimizing waste production, fuel cost, and burnup reactivity swing, and maximizing TRU burning. For TRU breakeven cores, the impact of fuel management scheme on TRU waste minimization was evaluated, using the lifetime TRU material to be processed as the figure of merit. A thirty-year period was used in the study. Because of the requirement that all the cores have the same power (300 MWt) and power density (50 W/cc), the long-life (single-batch) core was found to be the preferable design compared to multi-batch cores because of its low lifetime TRU requirements.

A carbide-fuel, SiC-matrix, Zr_3Si_2 -reflector PB-GCFR design was investigated and found workable over a wide range of cycle lengths and fuel loadings. With a typical LWR SNF TRU vector, this design results in a high reactivity swing, however. The study found that modifying the TRU feed to have a higher MA fraction than contained in LWR spent fuel, would reduce significantly the burnup reactivity swing for the long-life core design. The higher MA feed could be obtained in a multi-tier transmutation approach in which the plutonium is preferentially burned in the first tier. Without extensive optimization of the feed, the reactivity swing was reduced to less than $2\% \Delta k$. The higher MA content feed results in a total TRU destruction rate of less than 10%, but more than 30% of the minor actinides inventory is destroyed in a single pass. The 20% TRU enrichment limit imposed for non-proliferation reasons also limits the TRU burning.

The potential for a high TRU burning level in the PB-GCFR was investigated. Unacceptably high reactivity swings would occur unless the TRU contains a high fraction of minor actinides. The results indicated that a non-fertile-fuel, long-life PB-GCFR using a relatively high MA content could be designed to destroy a large fraction of the TRU, possibly 30%, if a high MA content can be used in the fuel. Such a design with 24% plutonium and 76% MA can operate for 17 full power years and achieve 25% burnup with a reactivity swing of 3% Δ k. The utilization of this fuel type would increase fuel cycle cost because of the difficulties associated with using it in the fuel cycle (e.g., handling problems due to high radiation field, manufacturing difficulties, low β_{eff} value, and production of helium gas in the fuel matrix).

At this point, only limited safety calculations have been performed and other design questions remain, but the design of a long-life PB-GCFR seems feasible neutronically.

REFERENCES

1. E.A. HOFFMAN, T.A. TAIWO, W.S. YANG, AND M. FATONE, "A Particle-Bed Gas Cooled Fast Reactor Core Design for Waste Minimization," Seventh Information Exchange Meeting on Actinide and Fission Product Partitioning and Transmutation, (2002).
2. B. J. TOPPEL, "A User's Guide to the REBUS-3 Fuel Cycle Analysis Capability," ANL-83-2, Argonne National Laboratory (1983).
3. H. HENRYSON II, B. J. TOPPEL, AND C. G. STENBERG, "MC²-2: A Code to Calculate Fast Neutron Spectra and Multigroup Cross Sections," ANL-8144, Argonne National Laboratory (1976).
4. K. L. DERSTINE, "DIF3D: A Code to Solve One-, Two-, and Three-Dimensional Finite-Difference Diffusion Theory Problems," ANL-82-64, Argonne National Laboratory (1984).
5. R.N. HILL, T.A. TAIWO, J.A. STILLMAN, D.J. GRAZIANO, D.R. BENNETT, H. TRELLE, M. TODOSOW, W.G. HALSEY, AND A. BAXTER, "Multiple Tier Fuel Cycle Studies for Waste Transmutation," Proc. 10th International Conference on Nuclear Engineering, Arlington, VA (2002).

1.9 Core Physics Design Alternatives (E. A. Hoffman, T. A. Taiwo)

Long-lived PB-GCFR Neutronics Design Optimization

The 300 MWt GFR based on the helium-cooled pebble-bed system was evaluated to determine the potential for developing a long-life core with a low burnup reactivity swing and a *more uniform power distribution*. As part of a nuclear park, the PB-GCFR may not be constrained to a TRU breakeven design, and fuel breeding could be used to reduce the reactivity swing. Based on this assumption, slightly breeding designs have been evaluated. The core is divided into 10 axial zones, each of which is loaded with fuel pebbles having different fuel enrichments. The fuel volume fraction is restricted to 30.5%. Radial enrichment zones were not permitted initially because it was assumed difficult to maintain the proper radial loading of the pebbles without adding radial barriers, which would significantly reduce the number of pebbles that would fit into the core.

Two separate fuel loading schemes were analyzed. The first has uniform fuel loading, with all pebbles identical, and the fuel volume fraction was adjusted until the core was just critical at the beginning of life (BOL) and end of life (EOL) or the maximum fuel volume fraction was reached. The second scheme adjusts the relative enrichment of each axial fuel zone to achieve a flat axial power distribution at BOL. The results are given in Table 1.

Table 1. Long-life PB-GCFR Design Optimization.

Power Density (W/cc)	H/D	Profile	Fuel Volume Fraction	TRU Average Enrichment	Peaking Factor BOL/EOL Max	Peak k_{eff}	Average Discharge Burnup
50	0.6	Uniform Fuel	Max (30.5%)	16.8%	2.07 / 1.92 / 2.10	1.036	8.4%
50	0.6	Flat Axial	Max (30.5%)	17.1%	1.81 / 1.87 / 1.95	1.026	8.4%
25	1.0	Uniform Fuel	29.8%	14.7%	2.23 / 2.08 / 2.47	1.011	8.6%
25	1.0	Flat Axial	29.2%	15.5%	1.76 / 2.01 / 2.17	1.007	8.7%
25	0.5	Uniform Fuel	Max (30.5%)	14.8%	2.22 / 2.09 / 2.46	1.010	8.4%
25	0.5	Flat Axial	30.0%	15.6%	1.87 / 2.04 / 2.24	1.008	8.5%

The 50 W/cc core has a relatively large reactivity swing because of the limit on fuel volume fraction. A larger inventory of fuel is needed to increase breeding and reduce the reactivity swing. The 25 W/cc core is twice as large as the 50 W/cc core. This reduces neutron leakage, which allows for substantially more breeding. The burnup reactivity swing of the 25 W/cc PB-GCFR can be reduced to less than 1% Δk .

Only marginal improvements were made in reducing the power density peaking factor. For the single-batch, long-life core, there is a significant redistribution of power over the core life. Even for a completely flat power distribution at the BOL, the power would shift to the center of the core and result in significant peaking by the EOL. An unrealistic RZ fuel zoning (5Rx10Z), which is not included in the table, was used for a 25 W/cc design. The power peaking factor was reduced to 1.37 at BOL, which by the EOL had shifted to a power distribution with a peaking factor of 1.86. The 1.37 peak at BOL was located on the centerline at 25% and 75% of the core height. By EOL, the power peak had increased to 1.86 and shifted to the center of the core.

Additional evaluation of the peaking factor has been done. In order to reduce the maximum peaking factor for the long-lived core, the ideal TRU enrichment zoning would peak the power distribution near the periphery of the core at the BOL. Over time, the power distribution would flatten and then peak in the center of the core. The minimum peaking is speculated to occur if the BOL peaking factor (near the periphery) and end of life (EOL) peaking factor (in the center) are equal. This leads to the largest power *redistribution*. This will also produce a more uniform fuel burnup, since each area of the core will operate at above or below average power densities over the life of the core.

This hypothesis was investigated for a 50 W/cc, 15 FPY design by allowing for an RZ TRU enrichment zoning using 10 axial region and 5 radial regions, which leads to 50 enrichment zones and 25 different enrichments because of symmetry. Figure 1 shows the peaking factor over the life of the core. If radial and axial fuel zoning are possible, the peaking factor can be kept below 1.5 for this design. The peak to average fuel burnup for this design was 1.3, whereas for the same design without TRU enrichment zones the peak to average fuel burnup was 2.1. Figure 2 shows the power density distribution at BOL, MOC, and EOL.

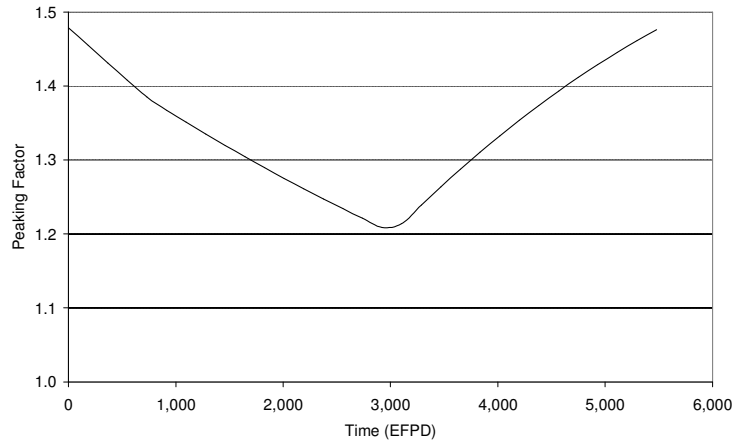


Figure 1. Time Dependent Peaking Factor for 3-D Fuel Zoning.

50 MWt Long-life PB-GCFR (Neutronics Study)

The potential for using a small (50 MWt) PB-GCFR for remote military heat and electrical needs was also evaluated during the second year. The smallest core size that could achieve a reasonable cycle length was determined. The performance at various cycle lengths and power densities was also evaluated. The core design for this evaluation was 39% He, 30.5% SiC matrix, and 30.5% carbide fuel. Core performance with enriched uranium and reactor-grade plutonium/depleted uranium was evaluated. Both fuel types gave similar core sizes and cycle lengths, with the plutonium-fueled reactor having a larger reactivity swing. The results are summarized in Table 2. If the fuel were not burnup limited (i.e., high burnup is not a problem), a very small core could be utilized. Depending on the desired operation time and reactivity control, it seems reasonable that a core volume of less than 1 m³ in size could operate for a decade or more using the PB-GCFR technology. Slightly larger cores would allow for reduced reactivity swing.

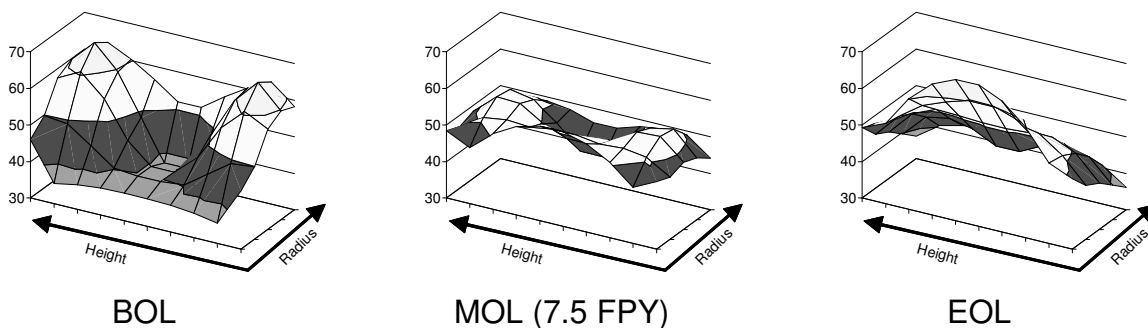


Figure 2. Evolution of Power Density Distribution.

Table 2. Long-life 50 MWt PB-GCFR Fueled with Enriched Uranium.

Cycle Length (FPY)	Enrichment	Power Density (W/cc)	BOL k_{eff}	Height & Diameter (m)	Volume (m ³)	Heavy Metal (MT)	Burnup (MWd/MT)
5	100%	717	1.254	0.45	0.07	0.28	330,634
10	100%	459	1.382	0.52	0.11	0.43	423,036
15	100%	343	1.460	0.57	0.15	0.58	470,943
30	100%	274	1.511	0.61	0.18	0.66	826,075
22	100%	250	1.539	0.63	0.20	0.79	512,823
15	75%	250	1.397	0.63	0.20	0.79	346,293
10	59%	250	1.282	0.63	0.20	0.79	230,862
5	45%	250	1.143	0.63	0.20	0.79	115,431
30	27%	50	1.216	1.08	1.00	3.96	138,517
15	22%	50	1.093	1.08	1.00	3.96	69,258
10	20%	50	1.054	1.08	1.00	3.96	46,172
5	18%	50	1.014	1.08	1.00	3.96	23,086

Task 2: Thermal-Hydraulic (T-H) and Safety Evaluations

The following are highlights of activities conducted in the safety and thermal-hydraulic area of the project.

2.1 *Point Design Concepts for a Gas-Cooled Fast Reactor (E. E. Feldman, T. Y. C. Wei)*

Twenty five years ago, when fast spectrum reactors employing gas-cooling were proposed and were being developed, it was evident that the safety case for this reactor type would be complicated by the poor heat transfer properties and low thermal inertia of the gas coolant. To survive a scrammed depressurization accident, without undue hazard to the public, when there is a concurrent loss of electrical power, would clearly be an attractive safety case feature of an advanced GCFR of the Gen IV class. Initial efforts focused on exploring a number of point design concepts that could potentially provide this safety feature through passive means. A fundamental assessment of heat transfer modes and the implications of the decay heat curve was first performed. Scoping type thermal calculations were then carried out. The conclusions are that:

- (a) Natural convection cannot be relied upon for the available selection of primary coolant gases, and that radiation through the coolant would dominate above 10^3 °C. Below this temperature, providing conduction pathways may be the better alternative.
- (b) However, for the period immediately following scram, substantial core thermal inertia is needed, as heat transfer on this timescale is not adequate for the core materials of the foreseeable future.

In addition, the results indicated that to improve the possibility of producing a truly passive core concept, it would be prudent to reduce the reactor power envelope to below 300 MWt. With these two fundamental tenets (a) and (b), three types of basic core elements were investigated which could possibly provide core configurations with the desired passive core safety feature:

- (i) block/plate
- (ii) pin/tube
- (iii) pebble/particle

The major focus of our work was devoted to the study of pebble/particle fuel element and, in particular, on the pebble-bed core configuration. However, some preliminary work was also performed on the two other basic fuel elements.

In the case of the plate/block element, the proposed core concept configuration was a small pancake core (0.3 meters height x 3 meters diameter) with radiation heat transfer from the top and bottom surfaces as the primary means of removing a decay heat of 1%. The radiation heat sink would be the top and bottom axial shielding. However, the peak core temperature for this concept is estimated to be ~ 2000 °C and no provisions have been made to address the issue of core thermal inertia. Additional work will be required on this core concept to determine what the showstoppers could be.

In the case of the pin/tube element, a small spaghetti core (long and thin) composed of ~ 3 or 4 tubes (0.3 meter diameter x 4 meters length) arranged in an array around the control rods was proposed (see Figure 1). The tubes would be filled with fuel pebbles and internally cooled with high-pressure helium (~ 7 MPa) while the tank (calandria) surrounding the tubes would contain low-

pressure carbon dioxide (1 MPa) to remove decay heat at natural convection conditions. This may decrease the need for substantial thermal inertia but follow-on calculations are required. Both of these designs are at a much earlier stage than the pebble-bed design. The issue of provision of thermal inertia to ride out the early decay heat period is a crucial one. The work reported here on the pebble-bed design addresses this issue for the pebble-bed concept. Future work is required on this design uncertainty for the two other designs.

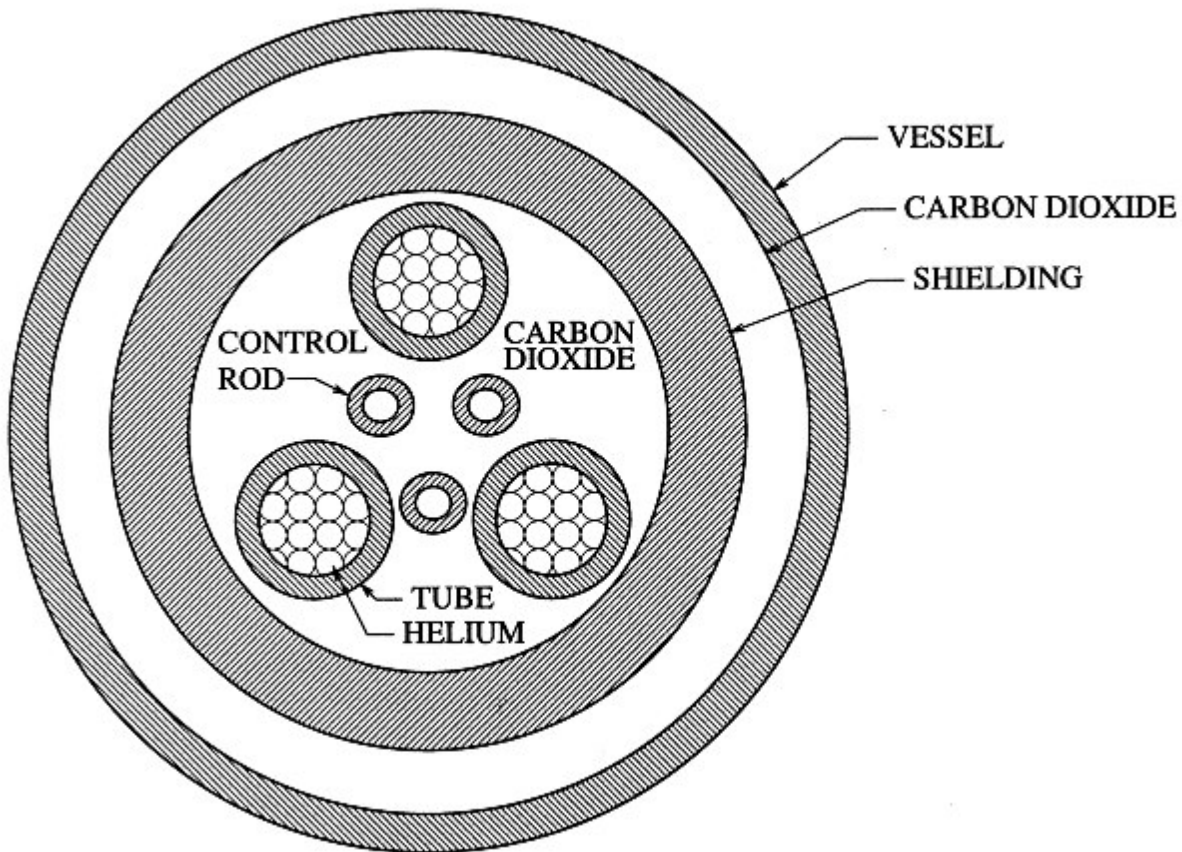


Figure 1. Tube Reactor Concept.

Most of the effort has been concentrated on the pebble-bed core design. Correlations for a pebble-bed equivalent thermal conductivity and pressure drop, and Nusselt number, were obtained from the published literature and were evaluated. A unique concept to increase the heat storage capacity of the fuel pebble was introduced. This concept uses fuel spheres in which the center is filled with a material that does not contain fuel and which can melt and absorb heat as latent heat of fusion. This concept also substantially lowered the temperature rise within each fueled pebble.

The scoping studies and the new pebble concept led to a conceptual design for a pebble-bed fast reactor. A one-dimensional CFD model of the conceptual design was used to study various thermal design options and parameters. This enabled more optimal values for the reactor dimensions to be found. A two-dimensional CFD model was developed to study the current annular core design choice believed to be among the closest to the thermally optimum. A severe

depressurization accident was simulated for this design choice. A plot from this study is displayed in Figure 2. The analysis predicted a maximum fuel temperature of 1627°C that is only 27°C above the current limit, which is arbitrarily based on the limit for graphite fuel. The reactor vessel temperature was observed to drop sharply at the initiation of the transient (which includes a scram) and then recover to a local maximum before the final decline, which lasted until the end of the accident. The local maximum, 489°C, is safely below the assumed allowed value of 537° C. However, the active core power density is limited to 23 W/cc.

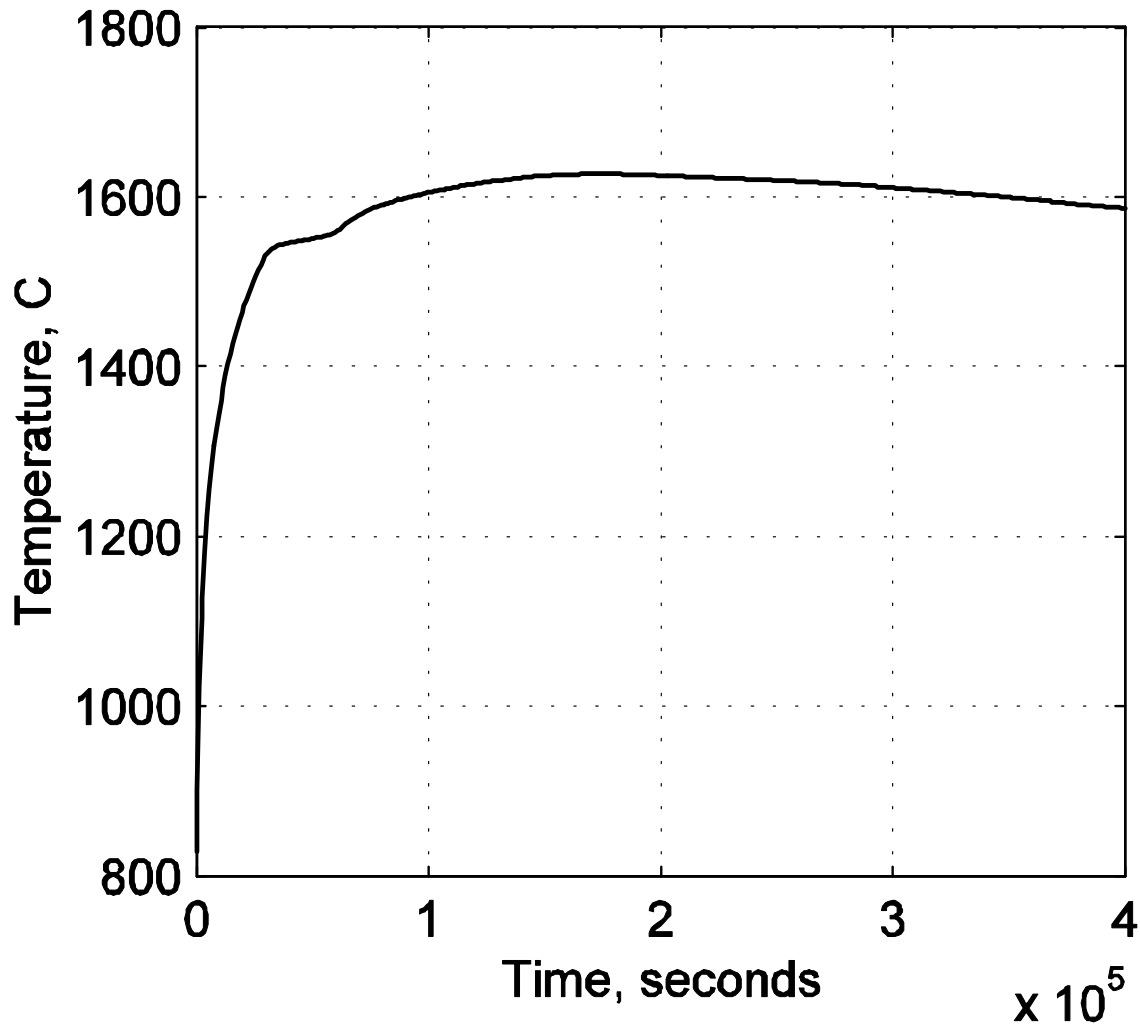


Figure 2. Fuel Temperature History at Location of Peak (2-D Calculation).

Future work could include an additional analysis with the two-dimensional CFD model to determine if the current inner core radius of 1.46 m actually does produce a lower peak temperature than would a somewhat smaller one. A study performed with a one-dimensional CFD model showed that the latent heat of fusion of the fuel pebbles reduces the peak temperature by 53°C. Other thermal studies will be deferred until the neutronics and materials studies can be incorporated into a more comprehensive design concept.

2.2 Thermal-Hydraulic and Safety Evaluation of the PB-GCFR Core Design (E. E. Feldman, T. Y. C. Wei)

ABSTRACT – This report documents the thermal hydraulic and safety analyses that have been completed for the pebble-bed design option in the past year and is a follow-on to the report of the prior year (Reference 1). During the past year, parametric studies corresponding to rated reactor operating conditions have been performed to determine the core diameter and height, and to investigate the design of the fuel pebbles. A parametric study was used to evaluate three candidate designs for a 50 W/cc core. Designs for a 25 W/cc cores were also considered. The model used to calculate natural convection in a closed-loop, introduced in Reference 1, has been improved and used to perform a parametric study for the tube reactor concept. The analytical results provide parametric curves of temperature versus system pressure for 0.5, 1.0, and 2.0% power and for no chimney and a 12.2 m (40 feet) one. Although it was anticipated that compressed carbon dioxide will be used for the natural convection-cooling mode, results are provided for both carbon dioxide and helium. These results show that, as expected, carbon dioxide provides much more natural convective cooling than helium under the same conditions.

The one-dimensional finite-element heat transfer model, which employs the FIDAP computational fluid dynamics, CFD, software package,² that was used in Reference 1 to simulate decay heat removal from a pebble bed reactor, has been used to analyze additional cases. The purpose of this study was to evaluate the performance of a gas-cooled reactor that did not have any special in-core decay heat removal devices, such as cold fingers, and also did not have any core coolant flow during the accident. The new cases considered new choices of pebble designs and materials from those of a year ago. The earlier tootsie pop pebble design was evaluated, but this time the latent heat of fusion due to the melting of the pebble core was set to zero. This enabled the effect of the latent heat to be quantified and shown to be relatively small. None of the new cases employed latent heat in the pebble. Several carbide, nitride, and oxide candidate fuel materials were considered along with graphite and tungsten for the pebble. The FIDAP results for silicon carbide and zirconium carbide approximate the results to be obtained for all the carbide and nitride material choices. In addition, a case was analyzed with both tungsten pebbles and a tungsten reflector. All of the new cases produced pebble temperatures higher than 1600° C, but often far below the melting or dissociation temperature of the pebble matrix material.

A new analytical model consisting of a set of simultaneous ordinary differential equations is presented and used to investigate the beneficial effects of flow and pressure coastdowns during a severe depressurization accident. A time constant of 1 minute was assumed for the compressor coastdown and a time constant of 10 minutes was assumed for the system depressurization. The analytical results show that it takes about 20 minutes for the relative flow rate to become less than the relative power, where the relative power and flow rate are both defined to be 1.0 at rated reactor conditions. After 20 minutes the flow rate continues to decrease rapidly toward zero while the decay power decreases slowly and the resultant high power-to-flow ratio causes the fuel temperatures to rise rapidly.

Two new concepts for decay heat removal are proposed and analyzed. In the first, the fuel pebbles are rapidly dumped into a series of lower storage tanks that are cooled externally by borated water. The transfer of the decay heat from the borated water to atmosphere is extensively analyzed. This heat transfer is accomplished by using the decay heat to boil the borated water and a natural-draft cooling tower to cool the steam and condense it back to liquid. The analysis indicates that this part of the decay heat removal scheme is feasible. Getting the fuel pebble to the storage tanks in a timely manner without overheating any of the structures

along the way and the heat transfer from the fuel pebbles to the borated water need further investigation.

The second new concept is the cold finger concept for decay heat removal. Both steady state and transient models were developed and used to evaluate the performance of these bayonet-type heat exchangers. The steady-state model is effective for scoping studies and provides the flow rates and heat transfer coefficients used in the transient model. For the steady-state model, a decay power level must be assumed, while the transient model uses the decay heat curve to represent local volumetric heat generation rate as a function of time. The transient model, which is a finite-element heat conduction model that employs the FIDAP software package,² considers heat storage effects in the fuel and in the cold finger. Thus, the transient model is essential in assessing the performance of the cold fingers and in determining the peak fuel temperature. Preliminary analytical results for the 4-cm and the 5-cm pebble core design choice for the 50 W/cc cores indicate that 15 cold fingers that occupy 15% of the total core volume are not enough to keep the transient peak fuel temperature below 1600° C. Hence, more cold fingers will be needed and/or a greater portion of the core volume must be occupied by cold fingers.

1.0 INTRODUCTION

The purpose of this report is to document the thermal hydraulic and safety analyses that have been completed for the pebble-bed design option in the past year. This report is a follow-on to the report of the prior year (Reference 1). During the past year, parametric studies corresponding to rated reactor operating conditions have been performed to determine the core diameter and height and to investigate the design of the fuel pebbles. These studies are described in Chapter 2.

The model used to calculate natural convection in a closed-loop, introduced in Reference 1, has been improved and used to perform a parametric study for the tube reactor concept. These results can be found in Chapter 3 and the equations for the model can be found in Appendix C.

Reference 1 used a one-dimensional finite-element heat transfer model, which employs the FIDAP computational fluid dynamics, CFD, software package,² to simulate decay heat removal from a pebble bed reactor and to study a series of parametric one-dimensional dynamic cases. Additional cases are provided in Chapter 4.0. In all of these FIDAP cases and in the two-dimensional one reported in Reference 1, the transient was initiated from the full-power rated steady-state condition and it was assumed that at time=0 the reactor flow rate instantaneously decreased in a step to zero and the system pressure decreased in a step to atmospheric pressure. The current report investigates these assumptions by considering the effects of flow and pressure coastdowns. The analytical models for the coastdown analysis can be found in Appendix A and the results can be found in Chapter 5.

Two new concepts for decay heat removal are proposed. Chapters 6 and 7 describe these concepts and provide analytical results based on the models provided in Appendices B, C, and D. Finally, Chapter 8 provides a discussion and conclusions.

2.0 REFERENCE DESIGN STEADY STATE PARAMETRICS

2.1 Core Parameters

A set of design parameters were established for steady-state operation and are as follows:

- core rated power of 300 MWt
- core inlet temperature of 480° C
- core outlet temperature of 850° C

- system pressure of 7.0 MPa
- helium coolant
- core pressure drop of no more than 0.31 MPa (45 psi)
- core length-to-diameter ratio in the vicinity of 1.0
- average core power density in the fuel region (including only the pebble-bed area) of 50 W/cc (This was later lowered to 25 W/cc.)

The basic geometric shape chosen for the core is a vertical right circular cylinder and the coolant flow is parallel to the axis of the cylinder. Special devices for decay heat removal, which are described Chapter 7, are part of the starting requirements. These special devices are cylindrical bayonet-style heat exchangers, called "cold fingers", which are oriented vertically and are distributed throughout the core. Because of neutronic design considerations, the combined cross sectional areas of all of the cold fingers is limited to 15% of the circular area of the core and the core aspect ratio is to be as close to 1.0 as is practical.

One of the first tasks was to establish design options for the pebbles. As described in Section 2.2, this required determining pebble sizes that resulted in acceptable fuel temperatures and core pressure drops. Then extensive analysis was performed, based on the assumption that the average core power density was to be 50 W/cc. It was decided that in the determination of core power density, the core volume includes only the regions occupied by pebbles, but not the volumes occupied by cold fingers. Neutronic analysis, performed by others, demonstrated that criticality could not be maintained over the desired core life for a 50 W/cc design that included the required number of cold fingers. The problem was that the fuel volume fraction was too small. Therefore, a 25 W/cc design that included cold fingers was proposed. Section 2.3 describes the 50 W/cc design, Section 2.4 describes the incorporation of cold fingers in this design, and Section 2.5 provides results for the 25 W/cc core.

2.2 Pebble Design Considerations

One of the first parameters to be determined is the pebble diameter. It is desirable to make this as large as possible for the following reasons:

- to minimize the core pressure drop
- to maximize the effective thermal conductivity of the pebble bed
- to minimize the total number of pebbles that must be manufactured

When smaller pebbles are used, more of them are needed to fill the same volume. Thus, the flow must travel across more pebbles and heat that is transferred across the core must pass through and around more pebbles. Hence, smaller pebbles result in a larger core pressure drop and a lower effective thermal conductivity. Unfortunately, as the pebble diameter increases, both the temperature rise from the coolant free stream to the pebble surface and the temperature rise from the pebble surface to the pebble center increase. These temperature rises are important because as they increase, the peak pebble temperature gets closer to its limit, which is currently assumed to be 1600° C.

For steady-state reactor operation at rated conditions, it is highly desirable to keep the maximum fuel temperature considerable below the 1600° C limit. This is necessary to provide a margin of safety so that the reactor can safely withstand an upset condition. Currently, a value of 1200° C is taken as a nominal value for the peak fuel temperature at operating conditions. There are several

incompletely known items that directly affect the peak fuel temperature, including the radial power peaking factor for the pebble bed, the axial power shape in the core, and the pebble design. All three of these items will become better defined as the design progresses. For now, only estimates of these quantities are available.

The peak temperature of each pebble is the sum of the local free stream coolant temperature and the temperature rise from the local free stream to the hottest location in the pebble. The latter quantity is directly proportional to the local power peaking factor, which is currently assumed to be about 2.0. The axial power shape is expected to resemble a chopped cosine. This implies that the peak pebble temperature will not occur at the core exit where the free-stream coolant temperature is the greatest. The coolant enters the core at 480° C and rise 370° C to reach the exit temperature of 850° C. For lack of better information at the time the analysis was performed, a reasonable estimate was made – namely that the hottest pebble is located where the coolant has risen 270° C from the exit and therefore is 750° C. This leaves 450° C to the arbitrarily set 1200° C limit. Since a peaking factor of 2.0 is assumed, the allowed nominal steady-state temperature rise from the local coolant free stream to the hottest point in the hottest pebble must be half this value, or 225° C.

Currently, the following three options are being considered for the pebble design: 1) a solid sphere in which fueled particles are evenly distributed throughout a graphite matrix, 2) a solid sphere in which the fuel metallurgically is a solid solution, and 3) a shell of metallurgically solid solution fuel with an unfueled core of the same or another material. The graphite option is assumed to yield a pebble thermal conductivity of 30 W/m-K. The solid solution material is assumed to be a metal that has a thermal conductivity of half of this value, or 15 W/m-K. The solid solution allows a greater fuel density and hence all of the fuel can be packed into half of the volume of the sphere. Thus, the third option has all of the fuel concentrated in an outer shell, which occupies half of the pebble volume and surrounds an unfueled core of the same volume. In the analysis of this pebble, the shell and core are assumed to be metallurgically bonded together and to have the same thermal properties. In these evaluations, the need for an exterior clad has not been fully addressed in any of the three options. The presence of the clad will certainly affect the thermal performance of the pebble, but if properly designed, should not have an overwhelming effect. The first option should be able to accommodate the fission gases by holding them within the fueled particles and an exterior thin layer of unfueled graphite potentially could be used in place of a clad. In the second option, the containment of the fission gases needs further consideration and in the third option, it may be possible to contain the fission gases in the unfueled core if it is porous.

2.3 50 W/cc Core

Published correlations for the pressure drop, effective thermal conductivity, and Nusselt number, which are needed to determine the film coefficient of the surface of the pebble, are provided in Reference 1. The reference also provides relationships for the temperature rise in heat generating spheres and shells. These correlations were evaluated with the aid of a computer spreadsheet and the results are provided in Table 1 for a series of design options. In the table the header "50/50" is used over three columns to indicate the pebble option where an outer heat-generating shell of half of the pebble volume surrounds a non-heat-generating core of the other half of the pebble volume. Pebble diameters of 2, 3, 4, 5, and 6 cm and two types of pebble – solid graphite (30 W/m-K) and 50/50 – are considered in the table and shading is used to identify the three design choices selected. The solid solution metal pebble design (15 W/m-K) is not in the table because its performance is always worse than the solid graphite pebble design (30 W/m-K). This is because the latter has twice the thermal conductivity of the former and hence half the pebble internal temperature rise.

The core length and the pebble diameter together determine the core pressure drop. Since core power density is assumed to be constant at 50 W/cc, increasing reactor power without changing core length or pebble diameter merely causes a proportionate increase in pebble-bed cross sectional area, with no increase in coolant flow velocity. Thus, if the power density is kept constant, for a given core length and pebble diameter, both the core pressure drop and the temperature rise through the pebble boundary layer and within the pebble are independent of reactor power. Increasing core power merely proportionately increases the number of pebbles without changing the thermal behavior of the individual pebbles. Changing the core length does not affect the total volume of pebbles. It just changes the core cross sectional area. Hence, changing the core length affects the film coefficient, since the velocity of the coolant is affected, but does not affect the temperature rise within the pebble.

Table 1. Parametric Study of Core Design Options (50 W/cc).

Core Length, m	Pebble Diameter, cm	Core Pressure Drop, MPa	Pebble Film Temperature Rise, C	Pebble Thermal Conductivity, W/m-K		Pebble Temperature Rise, C		Total Temperature Rise, C	
				Solid	50/50	Solid	50/50	Solid	50/50
2.0	6	0.252	139.5	30	15	407.8	179.6	547.3	319.1
1.5		0.108	171.2					579.0	350.8
1.0		0.033	227.5					635.3	407.1
2.0	5	0.303	110.4	30	15	283.2	124.7	393.6	235.1
1.5		0.132	135.2					418.4	259.9
1.0		0.041	179.2					462.4	303.9
2.0	4	0.388	82.7	30		181.3		264.0	
1.85		0.310	87.4					268.7	
1.5		0.169	101.1					282.4	
1.0		0.052	133.6					314.9	
2.0	3	0.533	56.9	15		203.9		260.8	
1.65		0.305	65.0					268.9	
1.5		0.232	69.4					273.3	
1.0		0.072	91.2					295.1	
2.0	2	0.834	33.4	15		90.6		124.0	
1.5		0.363	40.5					131.1	
1.0		0.112	53.0					143.6	

In examining the table to find candidate design options, one looks for instances where the core pressure rise is no greater than 0.31 MPa (45 psi) and the total temperature rise (i.e., film plus pebble) is no greater than about 225° C. These criteria clearly eliminate all of the 6-cm pebble choices and the “solid” 5-cm choices, which are the ones with the fuel evenly distributed throughout a solid graphite sphere. The length-to-diameter ratio is an important consideration that is not considered in Table 1. Since the fueled region, i.e., the pebble bed, is to occupy 85% of the core cross sectional area and the cold fingers are to occupy the other 15%, the core outer diameter can be determined and from that the core length-to-diameter ratio can be deduced. Alternatively, a simple formula can be derived for the core length-to-diameter ratio as follows:

$$\text{length-to-diameter ratio} = \frac{\text{length}^{1.5}}{\sqrt{\frac{4 \text{ power}}{0.85 \pi (\text{power density})}}}$$

Table 2, which provides the core length-to-diameter ratio for all of the core lengths considered in Table 1, shows that cores longer than 2.00 m would be needed to achieve a core length-to-diameter ratio of 1.0. Unfortunately, if the core pressure drop is not to exceed 45 psi, then a longer core would require a larger pebble diameter and this would result in excessive pebble temperatures. Thus, for each pebble type, the best choice is the greatest core length that does not exceed the 0.310-MPa limit.

Table 2. Core Length-to-Diameter Ratio (50 W/cc).

Length, m	Diameter, m	Length-to-Diameter Ratio
2.00	2.12	0.943
1.85	2.20	0.839
1.65	2.33	0.707
1.50	2.45	0.613
1.00	3.00	0.334

An equation analogous to the one given above can be used to determine the core diameter for each core length or it can be deduced from the core length and the core length-to-diameter ratio. The resultant core diameters are provided in Table 2. Making the core diameter smaller reduces both the required reactor vessel diameter and the required number of cold fingers. A longer core requires a longer vessel and longer cold fingers, but both of these are easier and less costly to achieve than a greater vessel diameter or more cold fingers.

Thus, close examination of Table 1 produced the following three design choices:

1. 2.0 m core length, 5 cm 50/50 metallic pebble
2. 1.85 m core length, 4 cm solid graphite matrix pebble
3. 1.65 m core length, 3 cm solid metallic pebble

These three are designated in Table 1 by a light shading. The 2.0-cm pebble diameter option was eliminated because it would require a very small length-to-diameter ratio, which implies a large reactor vessel diameter and many cold fingers, and it would require considerably more pebbles than any of the other choices. The total temperatures rises for the three selected pebble choices

are higher than the 225° C goal, with the highest being 268.9° C. Table 1 shows that for a given pebble design, lengthening the core has no effect on the pebble temperature rise, but does produce only a relatively small reduction in film temperature rise, and, of course, the same reduction in total pebble temperature rise. This however comes at the cost of a relatively large increase in core pressure drop. Since the fuel pebble has not been designed yet, its thermal properties and limits are just educated guesses. In addition, the maximum core peaking factor is not well known. Therefore, it was decided to accept the somewhat higher pebble temperature rises for now.

2.4 Incorporation of Cold Fingers in the 50 W/cc Core

The above three pebble design choices were selected essentially based on the operation of the reactor at its steady-state rated conditions. The only influence that upset conditions had on these designs is that the peak steady-state fuel temperature must be considerably below the assumed 1600° C temperature limit and that up to 15% of the core circular cross sectional area is to be reserved for cold fingers. The design of the cold finger system and the analytical process for determining the quantity and the dimensions of the cold fingers are provided in Chapter 7 and Appendices C and D. Table 3 summarizes key cold finger design results for the three design options listed above. As the table indicates, the first two design choices each require 12 cold fingers and the third requires 19. The maximum fuel temperature during a severe depressurization accident, as indicated at the bottom of the table, varies between 1551.5 and 1599.1° C among the three design choice. If the maximum fuel temperature for the third choice with 19 cold fingers had been several degrees higher, a 20th cold finger would have been needed and it would have caused the peak fuel temperature to be significantly below the 1600° C limit.

The table also lists the dimensions of the cold finger tubes for each design choice. The insulator and pressure tube inner diameters were selected in even increments of 0.5 cm. The insulator tube wall thickness was assumed to be 0.5 cm and the pressure tube wall thickness was assumed to increase linearly with the tube's inner diameter because the stress across the wall thickness of the pressure tube increases linearly with tube diameter. Thus, the pressure tube diameter selected may be slightly less than the one that results in exactly 15% of the core cross sectional area being occupied by cold fingers. Hence, it is likely that the mathematically exact core diameters of Table 2 will differ slightly from those actually used and indicated in Table 3. This difference would be obvious if the diameters were shown to more than two decimal places.

It should be noted that the cold finger analysis is based on the assumption that the cold fingers must remove 1% of rated power while operating in steady-state. As observed in Chapter 7, the decay power is above this level until about 2.5 hours after reactor shutdown. During this time period it is expected that the fuel temperature will rise as the core absorbs some of the excess decay power. Results for this transient behavior are provided in Section 7.4, which provides the fuel temperatures during this time interval. Also, the external heat exchanger that transfers the energy removed by the cold fingers to the atmosphere needs to be analyzed. This shortcoming is overcome by specifying a fixed value for the coolant temperature exiting the heat exchanger.

2.5 25 W/cc Core

After the three core design choices for a power density of 50 W/cc were provided, neutronic considerations required an increase in core volume and a corresponding decrease in power density. Therefore, the steady-state core design for rated conditions was evaluated for a 25 W/cc core. The lower power density allowed the core to be taller without exceeded the 0.31 MPa (45 psi) constraint on core pressure drop. Thus, the core choice with 5 cm metallic pebbles with the center

of each pebble unfueled, i.e., the 50/50 pebble design, could now be 3.1 m tall instead of 2.0 m and the choice with 4 cm graphite matrix pebbles could now be 2.9 m tall instead of 1.85. For these 25-W/cc cases, a preliminary judgment is that 18 cold fingers would be needed. Modeling with the dynamic cold finger model, describe in Chapter 7, is needed to determine the required number more accurately.

Table 3. Key Core and Cold Finger Parameters for the Three 50 W/cc Design Choices.

Quantity	Parameter		
design choice	1	2	3
pebble diameter, cm	5.0	4.0	3.0
pebble material/design	50/50 metallic	solid graph.	solid metallic
core length, m	2.00	1.85	1.65
actual core diameter, m	2.12	2.20	2.33
rated reactor power, MWt	300		
decay power level, %	1.00		
elevation difference (chimney height), m	10		
fuel region heat generation rate, W/cc	50		
control rod thimble O. D., cm	5.0		
carbon dioxide coolant inlet temperature, C	50		
pressure tube thermal conductivity, W/m-K	15.0		
number of cold fingers	12	12	19
insulator tube I. D., cm	18.5	20.0	16.0
insulator tube O. D., cm	19.5	21.0	17.0
pressure tube, I. D., cm	22.0	23.0	19.0
pressure tube O. D., cm	23.6	24.7	20.4
effective fuel region O. D., cm	61.2	63.6	53.4
fuel region thermal conductivity, W/m-K	10.9	11.9	7.8
cold finger carbon-dioxide flow rate, kg/s	3.58	3.10	2.38
carbon-dioxide coolant outlet temp., C	127.0	138.5	123.1
pressure tube I. D. temperature, C	336.5	340.7	309.8
pressure tube O. D. temperature, C	430.4	442.1	381.7
maximum fuel temperature, C	1560.1	1551.5	1599.1

3.0 TUBE REACTOR NATURAL CONVECTION MODE

The tube reactor concept is described in Reference 1. In the tube reactor, as shown in Figure 1, the pebbles are contained in a series of parallel tubes and are cooled by a high-pressure helium that flows between the pebbles. The tubes are surrounded by high-pressure carbon-dioxide that flows by natural convection. Figure 2 provides a schematic diagram of the carbon dioxide natural circulation loop. During normal operation most of the heat is removed by the flowing helium. However during severe helium depressurization accidents when the helium flow is essentially zero, the heat would be conducted and radiated from the fuel to the exterior of the tubes where, as shown in Figure 2, the flowing carbon dioxide would remove it via the external heat exchanger.

The analytical model for the natural circulation loop is presented in Appendix C. The temperature difference between the flowing carbon dioxide and fuel pebbles in the adjacent tubes should be small during shutdown decay heat conditions and is ignored in the current analysis. The core is assumed to extend the entire length of the fueled region, which is assumed to be 4 m and is shown in Figure 2, and to consist of four tubes that each produces 75 MWt at rated power. The tubes were assumed to be 0.3048 m (12 inches) in diameter and to be on a square pitch of 0.3302 m (13 inches). Thus, there is 2.54 cm (1.00 inches) between adjacent tubes. For this initial analysis, the hydraulic diameter and the flow area of the carbon dioxide regions outside the tubes were assumed to be those of the cusp formed at the center where the four tubes come together. This hydraulic diameter and flow area are 15.1 cm and 361 cm², respectively. The inlet and exit form losses, i.e., *k*-losses, for this region are assumed to be 0.5 and 1.0, respectively. At this time the heat exchanger used for heat rejection is not explicitly represented in the model and instead the carbon dioxide coolant at the heat exchanger exit, which is the same as at the tube reactor inlet, is taken to be 316° C (600° F).

The purpose of the analysis was to study the relationship between the carbon dioxide system pressure and the carbon dioxide temperature at the outlet temperature of the fueled region. Since the temperature rise from the coolant to the hottest fuel temperature should be very small, this coolant temperature is essentially a surrogate for peak fuel temperature. As show in Figure 2 the chimney is defined to be the vertical distance between the top of the fueled region and the bottom of the heat exchanger.

Figure 3 provides temperature predictions for both a 12.2 m (40.0 feet) chimney (solid curves) and no chimney (dashed curves). For each chimney option, temperature predictions for powers of 0.5, 1.0, and 2.0 % of rated power are provided. The analytical model represents steady-state conditions and was solved on a computer spreadsheet. In interpreting the results, one would choose the maximum allowed outlet temperature along the ordinate of the graph and read the minimum system pressure one would need from the abscissa. Since the fuel is assumed to be able to withstand temperatures up to 1600° C, one may be inclined to use this temperature. However, this would probably be non-conservative since the limits of much of the structural material are probably much lower. These structures may be made of various stainless steels whose melting point are considerably below 1600° C and have very little strength at temperatures approaching their melting points.

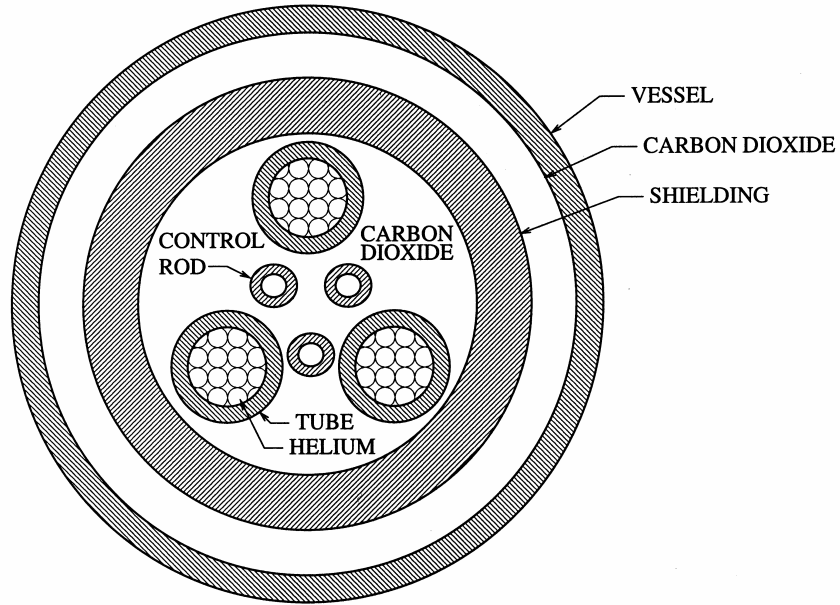


Figure 1. Tube Reactor Concept.

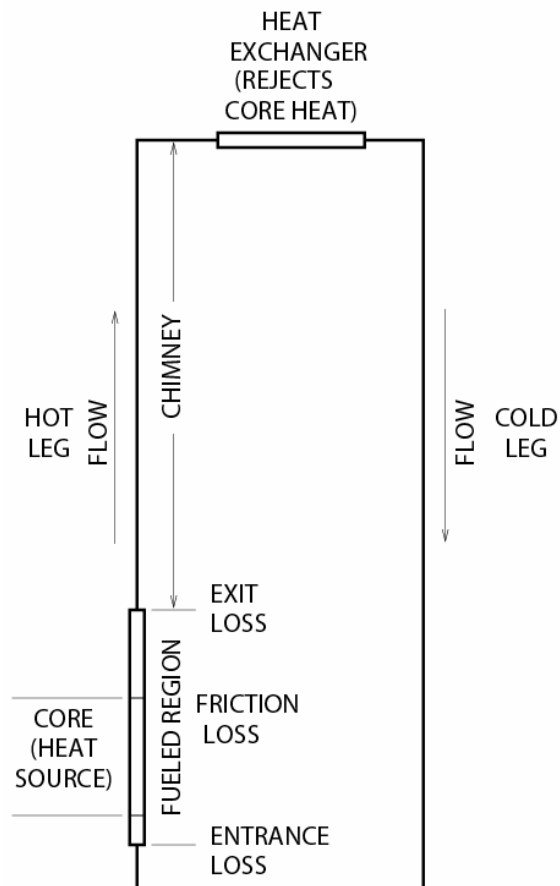


Figure 2. Carbon Dioxide Natural circulation Loop for the Tube Reactor Concept.

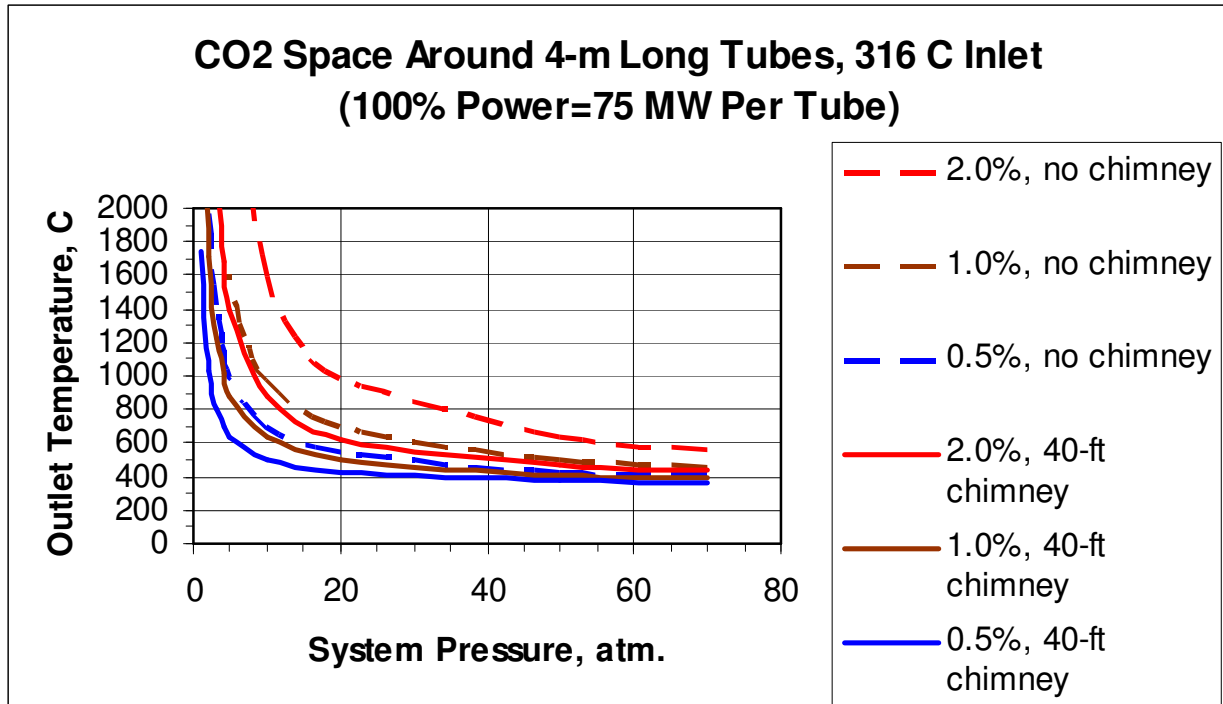


Figure 3. Tube Reactor Design Results for Carbon Dioxide Vessel Coolant.

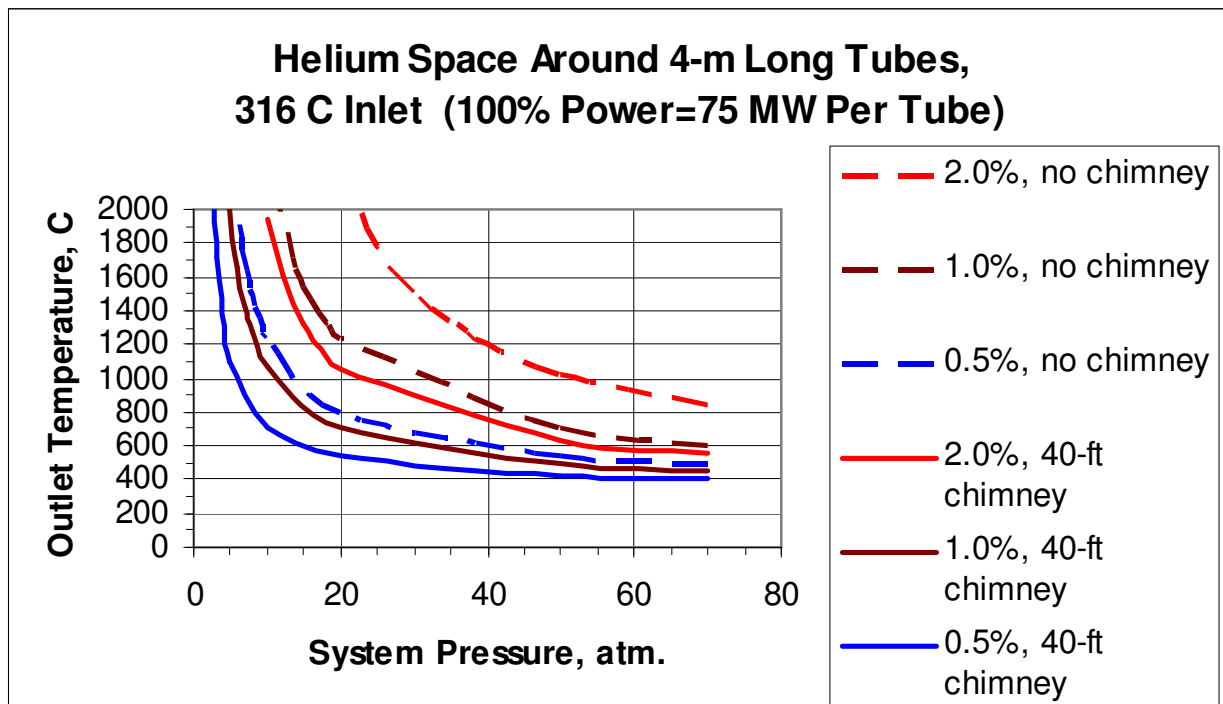


Figure 4. Tube Reactor Design Results for Helium Vessel Coolant.

An analogous set of results to those in Figure 3 are provided in Figure 4, but with the carbon dioxide coolant replaced by helium. The two sets of results when compared demonstrate that for the same set of conditions carbon dioxide produces much lower outlet temperatures than does helium. All of the results show that as the system pressure is lowered, a region is reached in each individual curve where the outlet temperature starts to increase dramatically. This is due, in part, to the increase in coolant gas viscosity with increasing temperature. As the system pressure decreases the density of the gas decreases and this decreases the flow rate of the gas. As the gas flow rate decreases the gas temperatures increase. The increasing gas temperatures increase the gas viscosity, which further decreases the flow rate and further increases the gas viscosity. Thus, a point can be reached where a small decrease in system pressure causes a large increase in gas outlet temperature. Decreasing gas density with decreasing pressure also has an adverse effect. For a given buoyancy pressure differential, the flow rate (kg/s) decreases as the density decreases.

The critical point for carbon dioxide is at 31.1° C and 7.38 MPa (87.8° F and 1070.6 psia). Thus, in some instances the carbon dioxide coolant will be close to the critical point. However, the steady-state loop natural convection model provided in Appendix C ignores this aspect of the carbon dioxide coolant state. The ideal gas relationship is assumed to apply for all conditions and the rapid changes in fluid properties that occur near the critical point have not been properly taken into account. Therefore, a better representation of the properties of carbon dioxide should be considered for future analysis. It is possible that such analysis may show better natural convective performance than is currently predicted. In addition, it may be desirable to avoid operation near the critical pressure and this could require that higher pressures be considered.

4.0 VESSEL CONDUCTION TRANSIENT DECAY HEAT REMOVAL

Chapter 5 of Reference 1 provides both a two-dimensional and a one-dimensional FIDAP finite-element heat transfer model of a 300 MWt gas-cooled reactor. The design dimensions and parameters used in these models represent an earlier version of the current reactor design. Because the two-dimensional model required a considerable amount of computational resources, the fast-running one-dimensional model was used for scoping studies where the effects of differences among design parameters were to be studied. Table 5-2 of Reference 1 provided the results of ten one-dimensional parametric cases. Three new one-dimensional cases were run to study the effects of various pebble designs and material choices and a fourth case was run to consider tungsten pebbles combined with a tungsten reflector. As in Reference 1, all of the cases assume a 6-cm diameter pebble, which is not one of the current design choices. The results, however, are valid on a comparative basis.

The standard for comparison is Case 19 of Reference 1. In this case the pebble has the properties of stainless steel and is of the "tootsie-pop" design. In this design it is assumed that all of the power is evenly distributed over the outer shell of the pebble and the volume of this shell is only 25% of the total spherical pebble volume. It is further assumed that the inner core of the pebble, which is the other 75% of the volume, will melt and all of the latent heat is absorbed between 1540 and 1550° C. Another assumption is that over the entire temperature range of this pebble and throughout its volume, the thermal conductivity, density, and heat capacity approximate those of stainless steel in the solid phase. The thermal conductivity of the pebble is assumed to be a constant 15 W/m-K. This conductivity was used to determine the effective thermal conductivity of the pebble bed, which was treated as a homogeneous region. The effective thermal conductivity of the pebble bed is a strong function of temperature because radiant heat transfer among the pebbles is a dominant effect.

As shown in Table 4, Case 26 is the same as Case 19 except that the latent heat in the core is set to zero in Case 26. The lack of latent heat causes the peak fuel temperature to rise by an additional 53° C and the peak reactor vessel to be 11° C higher. Thus, the benefits of a pebble whose central core can melt and absorb heat due to its latent heat of fusion may not justify the difficulties of designing it and dealing with the potential for molten metal inside the reactor core.

Table 4. Additional Vessel Conduction Decay Heat Removal Cases.

Case Name	Pebble Type	Core Maximum Temperature, C	Vessel Maximum Temperature, C
19	Steel (Tootsie Pop) with Latent Heat	1575	521
26	Steel (Tootsie Pop) without Latent Heat	1628	532
23	Silicon Carbide	1661	540
24	Zirconium Carbide	1774	564
22	Tungsten (with Tungsten Reflector)	1682	561

A number of materials that can withstand much higher temperatures than can stainless steel were considered for the fuel pebbles, as shown in Table 5. All of the property values in the table are based on Reference 3 except those for silicon carbide and graphite. The thermal conductivity of graphite depends on the type of graphite, which can be anisotropic, and it decreases with increasing temperature. Reference 4 shows the thermal conductivity for a reactor graphite to vary from 33.7 W/m-K at 427° C to 17.3 W/m-K at 1627° C. Densities and specific heat capacities for some graphites can be found in Reference 5. The values of thermal conductivity, density, and specific heat capacity for silicon carbide were taken from Reference 6 and are for the unirradiated material. Reference 7 indicates that irradiated silicon carbide can have a much lower value of thermal conductivity than does the unirradiated material. Reference 7 states: "In a neutral or reducing atmosphere, bare SiC can degrade through evaporation of silicon, leaving a porous carbon layer. The degradation becomes severe in a few hours at 2000° C (2273 K)."

The thermal conductivity for silicon carbide to be used in the current analysis should be much lower than the 35.7 W/m-K for unirradiated material shown in the table. When this is taken into account all three new materials can be expected to have a thermal conductivity within a factor of 2 of the 15 W/m-K used for the pebble conductivity of Case 19. The effective thermal conductivity for a pebble bed is a weak function of the thermal conductivity of the pebbles themselves since radiant heat transfer among pebbles is very important. Therefore, the effective thermal conductivity of the pebble bed in each case will be considerably less than a factor of 2 of that used in case 19. Hence, to a reasonable approximation the effective thermal conductivity of all of the carbides and nitrides in the table while in an irradiated condition will be close enough in value to each other and to the 15 W/m-K pebble conductivity assumed in Case 19 to warrant keeping the effective thermal conductivity of the pebble bed unchanged from that used in Case 19. Moreover, the emissivity at the surface of the pebbles may have a more significant effect than the pebble thermal conductivity. Thus, the uncertainty in effective thermal conductivity for the pebble bed may be bigger than the differences among the materials. Therefore, all cases in Table 4 used the same values of the Case 19 relationship for pebble bed effective thermal conductivity as a function of temperature.

Table 5. Thermal Properties of Candidate Pebble Materials.

Material	Thermal Conductivity at 1000° C, W/m-K	density, kg/m ³ (ρ)	specific heat capacity at 1500° C, J/kg-K (c _p)	Product of ρ × c _p , J/m ³ -K × 10 ⁻⁶	Melting Point or Dissociation Temperature, C
Silicon Carbide	35.7	3160	1336	4.22	~2000
Titanium Nitride	22	6400	595	3.81	3230
Zirconium Carbide	22	6510	250	1.63	3530
Uranium Oxide	3.6 / 3.2	10960 / 9660	339	3.72 / 3.27	2730 (2805)
Uranium Carbide	20 / 17.5	13630 / 12970	272	3.71 / 3.53	2400 (2525)
Uranium Nitride	24.6	14320 / 13510	272	3.90 / 3.67	2600 (2850)
Graphite	~30	1700	~2000	3.4	3650

Reference 6 provided specific heat capacity for silicon carbide as a function of temperature as follows:

temperature, C:	20	500	1000	1200	1400	1500
specific heat capacity, J/kg-K:	715	1086	1240	1282	1318	1336

A cubic interpolation routine in the Matlab software package⁸ was used to represent specific heat capacity as a function of temperature and then a Matlab quadrature relation was used to integrate it. From this one can obtain the average specific heat capacity over a specific temperature range. The average over 900 to 1500° C is 1280.1 J/kg-K. For 800 to 1500° C the average is 1269.0, and for 700 to 1500° C the average is 1257.3. This type of average is the best constant value to use because the product of temperature change and average specific heat capacity is the enthalpy change over the temperature change. Thus, 1269.0 J/kg-K is representative and was used in Case 23, shown in Table 4. The corresponding product of density and specific heat capacity is 4.01×10^6 J/m³-K. This differs somewhat from the value in Table 5 since specific heat capacity was evaluated at 1500° C there.

For transient thermal analysis, specific heat capacity and density always appear as a product and therefore only the product matters. In Table 5 one observes that all of the carbides and nitrides, except zirconium carbide have a product of specific heat capacity and density of about 4×10^6 J/m³-K. All of the materials that have the same relationship for pebble bed effective thermal conductivity as a function of temperature and about the same product of specific heat capacity and density will have about the same thermal performance. Therefore, the FIDAP results provided in Table 4 for silicon carbide, Case 23, are approximately applicable to all of the other carbides and nitrides in Table 5, except zirconium carbide, which is Case 24.

Case 22, in addition to having tungsten pebble in place of stainless steel ones, has a tungsten reflector. The effective thermal conductivity of the bed of tungsten pebbles was based on a constant thermal conductivity for tungsten of 100 W/m-K and an emissivity of 0.3. This is much lower than the 0.8 used in all of the other cases in Table 4 and better represents the behavior of tungsten. Also, the emissivity of the outer surface of the reflector, which faces the neutron shield, was reduced from the 0.6 values that was used for the stainless steel reflector (in Case 19) to 0.3 for the tungsten one.

Latent heat is included only in Case 19. The only difference among Cases 26, 23, and 24 is in the product of specific heat capacity and density. In Case 26 this product is about 25% larger than in Case 23 and it is more than twice as large in Case 23 than in Case 24. This explains the differences in core maximum temperature among these three cases.

5.0 EXTENDED FLOW COASTDOWN OPTION

In the previous thermal analyses provided in Chapter 4 and in Chapter 5 of Reference 1, it was assumed that the depressurization to one atmosphere and the stopping of the flow occurred instantaneously at the start of the depressurization accident. Thus, in these analyses, at the instant that the accident was initiated, the coolant flow rate became zero, the system pressure became 1 atmosphere, and the reactor power, which was full operating power, became the maximum initial decay power. In practice, the reactor scram does reduce the power level from full operating power down to decay levels in a fraction of a second and therefore is almost instantaneous. However, it can take many seconds for the system to depressurize fully and many seconds for the blowers to coast down and stop. Since the decay power decreases exponentially with time after scram, the previously ignored convective flow rate in the initial portion of the accident could potentially remove a substantial amount of decay energy and cause the predicted peak temperatures to be much lower than those predicted earlier. Thus, a dynamic model was developed, and is provided in Appendix A, to enable realistic pressure histories and flow coastdowns to be included in the analysis.

Figure 5 shows a model of the pebble bed core that was used to develop the dynamic model provided in Appendix A. The pebble bed core height was divided into ten axial slices of equal height. Each slice consists of a fuel node and a coolant node. Heat generated in each fuel node can be either stored or transferred to its adjacent coolant node. All of the heat leaving the fuel is assumed to be convection by the coolant. Heat is stored in both the fuel and the coolant, but no heat is assumed to be transferred through the external boundaries of the model except by convection by the flowing coolant. This representation can be viewed as that of the entire core or of an average channel in the core. The equations of this dynamic model were developed to represent the transient spatially varying coolant temperatures along the length of a representative coolant channel and the transient temperatures of its adjacent fuel pebbles. The resultant set of 20 simultaneous ordinary first-order total differential equations, representing the dynamic energy balance in the core, was numerically solved with the aid of the Matlab software package.⁷ The Matlab script developed to represent the analytical model was written so that the number of axial slices is an adjustable parameter. Hence, it would be a relatively simple matter to increase the number of axial slices to 20, for example, and to solve 40 simultaneous ordinary first-order total differential equations to obtain a solution for a finer nodal structure.

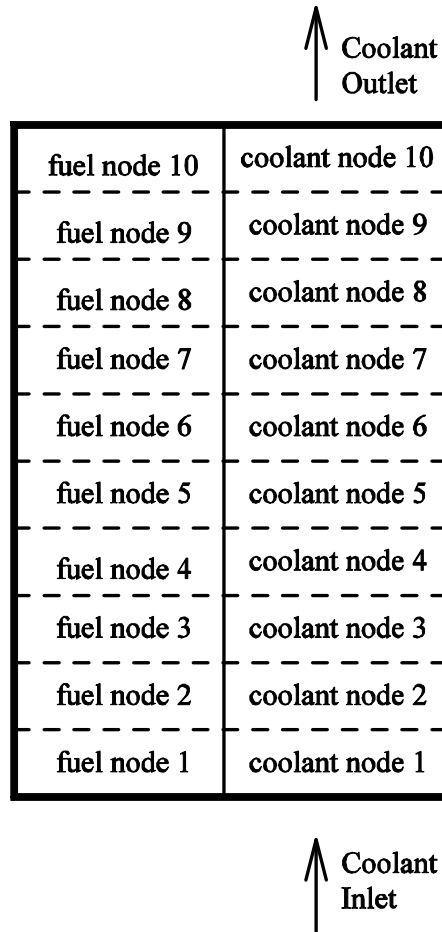


Figure 5. Core Model for Coastdown Analysis.

An analysis was performed in which the reactor was initially at the assumed rated conditions of 300 MWt and inlet and outlet temperatures of 537 and 900° C, respectively. The pebble diameter was assumed to be 6 cm in diameter and the thermal properties were assumed to be those of stainless steel in the solid form, i.e., no melting. These parameters correspond to an earlier design, but the results demonstrate the important phenomena. The normalized power, shown in the middle graph of Figure 6, follows the decay curve after a 0.3 s scram and the normalized pressure and blower speed are of the form $1/(1 + t/\tau)$, where t is time and τ is the time constant, which in this instance are taken to be 600 s for the pressure coastdown and 60 s for the blower coastdown. The pressure, shown in the top graph of Figure 6, is used to determine the coolant density. The blower speed, shown normalized in the middle graph of Figure 6, is used to determine the coolant velocity. The coolant density and velocity together determine the coolant flow rate, shown normalized in the middle graph of Figure 6. The results, the fuel exit node and exit coolant temperatures, are shown in the bottom graph of Figure 6. In this example the pressure and blower coastdowns are sufficiently protracted to enable the normalized flow rate to remain greater than the normalized power for about the first 1000 s. After that time the normalized flow rate drops considerably below the normalized power and this causes reactor temperatures to rise dramatically. Thus, the pressure and blower coastdowns delay and reduce the peak fuel temperature, but are of marginal value unless the normalized flow rate can be maintained above or reasonably close to normalized power for a very long period of time.

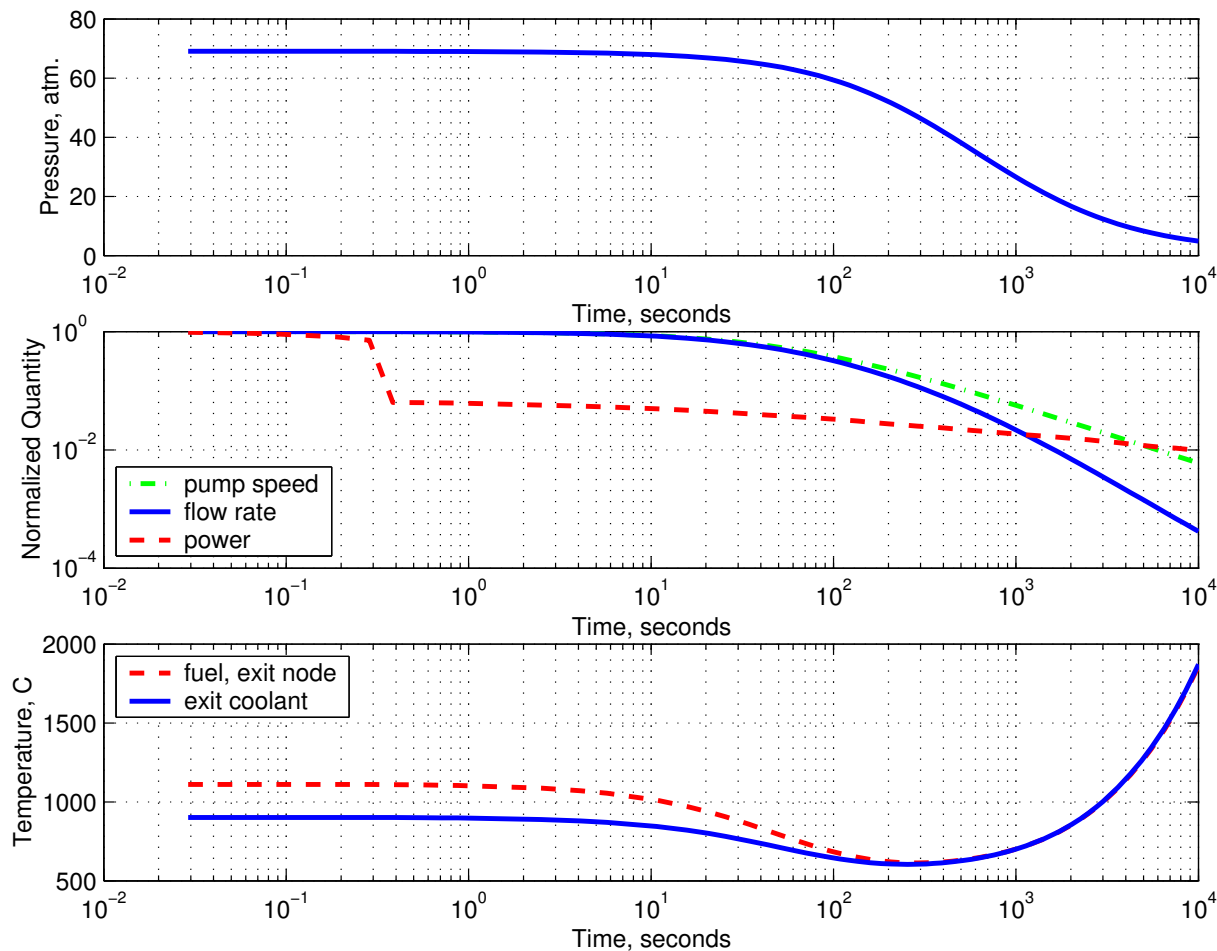


Figure 6. Dynamic Behavior Resulting from Assumed Flow and Pressure Coastdowns During a Depressurization Accident with Scram.

6.0 PEBBLE DUMP SYSTEM

This new concept is shown schematically in Figure 7. It is proposed that during a severe depressurization accident the fuel pebbles of a gas-cooled reactor be dropped into a series of tanks that are cooled externally. A borated water bath is proposed as a means of cooling the tanks. The water boils and the steam rises into an external condenser. A natural draft cooling tower draws air past the tubes of the condenser and condenses the steam back to water so that it can flow by gravity back to the water bath. A design concept with initial dimensions is provided in Reference 9, which has been reformatted to form Appendix B. This reference includes a steady-state analytical model that is solved on a computer spreadsheet. Mass, momentum, and energy equations and relationships for friction factors, heat transfer coefficients, and condenser fin efficiency are developed and solved for the water side. The assumed design dimensions result in a power removal capacity of several megawatts, which is adequate for the current application. The water-side model was successfully tested with published representative dimensions for a 375-foot tower that removes several hundred megawatts of power. If this new concept is further pursued then work will have to be focused on the heat transfer in the tanks from the beds to the walls of the tanks. This will provide sizing requirements.

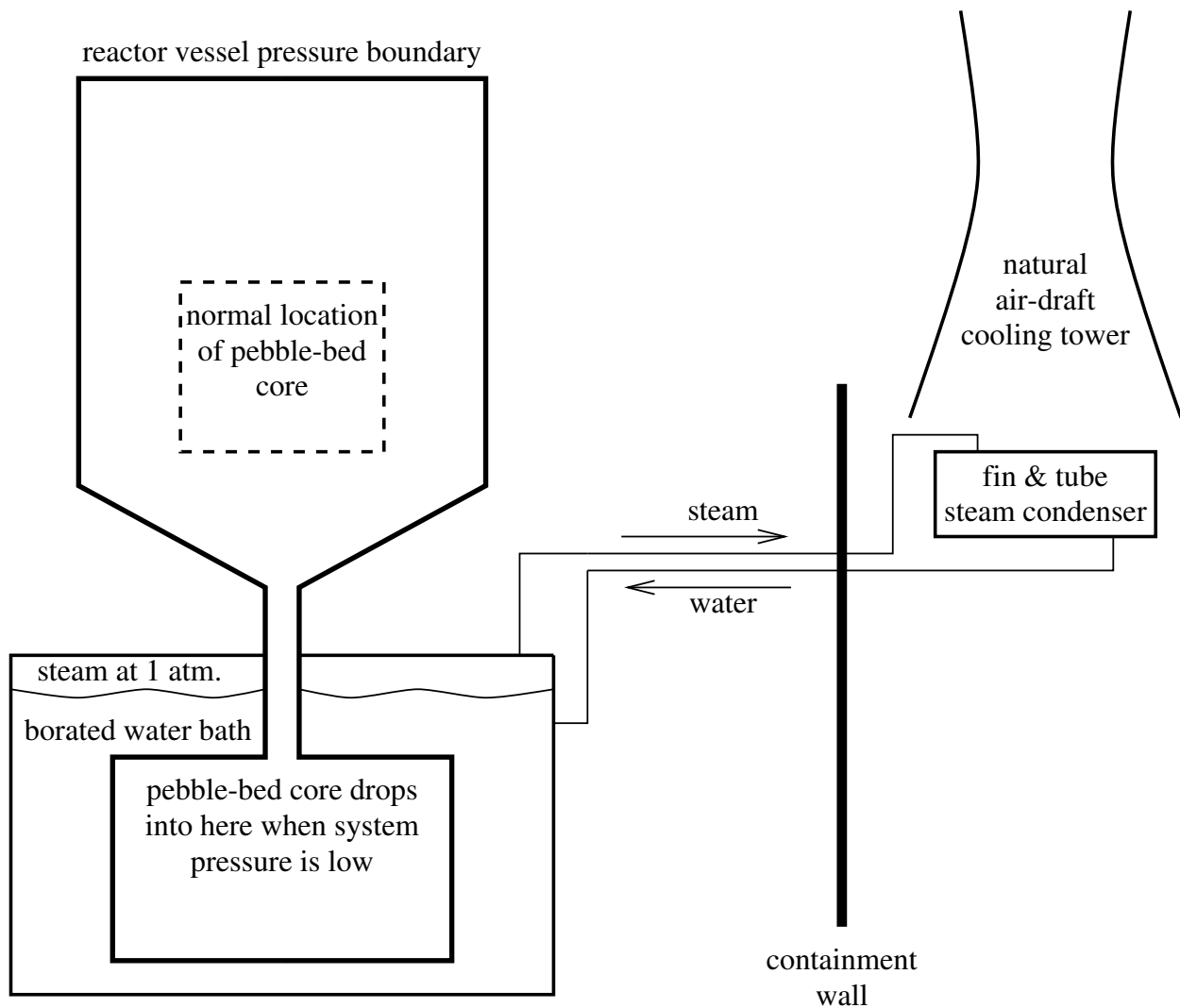


Figure 7. Design Concept for Pebble Dump and Decay Heat Removal .

7.0 IN-CORE DECAY HEAT REMOVAL COLD FINGER

7.1 Cold Finger Concept

As shown in Figure 8, the cold finger concept employs a series of bayonet heat exchangers, i.e., cold fingers, that are inserted vertically through the top of the reactor vessel. Each of these cold fingers, as shown in Figure 9, removes heat from the fuel in its immediate vicinity. In order to minimize the number of penetrations through the top of the reactor head, each cold finger would have a control rod along its centerline, as shown in Figure 9. Each cold finger, therefore, performs the dual functions of decay heat removal and reactivity control. High-pressure carbon dioxide at the same pressure as the reactor helium coolant, currently assumed to be 7 MPa, is used as the cold finger coolant.

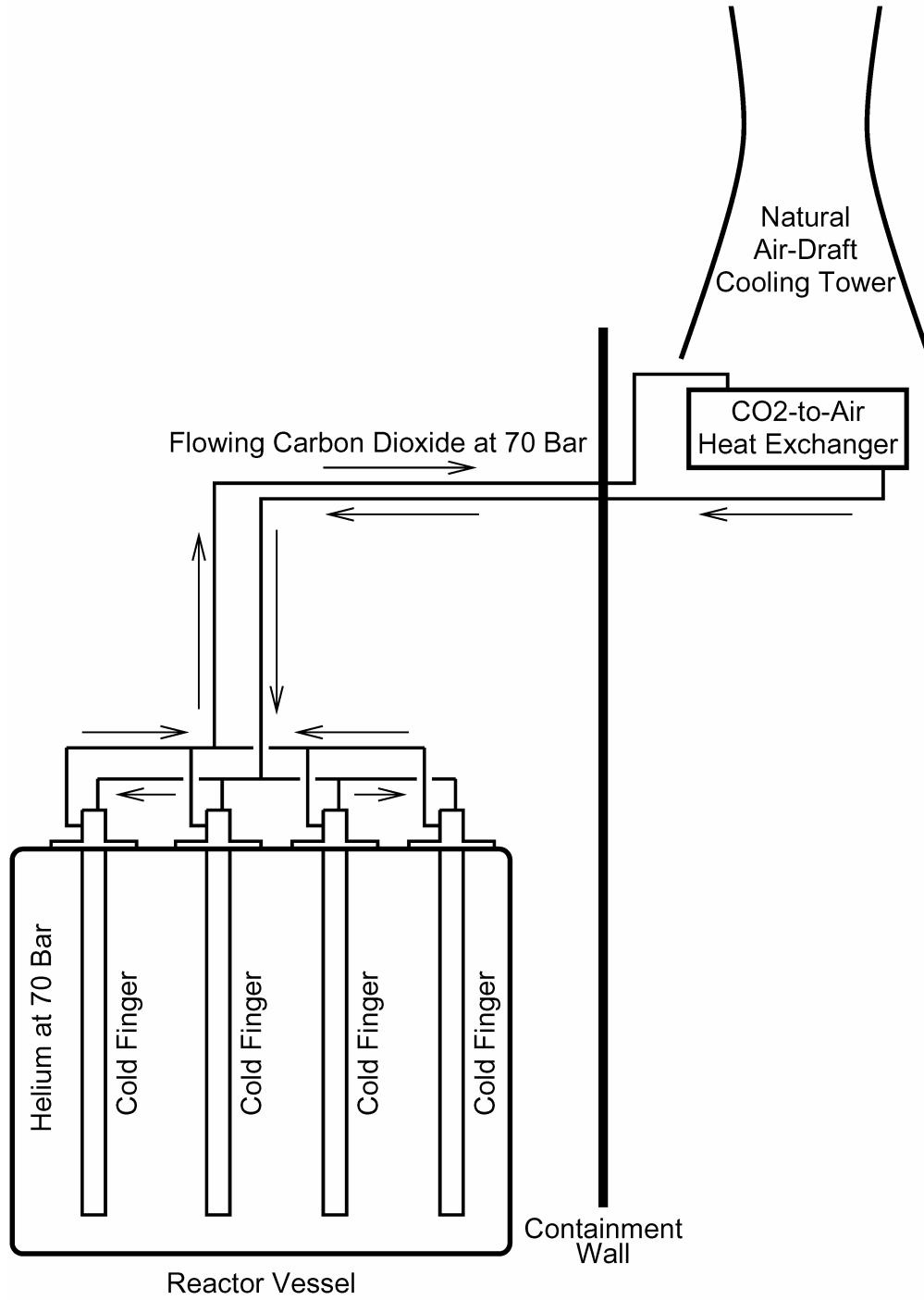


Figure 8. Cold Finger Concept for In-Core Decay Heat Removal.

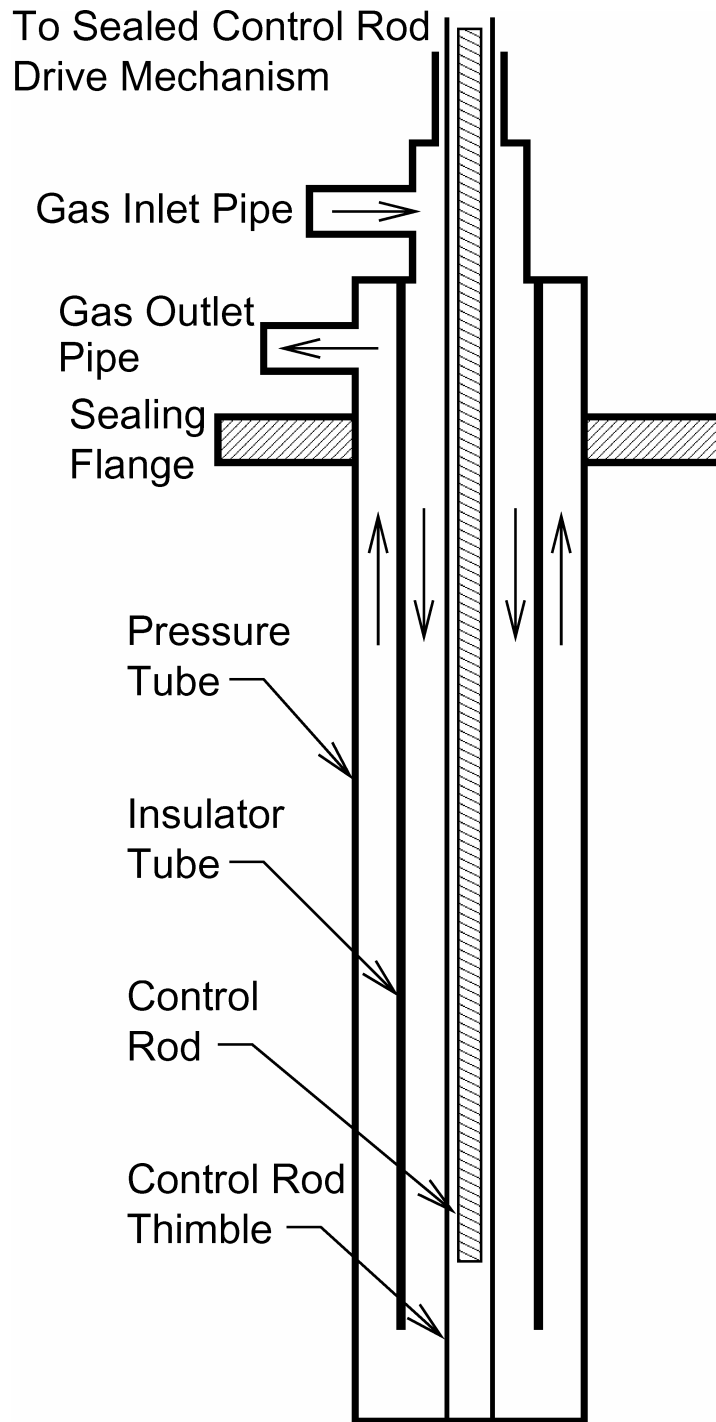


Figure 9. Cold Finger Design.

The coolant flow for the cold finger enters at the top of the finger and travels down an annulus around the outside of the control rod guide thimble. This flow also serves to cool the control rod. At the bottom of the cold finger the coolant flow makes a U-turn and travels upward along the outer annulus. An insulator tube separates the cold downward flow from the upward flow, which is heated by the adjacent pebble bed. The hot flow from the cold finger is convected to an external heat exchanger where the heated carbon dioxide is cooled by a stream of atmospheric air drawn through a natural-draft cooling tower. Several or all of the cold fingers would be attached to a single external heat exchanger or series of heat exchangers.

The bayonet design with the carbon dioxide flow making a U-turn at the bottom of the cold finger was chosen so that each cold finger would require only one penetration through the reactor vessel boundary, instead of one at the top and one at the bottom. The sealing flange, identified in Figure 9, is used to provide a leak-tight seal between the cold finger and the reactor head. The outer wall of the outer annulus is referred to as a "pressure tube" because it is a tube that separates the high-pressure carbon dioxide of the cold finger from the high-pressure helium of the reactor core. Whenever either gas is fully depressurized and the other is at full pressure, the pressure tube must withstand the full pressure of the pressurized gas.

There are no pumps in the carbon dioxide coolant circuit and all of the flow is by natural convection. Thus, the elevation difference between the cold finger and the external carbon-dioxide-to-air heat exchanger is important. Another observation is that a failure of a pressure tube would not cause a breach of the helium pressure boundary unless there was a concurrent breach of the external portion of the carbon-dioxide circuit. A pressure tube failure, however, would enable the two gases to mix.

The control rods and their drive mechanisms would be totally encased inside the carbon-dioxide pressure boundary. As is done in pressurized water reactors, all of the control rod latching and motion is accomplished by electromagnetic induction through the pressure boundary wall. This avoids the need for moving seals and the leakage associated with them. The flowing carbon dioxide will also serve to cool the control rods. The control rod guide thimble walls may need to be perforated near the top to allow coolant to be displaced easily, but may need to be nonperforated near the bottom so that compressed gas near the bottom can be used to slow the inserting rod. A tight clearance between the rod and thimble could be used for damping.

7.2 Cold Finger Models

For modeling purposes, the core fuel volume is assumed to be equally divided among all of the cold fingers so that if there are 20 fingers, for example, then 1/20th of the fuel volume would immediately surround each finger. A thermal conduction model representing the fuel volume associated with a typical cold finger and the pressure tube of the cold finger was developed. In this model the fuel volume was approximated as a concentric annulus with the pebble bed approximated as a homogeneous material. The pressure tube was represented as a concentric annular region that was inside and in perfect contact with the fuel annulus. The model was assumed to be axially symmetric and all variations were limited to the axial and radial directions. The top and bottom surfaces of the model and the exterior vertical surface of the fuel annulus were assumed to be zero heat-flux boundaries. Hence, the highest steady-state temperatures must occur along the exterior vertical surface. In the model, the inner annular surface of the pressure tube is the only place where heat is rejected from the system and hence must have the lowest steady-state temperatures. The carbon dioxide free stream coolant temperature and the film coefficient must be specified along this surface. These quantities are obtained from a solution of the cold finger loop hydraulics model, as explained below.

The height of the annular model is the height of the core. There are both a steady-state model of the annulus and a transient one. The former is solved on a computer spreadsheet and the latter is represented and solved via the FIDAP CFD software package.² Both up-flow and down-flow core designs are currently under consideration. Since the cold finger flow is driven entirely by natural convection, the hot leg in the cold finger, which is immediately adjacent to the pressure tube, is always in the upward direction. An up-flow core causes the exit core coolant to be adjacent to the exit cold finger flow. This is more limiting than a down-flow core, which places the hot core exit coolant adjacent to the cold finger inlet coolant. Since the coolant temperature rise in the cold fingers, as the results will show, is only about 100° C, the difference between an up-flow and a down-flow core is relatively small. However, the more limiting choice, an up-flow core, is assumed in all of the cold finger analyses.

In the steady-state model the power is assumed not to vary over the core volume, but in the transient model the core power distribution is allowed to vary axially. In the steady-state model a constant assumed representative power, typically 1 or 2%, was used, but in the transient analysis the decay heat varied with time and was assumed to be the ANS standard decay heat after shutdown of a uranium fueled LWR operating for infinite time.¹⁰ In both models the pebble bed was represented as a homogeneous region and an effective conductivity that was a function of temperature was used. For the steady-state model, heat conduction in the annular model was assumed to be one-dimensional – radial only – and the thermal conductivity was evaluated at the average of the temperatures on the inner and outer annular surfaces of the fuel. This approach is amenable to a hand calculation that is evaluated on a spreadsheet. The transient model was divided into many axial layers and both fuel and pressure tube annular regions were divided into many radial subregions, heat transfer was assumed to be both radial and axial, and fuel thermal conductivity was based on the temperature of each individual fuel node.

Of course, dividing the entire reactor core region into equal volumes that are thermally independent from one another is only an approximation. Additionally, representing these regions as symmetric annuli is a further approximation. At this stage of the design and analysis, however, this is a very reasonable approach to take since it provides very useful information without excessive amounts of modeling and the mathematical models to which it leads are relatively easy to understand and verify. In much more advanced stages of the design it may be necessary to represent the core geometry more realistically.

The hydraulic model for the cold finger is represented in Figure 10. This figure looks very similar to Figure 2, which correspond to the hydraulic model for natural convection in the tube reactor. The cold finger up-flow annulus, on the left side of Figure 10 corresponds to the fueled region on the left side of Figure 2. The modeling here is identical. The heated length of the reactor tube, labeled “core (heat source)” in Figure 2, is interchangeable with the heated length of the cold finger. The only real difference between the two analytical models is the unheated annulus on the right side of Figure 10, which does not appear in Figure 2. In the cold finger, the cold flow returning to the cold finger must travel down an annulus formed between the control rod thimble and the insulator tube, which are shown in Figure 9. This flow area can be as restrictive to flow as is the up-flow annulus. Therefore, in the cold finger model this down-flow hydraulic resistance was added and, analogous to the up-flow annulus (and also the heated region of the tube reactor), includes an entrance pressure loss, a friction pressure loss, and an exit pressure loss.

In the analysis of the natural convective loop, the up-flow and the down-flow annulus were each assumed to extend only over the length of the core. This assumption in retrospect is extremely optimistic since these two annuli must also extend from the reactor vessel cover, where the cold

fingers are attached, to and through the core. The added distance from the top of the core to the cover should significantly increase the hydraulic resistance of the loop and thereby decrease the performance of the cold finger. The analytical model of the hydraulic loop was designed to include unheated regions above and below the core and can be used, without modification, to consider this more realistic case.

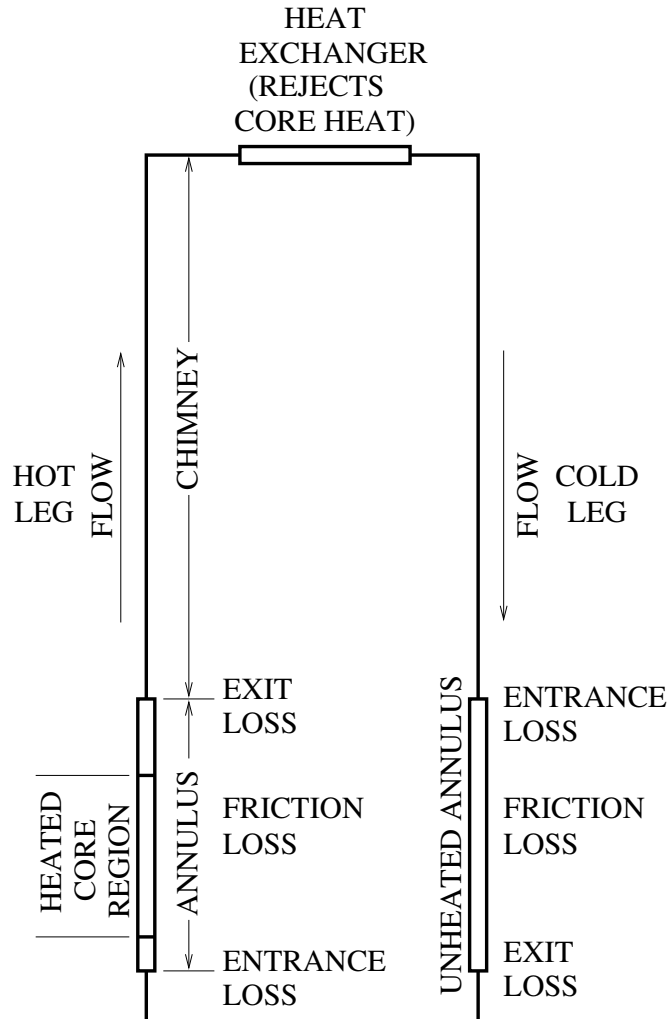


Figure 10. Carbon Dioxide Natural Circulation Loop for the Cold Finger Concept.

The external heat exchanger is currently not explicitly represented. Instead, in the model it is assumed that the coolant temperature exiting this heat exchanger and entering the cold finger is at 50° C and is a constant. In the future, a model for this heat exchanger may need to be developed. This would also need to include the modeling of the natural draft cooling tower and the air flow it draws through the heat exchanger. Something similar to this is included in the Appendix B model for the pebble dump concept of Chapter 6.

The steady-state heat transfer model of the annular fuel region was couple together with the steady-state loop hydraulics model and both were solved simultaneously on a computer

spreadsheet. Because of the significant heat capacity of the fueled pebble bed annulus and the pressure tube and the generally slow decrease of decay power with time, the dynamic thermal behavior of the loop is rather sluggish and therefore the loop hydraulics can be treated as if it were quasi-steady state. Thus, the dynamic behavior of the loop hydraulics, to a reasonable approximation, can be obtained via a series of steady-state solutions obtained from the combined steady-state model run for various power levels.

The boundary condition at the inner surface of the pressure tube needed for the transient model was approximated from the combined steady-state model. This model showed that the free stream coolant temperatures rise inside the pressure tube annulus and the film coefficient on this inner annular surface exhibit only modest variation over the decay power ranges of interest. Therefore, a steady-state solution at a single power level was used to represent the boundary condition at the inner surface for an entire transient solution. For the transient solution, the steady-state flow rate and power and the axial power distribution were used to calculate the axial distribution of coolant temperature along the pressure tube inner surface. The film coefficient from the combined steady-state solution was used in the transient analysis and was assumed to be constant over the surface. Hence, the boundary condition for the transient solution was assumed to be independent of time.

A transient solution with an inner surface boundary condition corresponding to a representative single steady-state power level was obtained and then repeated for a steady-state power level somewhat higher than the highest decay power possible. The differences in transient peak fuel temperature, as will be shown in Section 7.4, were found to be relatively small for the range of powers of interest. This is because, when a higher steady-state power is assumed the natural convective flow also increases and mitigates the increase in coolant exit temperature. This increase in coolant temperature is partially offset by the increase in film coefficient that accompanies the increase in flow rate. The peak fuel temperature typically occurs at about 45 minute to an hour into the transient. For the assumed decay heat curve, between 10 minutes and 66.7 minutes the decay power level decreases slowly from 2.11% to 1.28%. The equations for the cold finger loop hydraulics are provided in Appendix C and the equations for the steady-state cold finger thermal model are provided in Appendix D.

Since the cold finger coolant is to be carbon dioxide near the critical pressure, the same concerns with regard to properties around the critical point that were expressed in the last paragraph of Chapter 3 are also equally applicable to the cold finger modeling. The concern is not only for the flow rate, which is based on the Appendix C model, but also for the film coefficient used in the Appendix D model.

7.3 Results of Steady-State Analysis

Results for the steady-state analysis of the cold fingers were provided in Table 3 along with key parameters for the three design choices introduced in Section 2.4. For each of these three design choices, the steady-state cold finger model was used to determine the minimum number of cold fingers needed so that during a depressurization accident the maximum fuel temperature would not exceed 1600° C. It was assumed that the core rated power was 300 MWt and that on a steady-state basis, the cold fingers had to remove 1% of this amount during the accident. This assumed steady-state power level is critical. If this value is double, than the amount of power to be removed doubles and the number of cold fingers must increase significantly. A 1% heat removal capability may be adequate if sufficient benefit is realized from heat storage effects in the core. The transient analysis should provide a more definitive answer, but the steady-state model is much better for scoping studies and it includes the flow-loop hydraulics.

The core power density in the fueled regions (not including the cold fingers) was 50 W/cc at rated power conditions. It is possible to use the spreadsheet model to solve for the minimum number of cold fingers to produce a peak fuel temperature of 1600° C. The model does this by determining the thickness of the fueled annulus that results in a peak fuel temperature of 1600° C. The maximum number of cold fingers obtained in this manner is typically not an integer. Maximum non-integer values for the number of cold finger were determined for several values of insulator tube inner diameter, which were selected in 0.5-cm increments. Adjusting this diameter caused the up-flow and down-flow carbon-dioxide pressure drops to change. These solutions enabled an insulator tube diameter to be obtained that resulted in the minimum non-integer value for the number of fingers for the required fuel temperature limit. This number of cold fingers was rounded up to the nearest integer and then the model was used to solve for the maximum fuel temperature.

The total cross sectional area of all of the cold fingers was constrained to be no more than 15% of the total core cross sectional area of the core including the fueled region and the cold fingers within it. This helped to determine a maximum cold finger pressure tube outer diameter. Since the cold finger pressure tube has to withstand a 7 MPa pressure differential, the tube wall thickness was increased linearly as the pressure tube diameter was increased. The insulator tube was assumed to have a wall thickness of 0.5 cm and the control rod thimble outer diameter was taken to be 5 cm.

The fuel region is a pebble bed whose effective thermal conductivity is largely due to radiant heat transfer and is therefore highly temperature dependent. The effective thermal conductivity was evaluated at the average of the two boundary temperatures of the assumed annular fuel region. The effective thermal conductivity was represented in the model as a cubic function of temperature. This functional relationship was approximated by a curve-fit that was based on an evaluation of published correlations. A different cubic function was determined for each of the three design choices shown in Table 3. The pebble surface emissivity was assumed to 0.8 in all three cases. The representation of the pebble bed effective thermal conductivity is important because most of the temperature rise is across the fuel. This is to be contrasted with the temperature differential across the pressure tube, which is much smaller and for which a constant thermal conductivity of 15 W/m-K was assumed.

7.4 Results of Transient FIDAP Analysis

A steady-state model was used above to estimate the number of cold fingers that are needed for each of three candidate core designs. This model calculated the natural convective flow and the coolant exit temperature in the cold finger and assumed that all heat transfer between the cold finger coolant exit and the fuel was radial and one-dimensional. This conceptually simple model, which was solved on a computer spreadsheet, could not explicitly consider the nonuniform axial power shape, the decay power curve, or the heat storage capability of the fuel.

The FIDAP CFD software² was used to develop a model to investigate the dynamic behavior of the cold finger so that a more accurate estimate of the number of cold fingers could be made. In this model the decay power is represented as a function of time and the heat capacitances of the fuel and the cold finger pressure tube wall are explicitly represented. In the analysis it is important to use the appropriate initial axial fuel temperature distribution, which is considerably greater than the axial helium coolant temperature distribution. Because heat storage effects are important in this analysis, the fuel temperature distribution was based on the average temperature of each pebble rather than on the peak. In a separate steady-state hand calculation it was determined that for a core power density of 50 W/cc, the steady-state temperature increase from the flowing helium coolant to the pebble average temperature is 160° C for the 4-cm pebble that is identified

in Table 3 and 210° C for the 5-cm one. In determining the initial axial average fuel temperature distribution, the steady-state axial power shape was also included. This power shape was symmetric about the core mid-height.

As expected, the results of the dynamic modeling show that the fuel temperatures rise until the time is reached where the decay power has decreased to the power removal capability of the cold fingers. After that time, all of the decay power is removed as it is produced and the fuel temperatures enter a long gradual decline caused by the decreasing decay power.

Table 6. Summary of Transient Cold Finger Model Results

Case	1	2	3	4	5
Pebble Diameter, cm	4	4	4	4	5
Pebble Material	Graphite	Graphite	Graphite	Graphite	Metallic
Core Height, m	1.85	1.85	1.85	1.85	2.00
Axial Power Shape	Uniform	Non-uniform	Non-uniform	Non-uniform	Non-uniform
Cold Fingers Per Core	12	12	12	15	15
Steady-State Power for Boundary Condition, %	1.0	1.0	7.0	1.25	1.25
Peak Fuel Temp., C	1680	1863	1867	1743	1807
Time of Peak Temp., min	65.6	55.7	55.6	45.5	50.7

Five cases were analyzed, as summarized in Table 6. The first four correspond to the 4-cm graphite pebble core that is 1.85 m tall and the fifth corresponds to the 5 cm metallic pebble core that is 2.0 m tall. In all cases it was assumed that the core helium flow at rated reactor conditions was upward, since upward flow is at least as limiting as is downward flow and upward flow is what was assumed in the steady-state analysis. For both cores the steady-state model predicted that 12 cold fingers would be needed if the peak fuel temperature is to remain below 1600° C. For the first case a dynamic solution was obtained for a uniform axial power distribution so that this transient case would closely correspond to the steady-state solution for the 4-cm pebble core. The transient results, produced a peak fuel temperature of 1680° C, as is shown in the table, that is 129° C higher than that for the steady state. In the second case a realistic axial distribution of core power was included with a power shape that was symmetric about the core mid-height and the peak power 32% greater than the average. This caused the peak temperature to occur at the core mid-height and to be 183° C greater than in the previous case. In the first two cases the boundary condition, i.e., carbon dioxide coolant temperatures and film coefficient, at the inner surface of the pressure tube was based on results obtained in the steady-state analysis. Therefore, for the third case, the second case was altered so that this boundary condition was changed to correspond to a steady-state solution of 7% decay power instead of 1%. The third case produced a transient peak fuel temperature that was only 4° C greater than that of the second.

For the fourth case, first the steady-state model was solved for 15 cold fingers and 1.25% power. The higher power and number of cold fingers are deemed to be closer to the desired design. It should be noted that, although the number of cold fingers was increased, the total amount of core volume occupied by the cold fingers remained unchanged. Thus, the number of cold fingers was

increased, but the diameter of each was reduced. Then the fourth transient case was produced by modifying the third case to correspond to this new situation. For this case the boundary condition was changed to correspond to a steady-state solution for 1.25% power. The fourth case showed that for 15 cold fingers a peak fuel temperature of 1743° C occurred at 45.5 minutes into the transient. The fifth case was the same as the fourth except that it corresponds to the 5 cm metallic pebble core that is 2.0 m tall. It was analyzed in the same manner as the fourth case. First, the steady-state model was solved for 15 cold fingers and 1.25% power. Then the transient model was used to determine the peak fuel temperature, which occurred at 50.7 minutes and was 1807° C.

Clearly, all of the peak fuel temperatures are considerably above the 1600° C limit. It may be necessary to increase the fraction of core cross sectional area allotted for cold fingers. Before these issues are considered there are many other aspects of the cold finger modeling and design that should be addressed. These include the design and analysis of the external heat exchanger and finding materials that can withstand the high temperatures and temperature gradients and gas pressures to which the cold fingers will be subjected. In addition, as indicated in Section 7.2, the portion of the cold fingers annuli above the core should be included in the model. This will degrade the predicted performance of the cold fingers. It was decided to pursue the current transient heat transfer analysis in the next project phase.

8.0 DISCUSSION AND CONCLUSIONS

As innovative reactor designs that can better meet the Generation IV goals were conceived, analytical means were devised to investigate quickly and efficiently these concepts. Since designs and the selections of appropriate materials are in a state of flux, it is extremely important to obtain a good fundamental understanding of the behavior of each new design concept and to be able to reasonably quantify its performance without investing excessive amounts of time in new modeling efforts. Moreover, it is expected that along the way some design concepts will be discarded and others will be improved and, where appropriate, be accompanied by improvements in analytical models. A number of new and different concepts were therefore scoped with thermal-hydraulic performance calculations and safety evaluations.

In Chapter 2 a parametric study was used to determine three candidate designs for a 50 W/cc core. Cores of 25 W/cc were also considered. In establishing these designs it was necessary to use pebbles of sufficiently large diameter to minimize core pressure drop and maximize pebble bed effective thermal conductivity. If these were the only criteria, pebbles much larger than the 3 to 5 cm diameter ones chosen would have been selected. The countervailing requirement is the constraint on maximum fuel temperature. As the pebble diameter is increased, this temperature increases toward unacceptable values. Thus, for each pebble type an optimal diameter was chosen.

Chapter 3 provided analysis for the tube reactor design proposed in the previous year. These results provide parametric curves of natural circulation coolant temperature versus system pressure for 0.5, 1.0, and 2.0% decay power and for no chimney and a 12.2 m (40 feet) one. Although it was anticipated that pressurized carbon dioxide will be used in the vessel-cooling loop, parametric results are provided for both carbon dioxide and helium. These results show that, as expected, carbon dioxide provides much more convective cooling than does helium under the same conditions. The specific tube reactor geometry is one of many reasonable ones that could have been chosen. Thus, the results are important mostly because they lead to a better understanding of the behavior of the concept.

Chapter 4 provides additional parametric cases to extend a study that was performed in the year prior to the past year. This earlier study was a transient analysis of the transfer of decay heat from the reactor core to the reactor vessel and ultimately to the containment building during a severe depressurization accident. The purpose of this study was to evaluate the performance of a gas-cooled fast reactor that did not have any special in-core decay heat removal devices, such as cold fingers, and also did not have any core coolant flow during the accident. The new cases considered new choices of pebble designs and materials. First, the earlier tootsie pop pebble design was evaluated, but this time the latent heat of fusion due to the melting of the pebble core was set to zero. This enabled the effect of the latent heat to be quantified and shown to be relatively small. None of the new cases employed latent heat in the pebble. Several carbide, nitride, and oxide candidate materials were considered along with graphite and tungsten for the pebble matrix. The FIDAP results for silicon carbide and zirconium carbide approximate the results for all the carbide and nitride material choices. In addition, a case was analyzed with both tungsten pebbles and a tungsten reflector. All of the new cases produced pebble temperatures higher than 1600° C, but often far below the melting or dissociation temperature of the specific pebble matrix material.

In all of the cases studied in Chapter 4, it was assumed that instantaneously at the initiation of the transient the flow stopped and the system pressure went to atmospheric pressure. Thus, the beneficial effects of residual flow through the core during the initial portion of the accident, while the compressors are coasting to a stop, were ignored. Because the depressurization takes place over time as the coolant escapes through a breach in the pressure boundary, the system pressure can be many atmospheres for a considerable time after the initiation of the accident. A higher pressure implies a higher density and therefore a greater flow rate. Thus, it is conceivable that forced convective flow in the initial portion of the transient could remove a significant amount of the decay energy and mitigate the peak transient fuel temperature. Therefore, in Chapter 5 the beneficial effects of this residual flow were investigated. A time constant of 1 minute was assumed for the compressor coastdown and a time constant of 10 minutes was assumed for the depressurization. It takes about 20 minutes for the normalized flow rate to become less than the normalized power. After 20 minutes the flow rate continues to decrease rapidly toward zero while the decay power decreases slowly and the resultant high power-to-flow ratio causes the fuel temperatures to rise rapidly.

The flow coastdown analysis, however, ignores conduction and radiation from the core and assumes that all heat transfer from the fuel is by convection to the coolant. Within about an hour of the start of the transient, the peak fuel temperature has recovered to its initial steady-state value and is increasing rapidly. Thus, the effect of the convective flow is to delay the start of the transient. This effect could be approximately simulated with the Chapter 4 FIDAP model by shifting the decay heat curve by an hour so that at time=0 the decay power is about 1.3% instead of almost 7%. As Figure 5-8 of Reference 1 shows, the peak fuel temperature occurs at 2.0 days. As Figure 2-2 of Reference 1 shows, only a small fraction of the total decay energy produced in 2 days is produced during the first hour. However, if a significant portion of the total decay energy produced in 2 days were removed by conduction and radiation from the core to and through the reactor vessel wall, the amount removed by convection during the first hour would be a bigger fraction of what is left. Thus, the flow coastdown should reduce the peak fuel temperatures at least a moderate amount. Future more sophisticated transient models should include the core convective flow along with conduction and radiation from the fuel. Figure 5-8 of Reference 1 is for a 300 MWt (22.8 W/cc) core. Based on this figure, it is conceivable that with the appropriate reactor design and a power density of about 25 W/cc, sufficient decay heat could be removed – by the combination of heat

transfer through the vessel wall and core convective flow during the initial part of the transient – to yield an acceptable peak fuel temperature during a severe depressurization accident.

Chapter 6 describes a new concept for dealing with the decay heat. The fuel pebbles are rapidly dumped into a series of lower storage tanks that are cooled externally by borated water. The analysis in Appendix B extensively analyzes the removal of the decay heat from the borated water to the atmosphere. This heat transfer is accomplished by using the decay heat to boil the borated water and a natural-draft cooling tower to cool the steam and condense it back to liquid. Appendix B indicates that this part of the decay-heat removal scheme is feasible. A more difficult part, perhaps, is moving the fuel pebbles to the storage tanks in a timely manner without overheating any of the structures along the way. This issue and the heat transfer from the fuel pebbles to the borated water need further investigation.

Chapter 7 describes the cold finger concept for decay heat removal. Both steady state and transient models were developed and used to evaluate the performance of these bayonet-type heat exchangers. The steady-state model is effective for scoping studies and provides the flow rates and heat transfer coefficients used in the transient model. For the steady-state model, a decay power level must be assumed, while the transient model uses the decay heat curve to represent local volumetric heat generation rate as a function of time. The transient model is a FIDAP model that considers heat storage effects in the fuel and in the cold finger. Thus, the transient model is essential in assessing the performance of the cold fingers and in determining the peak fuel temperature. The analytical results for the 4-cm and the 5-cm pebble core design choice for the 50 W/cc cores indicate that 15 cold fingers that occupy 15% of the total core volume are not enough to keep the transient peak fuel temperature below 1600° C. If the total core volume occupied by cold fingers is not increased and the number of cold fingers is increased, the diameter of each cold finger must be made proportionately smaller. Cases 4 and 5 in Table 6 indicate that the peak fuel temperatures are about 200° C above the limit. Thus, to keep the transient peak core temperature below 1600° C, several more cold fingers are needed and/or a greater portion of the core volume must be occupied by cold fingers.

There are additional issues with regard to the cold fingers that should be addressed. First, the analysis of the natural circulation did not include the hydraulic resistance of the cold finger annuli between the top of the core and the reactor vessel cover. This resistance is included in the mathematical model capability but its value was effectively set to zero in the analysis. The effect of this resistance is to increase the number of cold fingers needed. Second, the external heat exchanger was not explicitly analyzed and analysis may show that the required size of the heat exchanger potentially could make the cold finger concept impractical. Third, the mechanical design and structural integrity of the cold fingers could be a major issue. Finding material that could withstand the fluence, temperatures, temperature gradients, and pressure-induced stresses that the cold finger could be subjected to is a serious challenge.

In conclusion, many diverse approaches and concepts have been analytically explored with regard to the thermal aspects of potential Generation IV gas-cooled fast reactor designs. Others, working in parallel, are exploring the neutronic, structural, and materials aspects of the reactor designs. When all of this collective knowledge is synthesized to produce the best candidate reactor designs, it should become clear which of the many approaches and concepts explored in this report deserve further consideration.

REFERENCES:

1. E. E. Feldman and T. Y. Wei, "Point Design Concepts for a Gas-Cooled Fast Reactor," Nuclear Energy Research Initiative Project #01-022: Particle-Bed-Gas-Cooled Fast Reactor (PB-GCFR) Design, Task 2.1 Milestone/Deliverable, Reactor Analysis and Engineering Division, Argonne National Laboratory, February 28, 2002.
2. FIDAP 8, (Fluid Dynamics Analysis Package), Fluid Dynamics International, Inc., USA, December 1998.
3. J. W. Holland and I. G. Prokofiev, "Assessment of Candidate Fuel and Structural Materials for Use in a Particle-Bed Gas-Cooled Fast Reactor," Nuclear Energy Research Initiative Project #01-022: "Particle-Bed-Gas-Cooled Fast Reactor (PB-BCFR) Design," Task 4 Milestone/Deliverable, Reactor Analysis and Engineering Division, Argonne National Laboratory, February 28, 2002.
4. G. Breitbach and H. Barthels, "The Radiant Heat Transfer in the High Temperature Reactor Core after Failure of the Afterheat Removal Systems," Nuclear Technology, Vol. 49. Aug. 1980, pp. 392-399.
5. L. D. Loch, Chapter 43, Graphite, C. R. Tipton, Jr., editor, Reactor Handbook, Second Edition, Volume I, Materials, Interscience Publisher, Inc., New York, 1960, pp.888-896.
6. "Sintered Silicon Carbide (SiC)," at NIST Web site, "<http://www.ceramics.nist.gov/srd/summary/scdscs.htm>," May 23, 2002.
7. R. J. Price, "Properties of Silicon Carbide for Nuclear Fuel Particle Coatings," Nuclear Technology, Vol. 35, 1977, pp. 320-336.
8. Matlab, The MathWorks, Inc., 24 Prime Park Way, Natick, Mass., 01760, Copyright 1984-2000.
9. Intra-Laboratory ANL Memo E. E. Feldman to T. Y. Wei, "A Design Concept and an Analytical Model for a Condenser and Natural Draft Cooling Tower Combination to Be Used for Decay Heat Removal for a Gas-Cooled Pebble-Bed Fast Reactor," August 1, 2002.
10. Yigal Ronen, Ed., CRC Handbook of Nuclear Reactors Calculations, Volume II, CRC Press, Inc., Boca Raton, Florida, 1986, p. 285.

APPENDIX A – FLOW COASTDOWN MODEL

Figure 5 shows a model of the pebble bed core that was used to develop the dynamic model. Although the figure shows 10 axial layers, the computer program that was developed to implement the analytical model does not restrict the number of layers to 10. Virtually any reasonable number of layers can be used, but all layers must be of the same thickness and each must be divided into a fuel volume and a gas volume. Thus, there are N layers, where N is an arbitrary integer. One Nth of the total core volume of pebbles is in each fuel volume and 1/Nth of the total gas volume in the void spaces among the pebbles is in each gas volume. This type of nodalization scheme is typical of what is done for pin and block cores. An alternative, perhaps more aesthetically pleasing, approach that leads to the same model is to analyze an average coolant channel instead of the entire core. This coolant channel would also be divided into N layers, or volumes, and each coolant layer would be thermally coupled to the solid fuel pebbles associated with the layer. A typical pebble associated with the layer would be modeled and appropriately scaled so that the energy flows between the coolant and all of the pebbles associated with the layer would be properly represented.

In the reactor, heat generated in the pebbles is transferred to the coolant and convected by the coolant from one coolant node to the next until the core coolant exit is reached. In the model, heat generated in a fuel node can be transferred only to its immediately adjacent coolant node, located in the same axial layer. Axial conduction among fuel nodes is not allowed, nor is axial conduction allowed among coolant nodes.

A simple energy balance relationship is developed for each fuel node and for each coolant node. Each relationship results in an ordinary first-order differential equation and the set of 2N simultaneous ordinary differential equations, ODEs, is

solved via a solver provide by the Matlab software package.A.1 Each energy balance relationship in mathematical terms merely states that the rate of energy transfer into the node minus the rate of energy transferred out the node plus the rate of energy generated in the node equals the rate of energy stored in the node. There is no energy generated in the coolant nodes and the energy generated in the fuel nodes is due to the decay power generated in the pebbles. The only heat transfer to or from the fuel nodes is at the interface of the fuel node and its directly adjacent coolant node.

Each coolant node, in addition to its thermal communication with its directly adjacent fuel node, can also transfer heat to the node immediately above it, if there is one immediately above it, or receive heat convected from the node immediately below it, if there is one immediately below it. The core inlet temperature is a boundary condition applied to the inlet of the first coolant node. The calculated exit temperature of the last coolant temperature provides the core exit coolant temperature.

The fuel nodal temperature is evaluated at the middle of the layer. In the coolant nodes the temperatures evaluated at the inlets and outlets of the node are need for the convective terms. The mean of the temperatures at the inlet and outlet of each coolant node is used to represent the temperature of the coolant volume. This mean temperature is used in the heat storage term and in accounting for the heat transfer between the coolant node and its adjacent fuel node.

When the fuel and coolant nodes in a single layer are considered, it is observed that there are five energy terms that must be considered. Each is listed below followed by its mathematical representation and the nomenclature is provided in Table A.1.

- 1) power generation in fuel node i

$$np_i \times vp \times q_i'''$$

- 2) rate of energy storage in fuel node i

$$np_i \times mp \times cpp \times \frac{dT_{p_i}}{dt}$$

- 3) heat transfer between fuel node i and its adjacent coolant node, where a positive value corresponds to heat transfer from the fuel to the coolant

$$np_i \times hp_i \times Ap \times (T_{p_i} - T_{g_{i-\frac{1}{2}}}), \text{ where } T_{g_{i-\frac{1}{2}}} \equiv \frac{(T_{g_i} + T_{g_{i-1}})}{2}$$

- 4) power convected into and out of coolant node i by the flowing gas, where a positive value corresponds to heat addition

$$\dot{m} \times cpg \times (T_{g_{i-1}} - T_{g_i})$$

- 5) rate of energy storage in coolant node i

$$Mg \times cpg \times \frac{dT_{g_i}}{dT}$$

The energy balance relationship for fuel node i is obtained by equating the difference of items 1 and 3 with item 2. An alternative way of arriving at this relationship is to write an energy balance relationship for a typical pebble in fuel node i.

Items 1, 2, and 3 would correspond to a single pebble instead of all of the pebbles in the volume if the common factor np_i were omitted from all three of them. The energy balance relationship for gas node i is obtained by equating the sum of items 3 and 4 with item 5. The resultant two equations, respectively are:

$$\frac{dT_{p_i}}{dt} = -\gamma_i \times T_{p_i} + \frac{\gamma_i}{2} \times T_{g_i} + \frac{\gamma_i}{2} \times T_{g_{i-1}} + \delta_i \quad (\text{A.1})$$

$$\frac{dT_{g_i}}{dt} = \alpha_i \times T_{p_i} - a_i \times T_{g_i} - b_i \times T_{g_{i-1}} \quad (\text{A.2})$$

where:

$$\gamma_i = \frac{hp_i \times Ap}{Mp \times cpp} = \frac{6 hp_i}{pp \times cpp \times dp}$$

$$\delta_i = \frac{q_i''' \times vp}{Mp \times cpp} = \frac{q_i'''}{pp \times cpp} = \frac{Q_i'''}{1 - vf} \frac{1}{pp \times cpp}$$

$$a_i = \frac{\alpha_i}{2} + \beta_i$$

$$b_i = \frac{\alpha_i}{2} - \beta_i$$

$$\alpha_i = \frac{np_i \times hp_i \times Ap}{Mg \times cpg} = 6 \frac{1 - vf}{vf} \frac{hp_i}{pg \times cpg \times dp}$$

$$\beta_i = \frac{\dot{m}}{Mg} = \frac{\dot{m}}{pg \times vf \times V}$$

In the above relationships, the product of volume and density is equated with mass for both the pebble and the coolant. The density of the pebble is assumed to be constant and the density of the gas, which is obtained from the ideal gas relationship for helium, is evaluated at the channel inlet conditions and assumed not to vary with position. Also, the volumes of the gas and of the pebbles are calculated from the total volume of a layer, V , which includes both the pebble and gas volumes, and the gas void fraction, vf , which is taken to be 0.387.

The film coefficient effect, i.e., thermal boundary layer effect, on the surface of the pebble and the thermal resistance of the solid material of the pebble itself together determine the thermal conductance between the interior of the pebble and the free stream of the helium gas, hpi . Therefore, hpi is obtained from the following:

$$\frac{1}{hpi} = \frac{1}{h_surf_i} + \frac{l_cond}{k_pebble} \quad (A.3)$$

where, h_surf_i is the film coefficient on the surface of the typical pebble in layer i , l_cond is the conduction length from the surface to the interior of the pebble, and k_pebble is the thermal conductivity of the pebble. The conduction length, l_cond , was taken to be the radial distance from the surface of the pebble to the radial location that divides the pebble into two equal concentric volumes. The film coefficient, h_surf_i , was obtained from Nusselt number correlations for forced flow through pebble beds provided in Reference A.2. For Reynolds numbers greater or equal to 500 equation 17 of Reference A.2 was used. For Reynolds numbers less than 500, equation 1 of Figure 1 of Reference A.2 was used with a typographical error corrected. As can be verified by Reference A.3, the apparent typographical error in this equation is that Reh in the second term of the square brackets should be replaced by Re .

Equations A.1 and A.2 are written once for each of the N layers to produce a simultaneous set of $2N$ ODEs with $2N$ unknown temperatures. The left side of the $2N$ ODEs, of course, is represented by a vector of $2N$ first derivatives of temperature with respect to time. The right sides of the $2N$ ODEs can be represented in matrix form by the sum of a vector of $2N$ known values and the product of a $2N$ by $2N$ array that has five nonzero diagonal bands and a vector of the $2N$ unknown temperatures. Several ODE solvers provided by Reference A.1 were tried and the one called "ode15s" was found to work best. The initial steady-state condition was obtained by solving the same set of $2N$ simultaneous equations with the left side, i.e., all of the time derivatives, set to zero.

References:

- A.1 Matlab, The MathWorks, Inc., 24 Prime Park Way, Natick, Mass., 01760, Copyright 1984-2000.
- A.2 E. Achenbach, "Heat and Flow Characteristics of Packed Beds," *Experimental Thermal and Fluid Science*, Vol. 10, 1995, pp. 17-27.
- A.3 E. Achenbach, "Heat Transfer and Pressure Drop of Pebble Beds Up to High Reynolds Number," U. Grigull, et al., Ed., *Proceedings of the Seventh International Heat Transfer Conference*, München, Fed. Rep. of Germany, Volume 6, pp. 3-8.

Table A.1 – Nomenclature

A_p	surface area of pebble, πdp^2
c_{pg}	specific heat capacity at constant pressure of gas
c_{pp}	specific heat capacity at constant pressure of pebble
dp	diameter of pebble
hp_i	thermal conductance of each pebble – including effects of film coefficient on the surface and heat conduction to the interior of the pebble – of volume node i
M_g	mass of gas in a single coolant volume node (or layer)
m_p	mass of one pebble
\dot{m}	gas flow rate through the coolant channel (same for all layers)
n_{p_i}	number of pebbles in volume node i
Q_i'''	average volumetric heat generation rate of volume node i (averaged over entire nodal volume)
q_i'''	volumetric heat generation rate of each pebble in volume node i
T_{g_i}	gas temperature at the exit of gas volume node i (The temperature at the inlet to the first gas volume node is T_{g0} .)
T_{p_i}	average temperature of each pebble in volume node i
t	time
V	combined volume of all of the gas and all of the fuel pebbles in a single layer (combined volume of both the fuel node and the gas node of a single layer)
v_f	gas void fraction
v_p	volume of one pebble, $\pi/6 dp^3$
ρ_g	density of gas
ρ_p	density of pebble

APPENDIX B – COOLING TOWER MODEL FOR PEBBLE DUMP CONCEPT

B.1 Introduction

One of the most rare, but difficult to accommodate, upsets in a passively-safe gas-cooled pebble-bed reactor is a severe depressurization accident. It is assumed that for a passively-safe response there are no external power sources or internal electric generators to provide power to coolant blowers. A novel design idea has been suggested. During the accident all of the pebbles are to be released and allowed to fall into a set of tanks located below the reactor core. These tanks would be able to withstand the full operating gas pressure of the reactor and would be located in a water bath. The decay heat from the fuel pebbles would be transferred through the tank walls and would cause the water to boil. The steam would rise through a pipe (or pipes) to a condenser located outside the reactor containment building. A natural-draft cooling tower located over the condenser would draw air through the condenser and condense the steam back to water. A pipe (or pipes) at the exit of the condenser would allow gravity to carry this water back to the water bath inside the containment. The boiling and condensing water in this concept behaves very much like the working fluid

in a heat pipe. Reference B.1, which describes the design of a heat pipe with water as the working fluid, provided the idea for using boiling/condensing water as the heat transfer mechanism. This memo explores this concept by suggesting a design and providing an analytical model for the condenser and the cooling tower. Representative dimensions are proposed to enable the system to remove about 6 MW of power on a steady-state basis. An additional advantage of the concept is that if greater amounts of power need to be removed in the early phases of the accident, this could be accomplished by allowing some of the steam to be released through a pressure relief valve. Once the decay power drops below the capacity of the unit, the steam pressure would drop and the relief valve would close. Of course, the steady-state power capability can be increased by enlarging the condenser and the cooling tower. The analytical is demonstrated in a validation test case by employing representative physical size parameters available in the published literature for cooling towers designed to remove hundreds of megawatts of power.

B.2 Conceptual Design

There are many ways of arranging tubes to form a condenser. In some designs, for example, the tubes are vertical and in others they are horizontal or have some other orientation. The boiling fluid can be on either the shell side or the tube side of the condenser. The tubes of the heat exchanger can be inside the chimney and cover the circular cross sectional area of the chimney or they can ring the circular perimeter at the base of the chimney. Handbooks that provide designs and correlations for cooling towers and steam condensers were consulted. Unfortunately, no design could be found in which both the cooling fluid and the condensing flow were both driven solely by natural convection. This is probably not a cost-effective combination. After much thought and analysis it was decided that 1) the tubes would be vertical, 2) the water would be inside the tubes, and 3) the tubes would ring the perimeter of the chimney at the base.

Putting the water on the inside of the tubes and the air on outside was an easy choice, since the effective film coefficient for the condensing water is very high compared to the film coefficient for the air side. This design choice enabled an extensive use of fins to enhance the heat transfer on the air side. Vertical tubes seemed to lead to a geometrically simple design and resulted in essentially symmetric water flow patterns inside the tubes. Horizontal or inclined tubes would be more complicated, but analytically manageable. The vertical tube could have been placed so that they cover the circular cross section of the chimney. This would have resulted in the condenser being a counter flow heat exchanger. However, putting the tubes inside the chimney limits the air flow area through the condenser to the circular cross section of the chimney minus the cross sectional area taken up by the tubes and the fins. When the base of the chimney is ringed with vertical tubes a cross flow heat exchanger is formed whose air flow area can be increased by making the tubes longer.

For structural reasons, natural air draft chimneys tend to be much wider at the base of the chimney than at the throat. Reference B.2 states: "For most towers, the main structure consists of a large concrete shell, roughly cylindrical in form with a vertical axis, but tapering inward and outward to form a throat that is located near the top." They provide typical proportions for natural draft air cooling towers. They state: "The ratio of the base diameter to the height usually lies in the range of 0.75-0.85; the ratio of the throat diameter to the base diameter is in the range of 0.55-0.65; and the ratio of vertical depth of air opening to base diameter lies in the range of 0.10-0.12." Thus, rings of tubes could fit inside the perimeter of the base of the chimney without being in line with the throat of the chimney. In the analytical model the chimney is assumed to be of uniform diameter and the diameter to be that at the throat.

For simplicity it was assumed that the rings of tubes would be made up of many identical smaller flat rectangular heat exchangers. These smaller units would be placed inside and along the circular perimeter at the base of the tower and could be in a jagged repeating pattern or, if desired, as secants of a circle. It was decided the tube fins would be a series of evenly-spaced rectangular horizontal parallel plate that intersect the vertical tubes to form structurally rigid units. The tubes in each unit are assumed to be on a square pitch forming an inline (as opposed to staggered) array. If the heat exchanger has ten rows of tubes, then its depth along the air-flow path is ten tube-to-tube pitches. In addition, if the heat exchanger has 20 tubes per row, its width is 20 such pitches. Each tube could be considered as being in the center of a square that is one pitch on a side and a 10-by-20 tube unit could be considered as being made of 200 such tubes each at the center of a one-pitch-by-one pitch square fin. This design of the fins and tubes is used below in modeling the fin efficiency of the units.

Another model is used in modeling the air flow through the heat exchangers. An air flow channel in this model is the rectangle formed by two adjacent plates and two adjacent (approximately radial) lines of tubes. The dimensions of this rectangle are, horizontally, the tube-to-tube pitch minus one tube outside diameter and, vertically, the plate spacing (i.e., plate pitch) minus one plate thickness. This defines the flow area of one flow channel. In determining the hydraulic diameter, only the plates are considered as part of the wetted perimeter. In this sense they are treated as infinitely wide parallel plates for which the hydraulic diameter is twice the channel spacing between the plates. In the actual design

the tube length may not accommodate an integral number of fin pitches. Therefore, in the analysis the tube length is divided by the plate-to-plate pitch. This number is truncated to obtain the number of plates. The total vertical air-flow height for the unit is taken to be the tube length reduced by the combined thickness of all of the plates. Similarly, the total air-flow width of the unit is the width of its plates, which is assumed to be an integer number of tube pitches, minus the combined outside diameters of all of its tubes. The total flow area is the product of the total air-flow height and width.

B.3 Analytical Model

The entire model for the condenser, the cooling tower, and the steam/water flow was developed on a computer spreadsheet. British units, which include feet, inches, and Btu's, were used. One exception is that the condenser power is represented in Watts because this is the unit commonly used for reactor decay power. The entire mathematical model is provided in the four sections which immediately follow this one. All of the models are for steady-state operation and do exclude dynamic behavior. Table B.1 provides the nomenclature and the units employed for the variables of the energy balance relationships in Section B.3.A., and the air-side momentum equation in Section B.3.B. The ancillary relationships of Section B.3.C. and the condenser heat transfer relationships of Section B.3.D., have their own nomenclature, which may conflict with each other and with that of Sections B.3.A. and B.3.B.. The models in Sections B.3.C. and B.3.D. came directly from published sources and are self-contained. The nomenclature for these two sections is largely that of the sources and the variable naming tends to follow common practice. However, each variable used in these four sections is defined the first time it is used.

B.3.A Energy Balance Relationships

The energy balance for the air flowing through the heat exchanger is given by:

$$Q \times 3.412/3600 = \dot{m}_{\text{AIR}} \text{cp}_{\text{AIR}} (T_{\text{OUT_AIR}} - T_{\text{ATM}}) \quad (\text{B.1})$$

where Q is the power in Watts, \dot{m}_{AIR} is the air flow rate in lbm/s, cp_{AIR} is the specific heat of air at constant pressure in Btu/lbm-F, $T_{\text{OUT_AIR}}$ is the temperature of the air at the heat exchanger exit in F, and T_{ATM} is the temperature of the air at the inlet in F, which is assumed to be the local atmospheric temperature. The factor 3.412/3600 is a conversion factor from Watts to Btu/s.

The energy balance for the steam condensing in the condenser is given by:

$$Q \times 3.412/3600 = \dot{m}_{\text{H}_2\text{O}} \text{hv}_{\text{FG}} \quad (\text{B.2})$$

where $\dot{m}_{\text{H}_2\text{O}}$ is the water/steam flow rate in the condenser and hv_{FG} is the heat of vaporization of water in Btu/lbm at the pressure inside the condenser. This pressure is taken to be atmospheric pressure in the cases considered below.

The condensing steam on the water side tends to keep the tube wall temperature, T_{WALL} , within several degrees Fahrenheit of the water/steam saturation temperature. Therefore, in the model this temperature is taken to be an unknown uniform (i.e., single) value. Since the tubes are typically made of metal that has a high thermal conductivity, the temperature drop from the outer to the inner surface of the tube is ignored. This temperature difference can easily be shown to be negligible compared to the temperature rise from the wall to the water or from the free steam air to the wall. Thus, the air-side model of heat transfer from the wall to the flowing air is that of air flowing through a duct whose entire surface is at a uniform temperature of T_{WALL} . The air enters the duct at a temperature of T_{ATM} , is heated by the duct walls, and exits at a temperature of $T_{\text{OUT_AIR}}$. The relationship can be easily derived and is:

$$\frac{T_{\text{OUT_AIR}} - T_{\text{WALL}}}{T_{\text{ATM}} - T_{\text{WALL}}} = \exp\left(-\frac{\text{UA}_{\text{HX}}}{3600 \dot{m}_{\text{AIR}} \text{cp}_{\text{AIR}}}\right) \quad (\text{B.3})$$

where UA_{HX} is the effective product of the film coefficient of the duct surfaces and the heat transfer area in Btu/hr-F and 3600 is the conversion factor from hours to seconds. A description for UA_{HX} is included below along with the models for air-side film coefficients and the fin efficiency in Section B.3.C.

The relationship for the heat transfer from the tube wall to the saturated liquid, which adheres to the inner surface of the tube wall, is given by the following well-know definition of film coefficient, $h_{\text{H}_2\text{O}}$:

$$Q \times 3.412 \equiv h_{H_2O} A_{H_2O} (T_{SAT} - T_{WALL}) \quad (B.4)$$

where h_{H_2O} is in Btu/hr-ft²-F, A_{H_2O} is the total tube wall inner surface area in ft², T_{SAT} is the water saturation temperature in F, and 3.412 is the conversion factor for Watts to Btu/hr. The relationships that provide h_{H_2O} are given below in Section B.3.D. in the special model for the condensing of vapor on the inside of vertical tubes.

B.3.B Air-Side Momentum Equation

The path the air follows from the heat exchanger inlet to the chimney to the atmosphere and back to the heat exchanger inlet can be modeled as a closed loop in which all of the heat gained from the heat exchanger is lost to the atmosphere at the chimney exit. The momentum equation for this loop is obtained by equating the combined friction pressure drops through the heat exchanger and the chimney, ΔP_{HX_FRIC} and ΔP_{CH_FRIC} , respectively, with the buoyancy pressure rise produced by the heated air in the chimney, ΔP_{GRAV} . Hence:

$$\Delta P_{HX_FRIC} + \Delta P_{CH_FRIC} = \Delta P_{GRAV} \quad (B.5)$$

where all three quantities are in psi.

The relationships for the two friction pressure drops are given by:

$$\Delta P_{HX_FRIC} = \left(K_{HX_AIR} + f_{FINS_AIR} \frac{L_{FINS}}{d_{H_FINS}} \right) \frac{1}{2} \rho_{AIR} (V_{HX_AIR})^2 \frac{1}{144 \times 32.2} \quad (B.6)$$

$$\Delta P_{CH_FRIC} = \left(K_{CH_AIR} + f_{CH_AIR} \frac{H_{CH} + \frac{L_{TUBES}}{2}}{d_{CH}} \right) \frac{1}{2} \rho_{AIR} (V_{CH_AIR})^2 \frac{1}{144 \times 32.2} \quad (B.7)$$

where K_{HX_AIR} and K_{CH_AIR} are the form-loss (or k-loss) for the heat exchanger and the chimney, respectively, f_{FINS_AIR} and f_{CH_AIR} are the Moody friction factor for the heat exchanger and the chimney, respectively, L_{FINS} is the depth of the heat exchanger (i.e., total length of the heat exchanger air flow path) in inches, d_{H_FINS} is the hydraulic diameter for the air flow path through the heat exchanger in inches, which can be shown to be twice the air gap spacing between adjacent fin plates, H_{CH} is the height of the chimney in ft, d_{CH} is the diameter of the chimney in ft., L_{TUBES} is the length of the condenser tubes in ft, ρ_{AIR} is the density of air in lbm/ft³, V_{HX_AIR} and V_{CH_AIR} are the air average velocity through the heat exchanger and the chimney in ft/s, respectively. The 144 factor is to convert ft² to in² and the 32.2 factor is to convert lbm to slugs. (A slug-ft/s² is a lbf.)

The buoyancy pressure rise is the differences in the weight per unit area between a vertical column of cold air at T_{ATM} and a hot one of the same length at temperature T_{OUT_AIR} . The length of the column is that of the chimney plus half the length of the tubes. The chimney is assumed to start at the top of the tubes. Only half the tube length is used because on average the air travels only half of the vertical length of the tubes after it exits the condenser. Thus, the buoyancy pressure rise is given by:

$$\Delta P_{GRAV} = \Delta \rho_{CH} \left(H_{CH} + \frac{L_{TUBES}}{2} \right) \frac{1}{144} \quad (B.8)$$

where $\Delta \rho_{CH}$ is the difference in density between the cold column of air and the hot one in lbm/ft³. $\Delta \rho_{CH}$ was obtained from the ideal gas relationship for air. Since a lbm weights a lbf, the acceleration due to gravity, g , does not appear in the above pressure drop relationship. The factor of 144 is needed to convert ft² to in².

Conservation of mass, i.e., the continuity equation, provides that:

$$\dot{m}_{AIR} = \rho_{AIR} V_{HX_AIR} A_{HX_FLOW} = \rho_{AIR} V_{CH_AIR} A_{CH_FLOW} \quad (B.9)$$

B.3.C Ancillary Air-Side Correlations

Reference B.3 recommends what they believe to be the most accurate relationships for friction factor and Nusselt number for turbulent flow inside smooth circular ducts. They also indicate that these are the ones they recommend for infinite parallel plates. Their relationships are based on the Fanning friction factor, which is a factor of 4 smaller than the Moody friction factor used above. Therefore, this factor was added so that the relationships are expressed in terms of the Moody friction factor. Hence:

$$f = 4 \left(A + \frac{B}{Re^{1/m}} \right) \quad (B.10)$$

where $A = 0.0054$, $B = 2.3 \times 10^{-8}$, and $m = -2/3$ for $2300 \leq Re \leq 4000$
 $A = 1.28 \times 10^{-3}$, $B = 0.1143$, and $m = 3.2154$ for $4000 \leq Re \leq 10^7$

$$Nu = \frac{\left(\frac{f}{8}\right)(Re - 1000)Pr}{1 + 12.7\left(\frac{f}{8}\right)^{1/2}\left(Pr^{2/3} - 1\right)} \quad (B.11)$$

where f is the Moody friction factor, Re is the Reynolds number, based on hydraulic diameter, Nu is the Nusselt number, based on hydraulic diameter, and Pr is the Prandtl number. These relationships were used to determine the friction factor on the air-side of the heat exchanger, which was treated as a series of infinite parallel plates, and in the chimney. The Nusselt number relationship was used to determine the film coefficient on the surfaces of the plates in the heat exchanger.

The temperature of the fins are coldest where they join the tubes and are warmest at the midpoints between adjacent tubes. If the fins were of infinite thermal conductivity, then the fin temperature would be uniform and at the coldest tube temperature everywhere. By definition, the fin efficiency is the ratio of the actual heat transferred by the fin to the ideal, i.e., infinite thermal-conductivity, case. Thus, in calculating the heat transfer from the surface of the fin to the flowing air, the tube temperature is assumed to be representative of all locations on the surface of the fin, but the film coefficient is multiplied by the fin efficiency, i.e., $h A \Delta T$ is replaced by $\eta h A \Delta T$, where η is the fin efficiency, h is the film coefficient, A is the fin heat transfer area, and ΔT is the difference between the surface temperature at the base of the fin (i.e., where it joins the tube) and the temperature of the flowing air.

Relationships for fin efficiency are a function of fin geometry and material. Reference B.4, p.17.45, provides a relation for a circular fin of outer diameter d_e , inner diameter d_o , and thickness δ . This fin is a flat disc with a hole of diameter d_o in the middle where it joins the tube. The fin efficiency, η , is given by:

$$\eta = \begin{cases} a(m l_e)^{-b} & \text{for } \Phi > 0.6 + 2.257(r^*)^{-0.445} \\ \frac{\tanh \Phi}{\Phi} & \text{for } \Phi \leq 0.6 + 2.257(r^*)^{-0.445} \end{cases}$$

$$a = (r^*)^{-0.246} \quad \Phi = m l_e (r^*)^n \quad n = \exp(0.13m l_e - 1.3863)$$

$$b = \begin{cases} 0.9107 + 0.0893r^* & \text{for } r^* \leq 2 \\ 0.9706 + 0.17125 \ln r^* & \text{for } r^* > 2 \end{cases} \quad (B.12)$$

$$m = \left(\frac{2h}{k_f \delta}\right)^{1/2} \quad l_e = l_f + \frac{\delta}{2} \quad r^* = \frac{d_e}{d_o} \quad l_f = \frac{d_e - d_o}{2}$$

where h is the film coefficient on the surface of the fin and k_f is the thermal conductivity of the fin. In the current application, each tube is considered to be at the center of a square fin that is one tube pitch on a side. The square fin is approximate by a circular one of the same horizontal surface area. Thus d_e in the above relationship is replaced by $(4/\pi)^{1/2} d_e$. Increasing the outer diameter of the fin in this manner reduces its efficiency, as it should.

The total heat transfer from the exterior surface of the heat exchanger to the flowing air must also include the heat transfer from the surfaces of the tubes. Thus, a film coefficient for the tube surface is also needed and this must be obtained for the appropriate Nusselt number relationship. This relationship is very much geometry dependent and is affected by the fin design and arrangement. Reference B.5 provides the Nusselt number, Nu, for heat transfer in banks of radial high finned tubes in cross flow for an in-line tube arrangement (as opposed to stagger tube arrangement), as follows:

$$\text{Nu} = 0.30 \text{Re}^{0.625} \epsilon^{-0.375} \text{Pr}^{0.333}, \quad 5 < \epsilon < 12, \quad 5 \times 10^3 < \text{Re} < 10^5$$

$$\text{where } \text{Nu} = \frac{h d}{k}, \quad \text{Re} = \frac{V d}{\nu}, \quad \epsilon = \frac{A_t}{A_o} \quad (\text{B.13})$$

and d is the tube outer diameter, h is the heat transfer coefficient to be applied to total fin and tube exposed surface area, A_t , A_o is the surface area of the bare tubes, V is the maximum velocity of the fluid, which occurs at the minimum free cross-section of the fin-tubed bank, and k and ν are the thermal conductivity and kinematic viscosity of the fluid, respectively. This relationship is intended to provide one overall film coefficient for the entire fin-tubed region of the heat exchanger. The heat transfer area is the entire combined exposed fin and tube heat transfer area, A_t . The effects of fin efficiency are included in the area ratio term. Thus, if one chose to approximate the heat exchanger as one of banks of radial high finned tubes, one could ignore equation B.12 and just use equation B.13 for both the fins and the tubes combined.. Instead, we chose to use equation B.13 with the area ratio ϵ set to 1 to approximate the Nusselt number (and film coefficient) for the exposed portions of the tubes. This approach is not totally correct, but it is reasonable. Thus, the UA_{HX} needed above is the sum of the $\eta h A$ for the flat plates, where η is obtained from equation B.12, h is based on Nu from equation B.11, and A is the horizontal surface area of all of the fin plates and the h A for the exposed tubed surfaces, where the tube h is obtained from the above equation B.13 and the tube A is all of the exposed tube surface area. Perhaps, in the future UA_{HX} should be set equal to the product of the total exposed tube and plate heat transfer area and the film coefficient, h, should be obtained from equation B.13 with ϵ set to the appropriate value. Then the results from the two modeling approaches could be compared. Although neither approach is totally correct, similar reasonably accurate results are anticipated.

B.3.D Condenser Heat Transfer Relationships

Reference B.6 provides the following analytical model for laminar film condensation on a vertical plate:

$$\delta(x) = \left[\frac{4k(T_{\text{sat}} - T_w) \nu x}{(\rho_f - \rho_g) g h'_{\text{fg}}} \right]^{1/4}$$

$$h'_{\text{fg}} \equiv h_{\text{fg}} \left[1 + 0.68 \frac{c_p (T_{\text{sat}} - T_w)}{h_{\text{fg}}} \right] \quad (\text{B.14})$$

$$h(x) = \frac{k}{\delta(x)} \quad \bar{h} = \frac{4}{3} h(L)$$

$$\text{Nu}(x) = \frac{hx}{k} = \frac{x}{\delta(x)} \quad \bar{\text{Nu}} = \frac{\bar{h}L}{k} = \frac{4}{3} \frac{L}{\delta(L)}$$

where x is the distance from the top of the plate and L is the length of the plate. $\delta(x)$ is the liquid boundary layer thickness along the inner surface of the plate, T_{sat} is the saturation temperature of the liquid, T_w is the wall temperature, h_{fg} is the heat of vaporization of the liquid, k is the thermal conductivity of the liquid, ν is the kinematic viscosity of the liquid, and ρ_f and ρ_g are the density of the liquid and the vapor, respectively, and g is the acceleration due to gravity. $\text{Nu}(x)$ and $h(x)$ are the local Nusselt number and film coefficient, respectively. $\text{Nu}(x)$ averaged over the plate length, L, is $\bar{\text{Nu}}$ and similarly $h(x)$ averaged over the length of the tube is \bar{h} . This model is valid for condensation inside round tubes when the maximum boundary layer thickness, $\delta(L)$, is small compared with the inner radius of the tube. In the current analysis, $\delta(L)$ is typically several thousandth of an inch, which is much smaller than the tube radius. Since the water/steam flow is not forced, the flow will tend to be in the laminar or transition range. Figure 14.5 on page 14.7 of

Reference B.4 show that the laminar theory (used above) always produces the same or a lower average film coefficient than does the turbulent theory. Pages 14.13-14.15 of Reference B.4 shows that the presence of a small amount of non-condensable gases in the condensing liquid can have a substantial adverse effect on the heat transfer. Thus, the presence of such gases, including air, may have to be controlled and included in future analyses.

An analytic model to describe the hydrodynamics of the water flow is not needed. It is assumed that the tubes are of sufficient diameter that steam can easily enter them from both the top and the bottom and that a very thin film of water on the inner surface will flow down by gravity and drip out the bottom. The number and the size of the tubes is governed more by the air side, where the thermal resistance is much greater, than by the water side.

B.4 Representative Results for Decay Heat Removal in a 300 MWt Reactor

The purpose here is to create a physically reasonable cooling tower and condenser design combination and analytically show that it will adequately remove the decay heat of a 300 MWt reactor. The initial decay power of a uranium-fuel reactor that has been operating at full power for a long time is about 7% of full power. Within 10 to 15 minutes after shutdown this power decreases to less than 2% and the total decay energy produced during this 10-to-15 minute time interval is about 20 full power seconds. Thus, a decay heat removal system that can remove about 2% for full power on a steady-state basis is deemed adequate.

There are many choices to be made in constructing a design. The creation of an optimal design would require a considerable amount of experience, testing, and development. All that is sought here is a reasonable design that can remove about 6 MWt on a steady-state basis. For this design it was decided to use 1-inch Schedule 10 stainless steel tubes that are commercially available. Table B.2 provides the inputs and the results for the proposed design. The variable names provided immediately to the left of each quantity were designed to be descriptive and intuitively obvious. The units are also included along with the variable names. Most of the input geometric parameters and the air and water/steam properties tend to be on the right half of the first page of the model. The calculated quantities tend to be on the left half of the first page. The second page contains the model used to calculate fin efficiency as provided by equation B.12. The fin efficiency equations are solved simultaneously with the rest of the model. The water/steam pressure is assumed to be atmospheric (14.7 psia). The heat removal capacity of the system decreases with increasing inlet temperature, which is assumed to be the atmospheric temperature. Since adequate performance must be guaranteed, even on very hot days, the atmospheric temperature was assumed to be 100° F.

The simultaneous non-linear equation solver that is part of the computer spreadsheet software was used in obtaining a solution. The first five quantities on the right half of the first page of Table B.2 represent equations B.1, B.2, B.5, B.3, and B.4, respectively. In the spreadsheet these five equations were recast so that their right-hand sides are equal to 0. The spreadsheet solver was used to find the correct values of the first five quantities on the left-hand side of the first page of the table that would simultaneously satisfy all five equations. The spreadsheet reevaluated all of the other derived quantities on both pages of the table accordingly.

The lower right portion of the first page of the table shows that 2400 6-foot vertical (1-inch Schedule 10) tubes were arranged in 20 rows on a square pitch of 6 tube outer diameters. The 20 rows and 6-tube pitches defined the length of the air flow path to be 120 tube diameters, which equals 157.8 inches. When 2400 tubes are arranged into 20 equal rows, each row must have 120 tubes. When 120 tubes are arranged so that 6 tube diameters are allowed for each of the 120 tubes, the length of the row is 720 tube diameters, which equals 78.9 ft and when this length is wrapped into a closed circle, the circle diameter is 25.11 ft. This diameter was also used for the diameter of the chimney. The 70-foot chimney height was arbitrarily chosen. It can be adjusted, but a lower height results in lower heat removal capability.

The fin thickness was arbitrarily chosen to be a tenth of the tube outer diameter, the fin pitch was assumed to be one tube outer diameter, and the fin thermal conductivity was assumed to be 200 W/m-K, which approximately corresponds to aluminum. Some experimenting with these parameters within the spreadsheet was used in arriving at these values. The air properties on the right-hand side of the table were chosen to correspond to 170° F. Perhaps, this temperature is a bit too high and 140° F would have been a better choice for an average air temperature. The effect on the solution should be small since these properties are only mildly temperature sensitive. The friction form-loss coefficients (k-losses) for the air-side of the heat exchanger and the chimney were both taken to be 1. These are representative values which may require closer examination in the future.

The calculated results at the top left-hand side of the table show that the air is heated 75° F to 175° F, the tube wall is cooled down to 209° F, which 3° F below the 212° F boiling point of water at 1 atm., and the decay heat removed by the condenser is 5.66 MW.

B.5 Results for a 500 MWt Cooling Tower – A Validation Case

Page 3.12.3-2 of Reference B.2 briefly mentions that several power stations in the United Kingdom use a pair of 375-foot tall natural draft cooling towers to serve one 500-MW turbo-generator. Typical proportions for natural draft cooling towers are also provided, as quoted in Section B.2, above. No other design details are provided. However, one would expect that pumps are employed on the water side of the condensers. This small amount of information was used in producing a scaled-up design of the Table B.2 design. The purpose was to show that the proposed basic design concept and analytical model could produce results that are reasonably consistent with published data. It was assumed that each of the two towers would be able to dissipate the full 500-MW load. Perhaps, it would have been better to assume that each tower dissipated only half of the full load. Based on the proportions provided in Reference B.2, as quoted in Section B.2, above, it was decided that the 375-foot tower would have a 300-foot diameter base and a 180-foot diameter throat and that the tubes would be 30-feet long. The tube diameter, tube pitch, and fin pitch were taken to be those used in the Table B.2 analysis. In addition, 20 rows of tubes on a square pitch, as in Table B.2, were assumed. The 300-foot diameter base corresponds to an arc length of 300π feet. This was used to determine that there would be 1433 tubes per row. The chimney diameter was taken to be the 180-foot throat diameter. The spreadsheet results, provided in Table B.3, show that the power removed by this design is 567 MW. An additional case was also done where the number of tubes was cut in half by reducing the number of tube rows from 20 to 10. For this case the calculated power was reduced to 319 MW. There are many arbitrary changes to the design assumptions that can significantly change the calculated power. Any result within a factor of five of 250 MW could be considered reasonable under the current circumstances.

B.6 Conclusions

A design concept has been proposed for the passive removal of decay heat during a severe depressurization accident in a pebble-bed gas-cooled fast reactor. The pebbles are to be dropped into tanks that are cooled by a water bath. The water boils and the steam is condensed back to liquid in a condenser in a natural draft cooling tower. A conceptual design with specific design dimensions has been proposed for the condenser and the cooling tower. An analytical model has been developed and solved on a computer spreadsheet. The results show that systems that range in power removal capability from a few megawatts to a few hundred megawatts are feasible. The spreadsheet model can be easily adapted and expanded as the design is developed and improved. Published representative dimensions for a 375-foot tall natural draft tower were used to show that the proposed design and analytical model provide reasonable results. Much more would need to be done, but an important first step has been taken.

References

- B.1 K. Ohashi, H. Hayakawa, and M Yamada, "Preliminary Study on the Application of the Heat Pipe to the Passive Safety Decay Heat Removal System of the Modular HTR," *Progress in Nuclear Energy*, Vol. 32, No. 3/4, pp. 587-594, 1998.
- B.2 G. F. Hewitt, coordinating editor, *Hemisphere Handbook of Heat Exchanger Design*, Hemisphere Publishing Corporation, New York, 1990. (Refer to section 3.12.3, J. R. Singham, "Natural Draft Towers").
- B.3 Sadik Kakac, Ramesh K. Shah, and Win Aung, *Handbook of Single-Phase Convective Heat Transfer*, John Wiley and Sons, New York, 1987, p. 4-145.
- B.4 Warren M. Rohsenow, James P. Hartnett, and Young I. Cho, editors, *Handbook of Heat Transfer*, Third Edition, McGraw-Hill Companies, Inc., New York, 1998, p. 17.45.
- B.5 *Heat Exchanger Design Handbook, Volume 2, Fluid Mechanics and Heat Transfer*, Hemisphere Publishing Corporation, 1989, p. 2.5.3-11.
- B.6 John H. Lienhard, *A Heat Transfer Textbook*, Prentice-Hall, Inc., Englewood Cliffs, New Jersey 07632, 1981, pp. 367-373.

Table B.1. Nomenclature for Sections B.3.A and B.3.B

A_{CH_FLOW}	flow area of the chimney, ft ²
A_{HX_FLOW}	total air flow area through the condenser (ignores area shadowed by aligned rows of vertical tubes), ft ²
A_{H_2O}	total combined water-side surface area of all of the condenser tubes, ft ²
cp_{AIR}	specific heat capacity of air (at 170° F), Btu/lbm-F
d_{CH}	diameter of chimney, ft
d_{H_FINS}	hydraulic diameter of air channels (2 times the air gap between adjacent fins), in
f_{CH_AIR}	Moody friction factor for chimney
f_{FINS_AIR}	Moody friction factor for air flow between horizontal plates in heat exchanger
H_{CH}	height of chimney, ft
h_{H_2O}	film coefficient on the water-side of the condenser tubes, Btu/hr-ft ² -F
K_{CH_AIR}	friction form-loss coefficient for the chimney
K_{HX_AIR}	air-side friction form-loss coefficient for the condenser
L_{FINS}	length of condenser fins (length of air flow path), ft
L_{TUBES}	condenser tube length, ft
\dot{m}_{AIR}	air flow rate through the condenser and the chimney, lbm/s
	\dot{m}_{H_2O} total water flow rate through all of the condenser tubes, lbm/s
Q	power removed by the condenser, W
T_{ATM}	Condenser air inlet temperature (taken to be atmospheric temperature on a hot day), F
T_{OUT_AIR}	Condenser air outlet temperature
T_{WALL}	Condenser tube wall temperature
UA_{HX}	effective product of conductance and heat transfer area for the air-side of the condenser, Btu/hr-F
V_{CH_AIR}	velocity of flow through the chimney, ft/s
V_{HX_AIR}	velocity of air flow through the condenser, ft/s
ΔP_{CH_FRIC}	friction pressure drop through the chimney, psi
ΔP_{GRAV}	buoyancy pressure rise through the air-side of the condenser and the chimney combined, psi
ΔP_{HX_FRIC}	friction pressure drop through the air-side of the condenser, psi
$\Delta \rho_{CH}$	difference in air density between the atmosphere and the chimney interior, lbm/ft ³
ρ_{AIR}	density of air (at 170° F), lbm/ft ³

Table B.2. Condenser and Cooling Tower Design Results for About 6 MWt of Decay Power Removal

power, W	5.66E+06	energy air flow	0
temp_air_out, F	174.687	energy steam flow	0
temp_tube_wall, F	208.9679	momen air flow	0
m_dot_air, lbm/s	297.7034	energy, wall to air flow	0
m_dot_water, lbm/s	5.527137	energy, water film	-3E-08
A_air_flow_hx, ft ²	355.5924		
A_air_flow_ch, ft ²	495.3865		
air_den_diff, lbm/ft ³	0.008338	rho_air, lbm/ft ³	0.063
dp_grav_air, psi	0.004227	cp_air, Btu/lbm-F	0.2412
		mu_air, lbm/hr-ft	0.0503
dp_fric_hx, psi	0.003588	nu_air, ft ² /hr	0.798413
dp_fric_ch, psi	0.000638	Pr_air	0.71
v_air_hx, ft/s	13.28895	k_air, Btu/hr-ft-F	0.0172
v_air_ch, ft/s	9.538916	latent_heat, Btu/lbm	970.3
Re_air_flow_hx	11819.05	cp_wat_satl, Btu/lbm-F	1.007
Re_air_flow_ch	1080193	k_wat_satl, Btu/hr-ft-F	0.3914
fric_fac_air_hx	0.029867	rho_wat_liq, lbm/ft ³	59.812
fric_fac_air_ch	0.011197	rho_wat_vap, lbm/ft ³	0.037315
k_loss_hx	1	Tsat_water, F	212
k_loss_ch	1	nu_wat_satl, ft ² /hr	0.01124
Nu_fin	34.07567	g_grav, ft/s ²	32.2
h_air_fin, Btu/hr-ft ² -F	2.971364	temp_atm, F	100
fin_surf_area, ft ²	109609.1		
efficiency_fin	0.801393	tube_OD, in	1.315
Re_air_tubes (tube OD)	6566.142	tube_ID, in	1.097
Nusselt_air (tube OD only)	54.09996	tube_length, ft	6
h_air, Btu/hr-ft ² -F (tube OD)	8.49143	num_tubes	2400
tube_area_air, ft ²	4468.506	rows_of_tubes	20
UA_hx, Btu/hr-F	298948.6	tubes_per_row	120
UA_over_mdot_cp	1.156466	tube_pitch, diameters	6
latent_heat_prime, Btu/lbm	972.3763	arc_length_of_row, ft	78.9
water_film_thick, in	0.004067	diam_row_of_tubes, ft	25.11465
Nusselt_wat	23602.48	fin_thickness, in	0.1315
h_wat, Btu/hr-ft ² -F	1539.668	fin_pitch, diameters	1
tot_area_wat, ft ²	4135.593	fins_per_tube	54
		plate_spacing, in.	1.1835
		depth_hx, in	157.8
		diam_chimney, ft	25.11465
		height_ch, ft	70

Table B.2. Condenser and Cooling Tower Design Results for About 6 MWt of Decay Power Removal (Fin Efficiency Model) (cont'd)

ID_fin, in.	1.315	
r_star_fin	6.770275	
delta_fin (thickness), in	0.1315	
k_fin, w/m-K	200	aluminum
h_fin, w/m ² -K	2.971364	
a_fin	0.624699	
b_fin	1.298123	
m_sq_fin, in ⁻²	0.01883	
m_fin, in ⁻¹	0.137222	
lf_fin, (Ro - Ri), in	3.793956	
le_fin, in	3.859706	
n_fin	0.267818	
phi_fin	0.883955	
phi_fin_criterion	1.563633	
m_lf_fin, (m*(Ro - Ri))	0.520615	
eta_fin (efficiency)	0.801393	

Table B.3. Condenser and Cooling Tower Design Results for About 500 MWt of Power Removal

power, W	5.67E+08	energy air flow	0
temp_air_out, F	158.8902	energy steam flow	0
temp_tube_wall, F	201.6762	momen air flow	0
m_dot_air, lbm/s	37835.98	energy, wall to air flow	0
m_dot_water, lbm/s	553.8842	energy, water film	0
A_air_flow_hx, ft ²	21206.02		
A_air_flow_ch, ft ²	25446.9		
air_den_diff, lbm/ft ³	0.006742	rho_air, lbm/ft ³	0.063
dp_grav_air, psi	0.018259	cp_air, Btu/lbm-F	0.2412
		mu_air, lbm/hr-ft	0.0503
dp_fric_hx, psi	0.014413	nu_air, ft ² /hr	0.798413
dp_fric_ch, psi	0.003846	Pr_air	0.71
v_air_hx, ft/s	28.32078	k_air, Btu/hr-ft-F	0.0172
v_air_ch, ft/s	23.60095	latent_heat, Btu/lbm	970.3
Re_air_flow_hx	25188.21	cp_wat_satl, Btu/lbm-F	1.007
Re_air_flow_ch	19154776	k_wat_satl, Btu/hr-ft-F	0.3914
fric_fac_air_hx	0.024678	rho_wat_liq, lbm/ft ³	59.812
fric_fac_air_ch	0.007605	rho_wat_vap, lbm/ft ³	0.037315
k_loss_hx	1	Tsat_water, F	212
k_loss_ch	1	nu_wat_satl, ft ² /hr	0.01124
Nu_fin	61.88694	g_grav, ft/s ²	32.2
h_air_fin, Btu/hr-ft ² -F	5.396478	temp_atm, F	100
fin_surf_area, ft ²	6617297	tube_OD, in	1.315
efficiency_fin	0.692722	tube_ID, in	1.097
Re_air_tubes (tube OD)	13993.45	tube_length, ft	30
Nusselt_air (tube OD only)	88.47007	num_tubes	28660
h_air, Btu/hr-ft ² -F (tube OD)	13.8861	rows_of_tubes	20
tube_area_air, ft ²	266482.7	tubes_per_row	1433
UA_hx, Btu/hr-F	28437566	tube_pitch, diameters	6
UA_over_mdot_cp	0.865581	arc_length_of_row, ft	942.1975
latent_heat_prime, Btu/lbm	977.3693	diam_row_of_tubes, ft	299.9108
water_film_thick, in	0.008251	fin_thickness, in	0.1315
Nusselt_wat	58172.5	fin_pitch, diameters	1
h_wat, Btu/hr-ft ² -F	758.9572	fins_per_tube	273
tot_area_wat, ft ²	246929.3	plate_spacing, in.	1.1835
		depth_hx, in	157.8
		diam_chimney, ft	180
		height_ch, ft	375

Table B.3. Condenser and Cooling Tower Design Results for About 500 MWt of Decay Power Removal (Fin Efficiency Model) (cont'd)

ID_fin, in.	1.315	
r_star_fin	6.770275	
delta_fin (thickness), in	0.1315	
k_fin, w/m-K	200	aluminum
h_fin, w/m ² -K	5.396478	
a_fin	0.624699	
b_fin	1.298123	
m_sq_fin, in ⁻²	0.034198	
m_fin, in ⁻¹	0.184928	
lf_fin, (Ro - Ri), in	3.793956	
le_fin, in	3.859706	
n_fin	0.274306	
phi_fin	1.206136	
phi_fin_criterion	1.563633	
m_lf_fin, (m*(Ro - Ri))	0.701607	
eta_fin (efficiency)	0.692722	

APPENDIX C – STEADY-STATE LOOP NATURAL CONVECTION MODEL

Figure 2 shows a schematic view of the natural convective flow circuit for the vessel carbon dioxide coolant that removes decay heat from the tubes of fuel in the tube reactor concept. This cooling would always be present while the reactor is running but would only be needed during accident situations to remove decay heat when other paths of heat removal were not available or not effective. The same schematic view could also be applicable to the main flow circuit in a reactor when the flow compressors are not turning. For example, it could be used to analyze the helium flow in a gas-cooled reactor under shutdown conditions with the compressors not running. In this case the fueled region could be the pin-bundle length in a pin core or the lengths of the fuel blocks in a block core. In the model, only the region labeled "core (heat source)" provides heat to the flowing coolant. All three sections of the fueled region, however, contribute to hydraulic resistance, but the core section and the one above it also contribute to buoyancy. The bottom section does not contribute to buoyancy because it is at the same temperature as the cold leg.

In the model all of the coolant between the core exit and the heat exchanger inlet is at the hottest temperature in the loop. All of the heat produced is produced in the core and is rejected by the heat exchanger, located at the top of the loop. This heat exchanger is not explicitly included in the model. Its hydraulic resistance is assumed to be zero. However, other hydraulic resistances, in particular, the entrance and exit losses of the fueled region, can be increased to account for the heat exchanger resistance. The exit coolant temperature of the heat exchanger, which is also the uniform temperature of the cold leg, is an input quantity to the model.

The fluid flows around the loop because the coolant in the cold (down-flow) leg is on average denser than the coolant in the hot (up-flow) leg. The differences in density are a direct result of temperature differences around the loop. The speed at which the coolant flows around the loop is the result of a balance between the buoyancy pressure rise around the closed loop and the sum of the friction-type pressure drops caused by the fluid flowing around the loop.

The model for the natural convective flow around the cold finger loop, which is shown schematically in Figure 10, is conceptually the same as that shown in Figure 2. As explained in Chapter 7, the hot leg side is the same as in Figure 2, except that the names of some of the sections have been changed. Also, as explained in Chapter 7, additional hydraulic resistances have been added to the cold leg in the cold finger model. This added resistance is to account for the hydraulic resistance of the down-flow annulus in the cold finger.

The vertical separation between the heat source and the heat sink, label "chimney" in Figures 2 and 10, is very important. As the length of the chimney increases the buoyancy force increases and causes the flow to increase. In the current idealized model there are no hydraulic losses associated with either the chimney or any of the down-flow piping. However, in some situations these losses may be significant. In such instances, part of the increase in performance caused by a longer chimney will be diminished by these increased losses.

The mathematical model for the steady-state natural convective flow consists of the continuity, momentum, energy equations. The continuity equation simply states that the flow rate at all points in the loop is a constant. The momentum equation just equates the net buoyancy pressure rise with the total pressure drop due to hydraulic resistances. The energy equation provides the temperature at the exit of the core, or heated section, given the inlet temperature of the core, the flow rate, and the specific heat capacity of the fluid. Since all of the heat is assumed to be added at a uniform rate over the length of the core the coolant temperature rises linearly over the length of the core. The precise variation of coolant temperature with length over the core length is not important when core length is short compared to the height of the loop.

The energy equation can be easily manipulated to provide, $T(x)$, the gas temperature along the heated length, as follows:

$$T(x) = T_{in} + \frac{q'}{\dot{m} c_p} x = T_{in} + (T_{out} - T_{in}) \frac{x}{L_{core}} \quad (C.1)$$

where T_{in} is the inlet temperature to the core or cold finger, q' is the power per unit length over the core region, \dot{m} is the coolant flow rate, c_p is the specific heat capacitance of the coolant, and x is the distance from the inlet, T_{out} is the outlet coolant temperature, and L_{core} is the core length. The last part of equation C.1 states that the temperature is linear with length and is T_{in} at the inlet and T_{out} at the exit.

The buoyancy pressure drop, ΔP_{buoy} is given by:

$$\Delta P_{buoy} = g \int_{loop} \rho dx \quad (C.2)$$

where g is the acceleration due to gravity, ρ is the local density of the coolant, and x is the distance along the length of the closed loop going upward along the hot leg and downward along the cold leg.

The ideal gas law allows the density of the gas to be related to its absolute temperature, T , and its absolute pressure, P , as follow:

$$P = \rho R T \quad (C.3)$$

where R is the ideal gas constant for the gas under consideration. In all cases studied, the variation in pressure around the flow circuit was small compared to the system absolute pressure. Therefore, P was always taken to be the system pressure.

Combining equations C.1 through C.3, one obtains:

$$\Delta P_{buoy} = \frac{gP}{R T_{in}} \left[\left(1 - \frac{\ln \frac{T_{out}}{T_{in}}}{\frac{T_{out}}{T_{in}} - 1} \right) L_{core} + \left(1 - \frac{T_{in}}{T_{out}} \right) (L_{above} + L_{chim}) \right] \quad (C.4)$$

where, L_{above} is the unheated vertical section between the top of the core and the bottom of the chimney and L_{chim} is the length of the chimney. In equation C.4 these two length could be combined and into one quantity since both are unheated lengths above the core. However, the distinction is maintained because L_{above} can contribute considerably to the friction pressure drop while L_{chim} contributes nothing in the model.

The friction pressure drop due to a form loss, ΔP_K is given by:

$$\Delta P_K = K \frac{1}{2} \rho v^2 = K \frac{1}{2} \frac{\dot{m}^2}{\rho A^2} \quad (C.5)$$

where K is the form loss, v is the coolant velocity, and A is the flow area of the channel for which the inlet or exit form loss is to apply. The part of equation C.5 to the right of the second equals sign was derived by using the continuity equation to obtain the local velocity from the applicable flow area and density. The continuity equation is given by:

$$\dot{m} = \rho v A \quad (C.6)$$

The friction pressure drop (not including form loss), ΔP_f , for a uniform channel of flow area A, hydraulic diameter, d_h , and length, L, is analogous to that of the form loss provided in equation C.5 with K replaced by the product of Moody friction factor, f, and the ratio L/d_h . Because both friction factor and density are functions of x, the distance along the length of the channel, ΔP_f , is given by:

$$\Delta P_f = \frac{1}{2} \frac{\dot{m}^2}{A^2 d_h} \int_0^L \frac{f(x)}{\rho(x)} dx \quad (C.7)$$

Friction factor and density vary over the core region because of the heat transferred to the coolant from the core. When there is no heat addition, the integral in equation C.7 is simple $f \times L/\rho$.

In the model it was assumed that for laminar flow $f = 64/Re$, where Re is the Reynolds number, and that for turbulent flow the Blasius formula, $f = 0.316/Re^{0.25}$, applies. The transition between laminar and turbulent flow was assumed to occur at the value of Re where the two relationships for f intersect, i.e., $Re = 1189.4$. By definition Reynolds number is given by the following:

$$Re \equiv \frac{\rho v d_h}{\mu} = \frac{\dot{m} d_h}{\mu A} \quad (C.8)$$

where μ is viscosity.

For a given flow rate and geometry, the only independent variable in Re is μ , which is a function of temperature. Hence, for laminar flow friction factor is proportional to μ and for turbulent flow it is assumed to be proportional to μ to the 0.25 power. Viscosity, μ , increases with temperature in both carbon-dioxide and helium. For example, between 480° C, the proposed reactor coolant inlet temperature, and 1600° C, the expected allowed peak fuel temperature, the viscosity of both carbon dioxide and helium increases by a factor of 1.9. In the current analysis, f in equation C.7 was treated as a constant and was evaluated at the average of the channel inlet and outlet temperatures. This approximation may be reasonable in some instances, but should be investigated further in the future. For a more precise treatment of the effects of temperature on the friction pressure drop in a heat channel with gas coolant, refer to Reference C.1.

The pressure drop due to hydraulic resistance for the up-flow (hot) leg of both the Figure 2 and the Figure 10 model, $\Delta P_{\text{fric_up}}$, is given by:

$$\Delta P_{\text{fric_up}} = \frac{1}{2} \frac{R T_{\text{in}}}{P} \frac{\dot{m}^2}{A^2} \times \left[\left(K_{\text{up_in}} + f_1 \frac{L_1}{(d_h)_1} \right) + \frac{f_2}{2} \frac{L_2}{(d_h)_2} \left(1 + \frac{T_{\text{out}}}{T_{\text{in}}} \right) + \left(K_{\text{up_out}} + f_3 \frac{L_3}{(d_h)_3} \right) \frac{T_{\text{out}}}{T_{\text{in}}} \right] \quad (C.9)$$

where the subscripts 1, 2, and 3 refer the section below the core, the core section, and the section above the core, respectively, of the fueled region in Figure 2 or the (heated) annulus in Figure 10. The flow area, A, was assumed to be the same for each of these three sections. The subscripts "in" and "out" refer the entrance and the exit of the fueled region in Figure 2 or the (heated) annulus in Figure 10, respectively. The quantity P is the system pressure. In the model,

typically, K_{up_in} was taken to be 0.5 and K_{up_out} was taken to be 1.0. In equation C.9, the quantity (RT_{in}/P) was obtained from the ideal gas relationship and is the reciprocal of the inlet fluid density. In the ideal gas relationship, T_{in} must be in units of absolute temperature. Therefore, T_{out} also must be in units of absolute temperature. Equation C.9 was obtained by summing three pressure drops, one for the entrance form loss, one for the friction over the heated region, and one for the exit form loss.

For the Figure 2 model, the entire pressure drop due to hydraulic resistance is given by ΔP_{fric_up} . However, the cold finger model has this pressure drop and another one due to its down-flow annulus. This additional pressure drop, ΔP_{fric_down} is given by:

$$\Delta P_{fric_down} = \frac{1}{2} \frac{RT_{in}}{P} \frac{\dot{m}^2}{(A_{down})^2} \left[K_{down_in} + f_{down} \frac{L_{down}}{d_{down_h}} + K_{down_out} \right] \quad (C.10)$$

where A_{down} is the flow area of the down-flow annulus, K_{down_in} and K_{down_out} are the entrance and exit form losses, respectively, for the down-flow annulus, and f_{down} is the friction factor for the down-flow annulus.

The momentum equation is obtained by equating the buoyancy pressure rise, equation C.4 with the sum of the pressure drops due to hydraulic resistance. For the cold finger model the sum of the pressure drops due to hydraulic resistance is the sum of ΔP_{fric_up} and ΔP_{fric_down} . For the other loop model, which is the one used for the tube reactor analysis and for natural convection involving flow through pin and block reactor cores, ΔP_{fric_down} is zero and hence in this case the sum of the pressure drops due to hydraulic resistance is just ΔP_{fric_up} .

The energy equation may be used to find the outlet temperature from the heat vertical section in the model given the power transferred to the coolant, q , and the coolant flow rate. Hence:

$$q = \dot{m} \times c_p \times (T_{out} - T_{in}) \quad (C.11)$$

This is just a variation of equation C.1.

The momentum and energy equations and all of the needed ancillary relationships, identified above, were represented on a computer spreadsheet and an automatic solver was used. Separate spreadsheets were devised for each of the two types of natural convective loop. A thermal model for the cold finger, as described in Appendix D, was developed and included with the cold finger loop hydraulics model. This enabled cold finger hydraulic and thermal models to be solved simultaneously. This is the combined steady-state model identified in Chapter 7.

The critical point for carbon dioxide is at 31.1° C and 7.38 MPa (87.8° F and 1070.6 psia). Thus, in some instances when carbon dioxide coolant is used, it will be in a supercritical state. However, the above steady-state loop natural convection model does not specifically consider coolant behavior near the critical point or in the supercritical range. The ideal gas relationship is assumed to apply for all conditions and the rapid changes in fluid properties that occur near the critical point have not been taken into account. Therefore, a better representation of the properties of carbon dioxide should be considered for future analysis. It is possible that such analysis may show better natural convective performance than is currently predicted. Also, it may be desirable to avoid operation near the critical pressure and this could require that higher pressures be considered.

References:

- C.1 E. E. Feldman and T. Y. C. Wei, "Core Key Mechanical Design Evaluation for a Pebble-Bed Gas-Cooled Fast Reactor," Nuclear Energy Research Initiative Project #01-022: Particle-Bed-Gas-Cooled Fast Reactor (PB-BCFR) Design, Task 2.1 Milestone/Deliverable, Nuclear Engineering Division, Argonne National Laboratory, February 2003

APPENDIX D – STEADY-STATE THERMAL MODEL FOR COLD FINGERS

As described in Chapter 7, the steady-state thermal model for an individual cold finger model is axially symmetric. If there are to be N cold fingers in the reactor core, then $1/N$ th of the fuel is assumed to be formed into a uniform concentric annulus whose height is the height of the reactor core and whose inside diameter is that of the outer diameter of the pressure tube of the cold finger. The outside diameter of the fuel annulus is calculated so that the volume of the annulus is $1/N$ th the total volume of fuel in the core.

The geometry of the model is a two-region concentric annulus with the outer region representing the fuel and the inner one representing the pressure tube of the cold finger. All exterior surfaces of the model are insulated except for the inner surface of the pressure tube. This surface has a convective boundary condition consisting of a film coefficient, h , and a free stream fluid temperature. Since axial heat conduction is not considered in the model, the model is actually one-dimensional with heat transfer only in the radial direction. The hottest temperature is at the insulated boundary at the outer radius of the fuel annulus. Since the axial power distribution is assumed to be uniform, the hottest fuel temperature occurs at the exit plane of the cold finger coolant channel where the coolant temperature is the hottest. Thus, the free stream fluid temperature is set to the coolant outlet temperature, T_{out} .

The assumption of a uniform axial power distribution is too optimistic because the heat generation rate at the middle plane of the core, which is where the peak is expected to occur, is expected to be about 32% greater than the average. Thus, the hottest fuel temperature would be at a short distance above the middle plane, where the heat generation rate is just below the peak value and where the cold finger coolant temperature is less than its exit value. This effect could be approximated with the current steady-state model by increasing the core decay power proportionately to correspond to the peak. Such an approximation would predict peak temperatures (at the exit) that are too high by perhaps about 60 to 70° C. The temperature would be too high mostly because the coolant temperature to be used in such a calculation is the one at the axial location where the peak fuel temperature occurs and not the one at the exit for a core with much more than the average power.

The temperature rise from T_{out} to the maximum fuel temperature, located on the outer surface of the fuel, is the sum of three temperature rises – the film temperature rise from the free steam to the inner surface of the pressure tube, the temperature rise across the pressure tube annulus, and the temperature rise across the fuel annulus. The film temperature rise is just the heat flux at the surface, q'' divided by the film coefficient, h . Thus, T_1 , the temperature at the inner surface is given by:

$$T_1 = T_{out} + \frac{q''}{h} \quad (D.1)$$

The relationship for h was obtained from the following equation:

$$Nu = \frac{h d_h}{k} = 0.22 Re^{0.8} Pr^{0.4} \quad (D.2)$$

where Nu is Nusselt number, d_h is the hydraulic diameter of the annular flow region, k is the thermal conductivity of the coolant, Re is the Reynolds number of the coolant, and Pr is the number of the coolant. The Reynolds number is defined as follows:

$$Re = \frac{\rho v d_h}{\mu} = \frac{\dot{m} d_h}{\mu A} \quad (D.3)$$

where ρ and μ are the density and viscosity of the gas, respectively, \dot{m} is the flow rate of the gas, and A is the flow area. Equation D.2 is typical of the Dittus-Boelter-type of relationships used for predicting Nusselt numbers in turbulent gas flows in round tubes and annuli. The fluid properties of k , ρ , and μ must be evaluated at the average of free stream and surface temperatures. This is easily accomplished on a computer spreadsheet where nonlinear relationships can be easily represented and solved simultaneously.

The equation for steady-state one-dimensional heat conduction with constant conductivity, k , in radial coordinates, r , is:

$$\frac{1}{r} \frac{d}{dr} \left(r \frac{dT}{dr} \right) = -\frac{q'''}{k} \quad (D.4)$$

where T is temperature and q''' is volumetric heat generation rate. For the pressure tube region this equation can be solved with q''' set to zero and with boundary conditions of a known heat flux at the outer radius and a known temperature, T_1 , at the inner radius. Since all of the power leaving the fuel annulus exits uniformly through its inner surface and enters the outer surface of the pressure tube, the heat flux at the outer surface of the pressure tube is just the power per unit length of the fuel annulus, q' , divided by the circumference of the annulus. Thus, equation D.4 can be solved to obtain a relationship for the temperature at the outer surface of the pressure tube, T_2 , as follows:

$$T_2 = T_1 + \frac{q'}{2\pi k_t} \ln \frac{d_2}{d_1} \quad (D.5)$$

where k_t is the thermal conductivity of the tube and d_1 and d_2 are the inner and the outer diameter of the pressure tube, respectively. Equation D.4 can also be solved over the fueled annulus with boundary conditions T_2 at the inner surface and an insulated condition, i.e., $dT/dr = 0$, at the outer surface. The resultant equation can be solved to obtain a relationship for the temperature at the outer surface of the pressure tube, T_3 , as follows:

$$T_3 = T_2 + \frac{q''' (d_3)^2}{16k_f} \left[\ln \left(\frac{d_3}{d} \right)^2 + \left(\frac{d_2}{d_3} \right)^2 - 1 \right] \quad (D.6)$$

where q''' is the volumetric heat generation rate of the fuel, k_f is the effective thermal conductivity of the fuel and d_2 and d_3 are the inner and outer diameter of the fuel region, respectively.

The thermal conductivity of the tube was assumed to be a constant and 15 W/m-K was typically used. The fuel is configured as a pebble bed and was modeled as a homogeneous region. The effective thermal conductivity was calculated as a function of temperature as described in Chapter 5.1 of Reference 1. This produced a table of temperature versus conductivity. A third-order polynomial was fitted to this data. The value of k_f used in the solution was obtained by evaluating the third-order polynomial at the average of T_2 and T_3 .

Task 3: Mechanical Design

The following paragraphs are highlights of activities conducted in the mechanical design area in the two years of the project. These activities investigated the vibration response of fuel element/assembly, flow instability, and thermal stress issues for the PB-GCFR design using cold fingers.

3.1 Core Key Mechanical Design Evaluation for a Pebble-Bed Gas-Cooled Fast Reactor (E. E. Feldman, T. Y. C. Wei)

ABSTRACT -- *The subject of this report is the investigation of key mechanical design issues that affect the engineering feasibility of a gas-cooled fast reactor core design based on the use of pebble fuel elements. The key driving safety issue identified to date is the passive removal of decay heat under depressurized conditions. A novel concept, labeled "cold fingers", was introduced to resolve this issue. Since this is a first-of-a-kind device, the mechanical design of the cold fingers requires initial scoping analyses to determine feasibility to solve the driving safety issue. The focus of this report is therefore the analysis of the mechanical design of the cold fingers. These bayonet-type heat exchangers are attached to the upper head of the reactor vessel, extend through the upper plenum, and are immersed in the fueled pebble bed. Thus, they are subjected to a very severe thermal and neutronic environment. In addition, the flow in the upper plenum potentially can cause unacceptable vibrations in the cold fingers. Because the viscosities of the gases being considered for coolants increase with temperature, there is a potential for flow instabilities in the pebble bed that could also lead to cold finger structural failures.*

All of the above issues have been addressed, although some are treated in only a preliminary manner. Finding a material that could meet all of the structural, thermal, and neutronic requirements could be a daunting task. Materials that are currently being developed for future fusion reactors may be the best choices, but none of them are completely suitable. However, the properties of some of the SiC/SiC composites seemed to indicate that these composites are the best choice at this time and hence their properties were used for the current analysis.

A reasonably complete and definitive theoretical analysis of flow instability was performed. This analysis clearly demonstrates that while flow instability is theoretically possible under some extreme conditions, none of those conditions is anticipated in a gas-cooled power reactor of the type being considered. The initial preliminary analysis of flow-induced vibration indicates that it is too early in the design phase to be able to provide a definitive answer, but there is a potential problem here. Hence, there is a need to do analysis of flow-induced vibration in parallel with the development of the design, so that the problem can be avoided before the reactor is constructed and while design changes are relatively easy and inexpensive to make.

1.0 INTRODUCTION

The subject of this report is the investigation of key mechanical design issues that affect the engineering feasibility of a gas-cooled fast reactor core design based on the use of pebble fuel elements. The key driving safety issue identified to date is the passive removal of decay heat under depressurized conditions. The "cold fingers" concept was introduced to resolve this issue. Since this is first-of-a-kind, the mechanical design of the cold fingers requires initial scoping analyses to determine feasibility to solve the driving safety issue. The focus of this report is the mechanical design of the cold fingers, which are a series of bayonet heat exchangers used for passive decay heat removal. These heat exchangers are inserted vertically through the top of the reactor vessel

(see Figure 1). Each of these cold fingers removes heat from the fuel pebbles in its immediate vicinity. In order to minimize the number of penetrations through the top of the reactor head, each cold finger would have a control rod along its centerline, as shown in Figure 2. High-pressure carbon dioxide at the same pressure as the reactor helium coolant, currently assumed to be 7 MPa, is used as the cold finger coolant. A cold finger therefore serves the dual purpose of reactivity control and passive decay heat removal. It provides the housing for the control rod as well as the means of decay heat removal by the carbon dioxide circuit.

As shown in Figure 2, the coolant flow for the cold finger enters at the top of the finger and travels down an annulus around the control-rod guide thimble. This flow also serves to cool the control rod. At the bottom of the cold-finger, the coolant flow makes a U-turn and travels upward along the outer annulus. An insulator tube separates the cold downward flow from the upward flow, which is heated by the adjacent pebble bed. As shown in Figure 1, the hot flow from the cold finger is convected to an external heat exchanger where the heated carbon dioxide is cooled by a stream of atmospheric air drawn through a natural-draft cooling tower. There probably would be only one of these towers. Several or all of the cold fingers would be attached to a single external heat exchanger or a series of heat exchangers.

The bayonet design with the carbon dioxide flow making a U-turn at the bottom of the cold finger was chosen so that each cold finger would require only one penetration through the reactor vessel boundary, instead of one at the top and one at the bottom. As indicated in Figure 1, the sealing flange, identified in Figure 2, is used to provide a leak-tight seal between the cold finger and the reactor head. The outer wall of the outer annulus is referred to as a "pressure tube" because it is a tube that separates the high-pressure carbon dioxide of the cold finger from the high-pressure helium of the reactor core. Whenever either gas is depressurized and the other is at full pressure, the pressure tube must withstand the full pressure of the pressurized gas.

There are no pumps in the carbon dioxide coolant circuit and all of the flow is by natural convection. Thus, the elevation difference between the cold finger and the external carbon-dioxide-to-air heat exchanger is important. Another observation is that a failure of a pressure tube would not cause a breach of the helium pressure boundary unless there was a concurrent breach of the external portion of the carbon-dioxide circuit. A pressure tube failure, however, would enable the two gases to mix.

The control rods and their drive mechanisms would be totally encased inside the carbon-dioxide pressure boundary. As is done in pressurized water reactors, all of the control rod latching and motion is accomplished by electromagnetic induction through the pressure boundary wall. This avoids the need for moving seals and the leakage associated with them. The flowing carbon dioxide will also serve to cool the control rods. The control rod guide thimble walls will need to be perforated near the top to allow coolant to be displaced easily, but may need to be nonperforated near the bottom so that compressed gas near the bottom can be used to slow the rod as it approaches the end of its travel. A tight clearance between the rod and thimble could be used here for damping.

The cold fingers extend from the reactor vessel head to the bottom of the pebble bed. Thus, they are very long, about 8.5 m, and relatively small in outside diameter, about 24 cm. The reactor coolant must flow along and across them and thus flow-induced vibration is a potential problem. Since the bottom approximately 2 m of the cold finger is located in the pebble bed, it is subject to high temperatures and neutron fluences. Because it serves as a heat exchanger, there can be substantial temperature gradients across its external (pressure tube) wall. Since it provides the boundary between the pressurized reactor helium coolant and its own high-pressure carbon

dioxide coolant, it must withstand large pressure gradients during depressurization accidents. These accidents can be caused by a depressurization on either the helium side or the carbon dioxide side.

Another issue addressed by this report is the potential for flow instability. For gases, including helium and carbon dioxide, viscosity increases with temperature. This phenomenon enables one to postulate that a single value of pressure drop can correspond to two values of flow and that a self-initiating oscillation or flow instability could occur at a fixed pressure drop as the flow varies between its two values. Although this phenomenon is purely thermal-hydraulic, its effects can be extremely detrimental to the internal structures of a reactor.

Chapter 2 addresses the selection of a suitable material for the pressure tube of the cold finger, Chapter 3 briefly examines thermal stresses in this tube, Chapter 4 provides an analytical criteria to assure flow stability, Chapter 5 provides an initial analysis of the potential for cold finger flow-induced vibrations, and Chapter 6 provides conclusions to the work.

2.0 SELECTION OF MATERIALS

The portions of the cold finger of particular interest here is the pressure tube. During normal operation, it has a 7 MPa (~1015 psia) internal carbon dioxide gas pressure and the same external gas pressure of helium. During a core depressurization accident the external pressure could go to one atmosphere. The cold finger must also be able to withstand the full helium pressure (7 MPa) should the carbon dioxide gas inside it depressurize to one atmosphere.

Another requirement is that the cold finger pressure tube must withstand high temperatures and possibly large temperature gradients. The cold finger pressure tube is in direct contact with the pebble bed. Under normal operating conditions the helium exit coolant gas is at 850° C. The pebble surface temperature will be about 100° C above this temperature, or 950° C. The cold fingers serve as the heat sinks and have carbon dioxide gas temperatures in the range of 50 to 150° C. If during normal reactor operation, the flowing carbon dioxide gas in the cold finger should become depressurized, the cold fingers would essentially stop removing heat from the core and the pressure tube could reach temperatures between 850 and 950° C. During an upset condition in which the helium is depressurized to one atmosphere, which is when the cold fingers are needed to prevent excessive fuel temperatures, the fuel pebble temperatures could go to 1600° C or higher, but this is at locations furthest from the cold fingers. Accurately, specifying the peak temperature that the cold finger pressure tubes must withstand may require more detailed thermal analysis of the interface between the cold finger and the pebble bed. The current estimate is that the peak pressure tube temperature is 1000° C, but it could be 1200° C, or more. Of course, it would be desirable to use a material that can withstand much more than 1000° C if all other things are equal.

Another consideration is that the pressure tube should also have a relatively high thermal conductivity so that heat can flow through it without producing a large temperature gradient. A thermal conductivity at least in the range of stainless steels (~15 W/m-K) would be highly desirable.

However, if the material is much stronger than stainless steel, then the tube wall thickness could be made much thinner. This could compensate for a lower thermal conductivity.

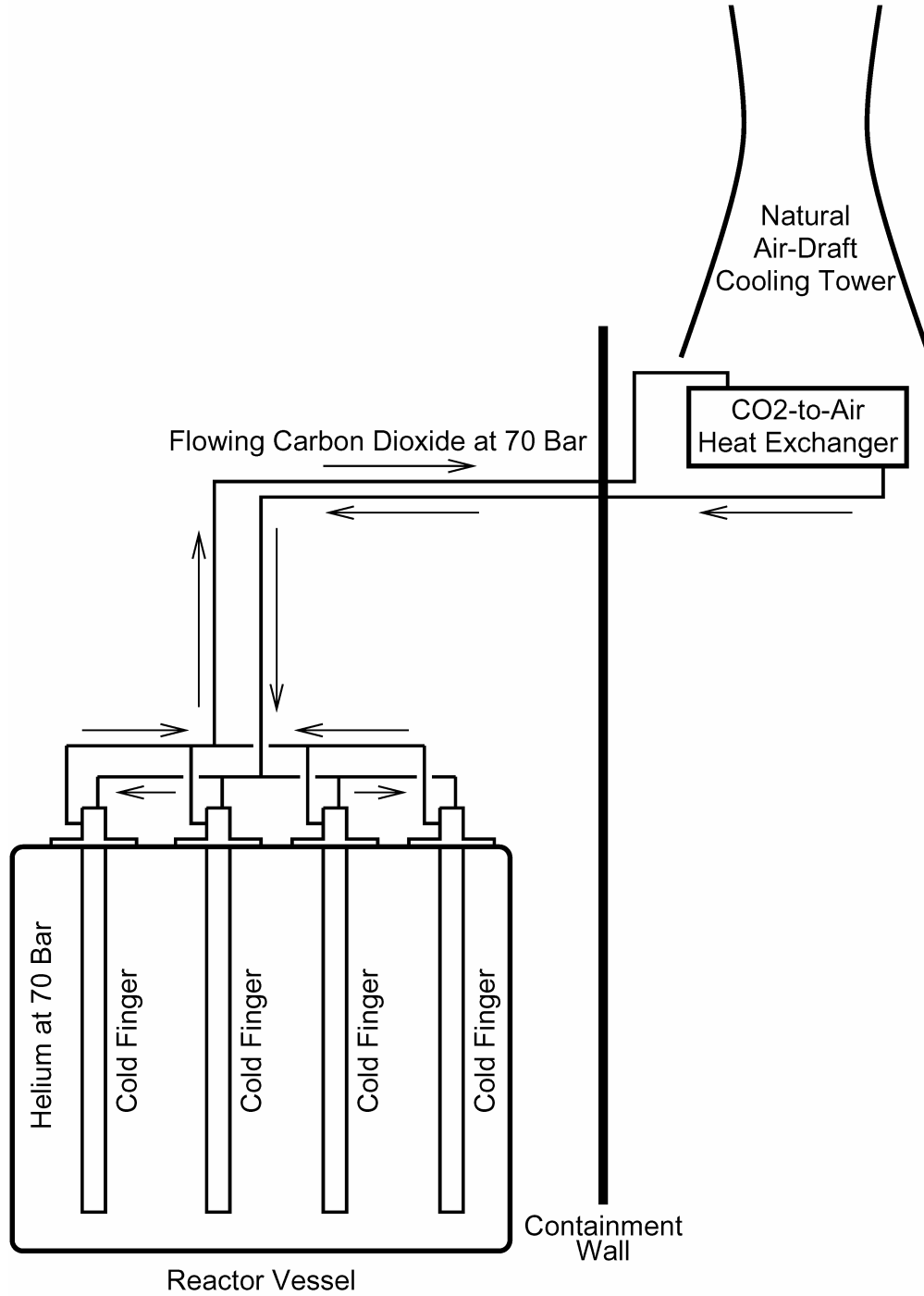


Figure 1. Cold Finger Concept.

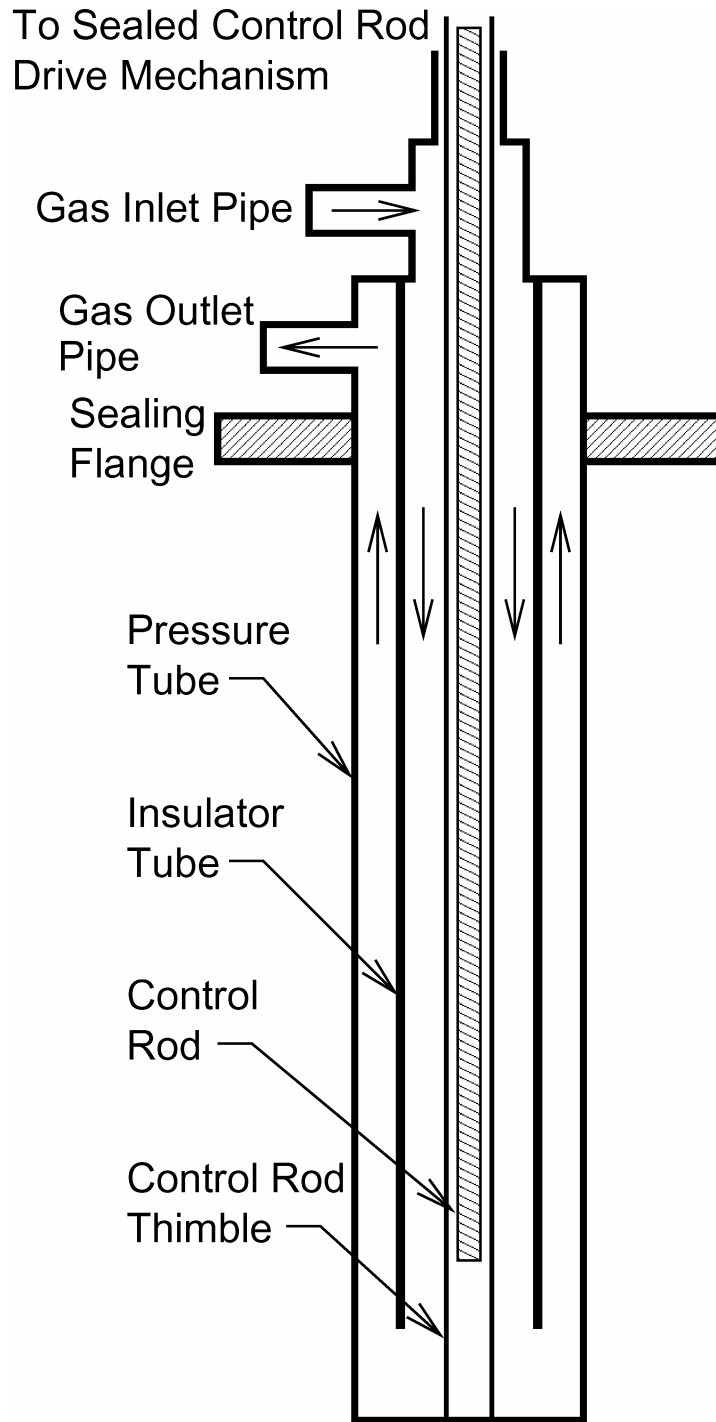


Figure 2. Cold Finger Design.

The coefficient of linear expansion is important because thermally-induced stresses tend to be proportional to this property. Therefore, the lower this parameter is the better it is. How important and limiting or unimportant this parameter is will become more obvious in Chapter 3.0

The next two considerations are neutronic. First, the material must be a poor neutron absorber and second, it must be able to withstand a high neutron fluence. A one-batch core, i.e., no refueling, is to be used. For 15% burnup the fluence is estimated to be about 1×10^{24} neutrons/cm² at the end of the one-batch core life.¹

During a major depressurization accident there could be an ingress of air, which could cause oxidation of the material. Thus, resistance to oxidation also could be an additional criterion.

Information from the ANL/CEA I-NERI project² was obtained regarding choices for materials selection. There is no material available that could meet all the above criteria. It is noted in Reference 2 that the required fluence capability, in particular, is beyond anything ever measured. Reference 2 also indicated that some of the materials research for the fusion reactor program could be helpful and that based on the above requirements the following materials could be considered as possible candidates:

- W
- Mo(TZM)
- Ta-8W-2Hf
- Nb-1Zr-0.1C
- SiC/SiC composites

The reference further stated that:

The Ta and Nb alloys have unacceptable oxidation above $\sim 600^\circ\text{C}$ for any significant oxygen concentration so Ta and Nb alloys are unlikely to be acceptable unless a coating method can be found that be applied and can handle the possible harsh temperature transients. Tungsten and Mo have a similar problems above $\sim 800^\circ\text{C}$, although recent success has been made with a Mo-6Ti-2.2Si-1.1B alloy.

The reference then concluded that the only potentially viable material in the above list of five is SiC/SiC composites. The reference also stated that unfortunately, this alloy is not well studied and nothing is known about the irradiation response and that additionally, Mo alloys cannot be operated in a neutron irradiation environment at temperatures less than ~ 1000 K due to low temperature radiation embrittlement effects. It also pointed out that currently no production capability exists for the Ta, Mo, and Nb alloys. It then concluded that the best candidates to consider for now are the SiC/SiC composites and included the caveat that there are major holes in the experimental database, especially given the high fluence targets. Reference 2 provided four publications, including References 3 and 4, and also Figure 3, which came from Reference 4. Reference 4 stated: "The light shade bands on either side of the dark bands represent the uncertainties in the minimum and maximum temperature limits."

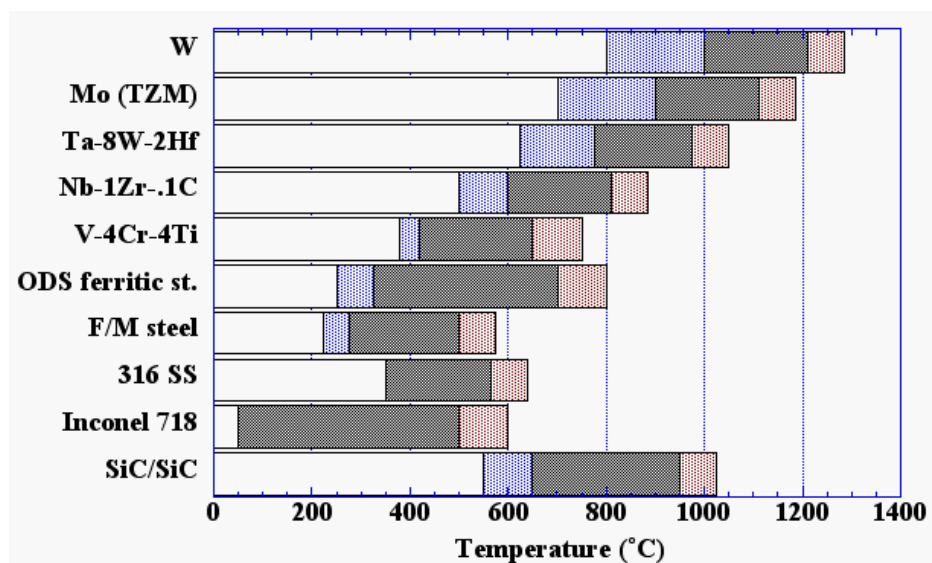


Figure 3. Estimated Operating Temperature Limits for Structural Alloys in Fission Reactors: 10-50 dpa. [4]

Based on previous information and that in Table 1, [3] it is assumed for now that the pressure tubes will be made of SiC-based composite material. An appropriate choice of composite will probably require further development and testing and may not be available until far into the future when the reactor currently under consideration is to be built. For the current analytical requirement, representative property values will be taken from the table. Where appropriate, these will be compared with their counterparts for iron or steel, as a means of gauging the values utilized in this study.

Table 1. Comparison of properties of commercial SiC-based fibers and bulk SiC. [3]

Property	cg-Nicalon	Hi-Nicalon	Hi-Nicalon type S	Dow Sylramic	Bulk SiC
Diameter (μm)	14	12-14	12	10	--
Tensile strength (GPa)	2.0-3.0	2.8-3.4	2.6-2.7	2.8-3.4	~0.1
Elastic modulus (GPa)	170-220	270	420	390-400	460
Density (g/cm^3)	2.55	2.74	2.98-3.10	3.0-3.10	3.25
Coefficient of thermal expansion ($10^{-6}/\text{K}$)	3.2	3.5	--	5.4	4.0
Thermal conductivity at 20°C (W/m-K)	1.5	4	1.8	40-45	100-350
Oxygen Content (w%)	11.7	0.5	0.2	0.8	0.0
C/Si atomic ratio	1.31	1.39	1.05	1.0	1.0

3.0 THERMAL STRESS ANALYSIS

A detailed structural analysis would necessarily consider the combined stress state produced by all of the loads simultaneously applied to the pressure tube of the cold finger, including those caused by internal or external pressures and also variations in temperature throughout the volume of the cold finger. In addition, the failure modes would have to consider the composite material and its anisotropic nature. For example, delamination and the breaking of individual fibers may need to be considered. However, for the current initial preliminary assessment a very simple approach will be used to analyze the pressure tube. The heat transfer through the pressure tube under steady-state conditions will produce an essentially linear temperature drop from the outer surface of the tube to the inner. At points far from the ends of the tube, the thermal stress can be estimated from the following formula provided by Reference 5.

$$\sigma_{\max} = \frac{\alpha E (t_1 - t_2)}{2(1 - \mu)} \quad (15)$$

where σ_{\max} is the peak stress, α is the coefficient of thermal expansion, E is Young's (or the Elastic) modulus, t_1 and t_2 are the temperatures at the inside and outside surfaces of the tube, respectively, and μ is Poisson's ratio.

Based on the Table 1 in Chapter 2.0, E is taken to be 200 GPa, α is taken to be $3.5 \times 10^{-6} \text{ K}^{-1}$, and the maximum allow stress is taken to be 2.0 GPa. Iron has an E comparable to that being used here and an α of about $12 \times 10^{-6} \text{ K}^{-1}$. For 18-8 stainless steel the tensile strength is about 0.6 GPa. Although Reference 2 does not provide a value for μ for SiC-based fiber materials, it does provide a value of 0.18 for bulk SiC. This is to be compared with 0.25 to 0.33 for steel. Therefore, 0.18 will be assumed here. Since t_2 is greater than t_1 , σ_{\max} is negative. This merely implies that the maximum stress is compressive instead of tensile. Thus, equation 1 can be solved to obtain the maximum allowed temperature difference and for the SiC properties assumed here a value of about 4700° C is obtained.

Steady-state thermal analysis of the cold fingers indicates the temperature drop across the pressure tube wall thickness is about 100° C (Reference 6) when the thermal conductivity of the wall is taken to be 15 W/m-K. The values of thermal conductivity shown in the table of Chapter 2.0 indicate that the thermal conductivity for the SiC material will be about an order of magnitude lower. That would yield a temperature differential of about 1000° C and probably yield an acceptable thermal stress level. However, a 1000° C wall temperature drop would not be acceptable from a heat transfer perspective and would challenge fuel limits. A possible fix is to take advantage of the much greater strength of the SiC material to design a much thinner wall. In addition, perhaps a SiC material with a thermal conductivity of at about 4.0 W/m-K can be selected, based on the table in Chapter 2.0. However, a very thin wall could make the pressure tube susceptible to a buckling failure when it is subjected to a compressive external pressure load. In conclusion, obtaining a material with a suitable combination of structural and thermal properties will be a challenge.

4.0 FLOW INSTABILITY

A flow instability in the pebble bed near a cold finger can have a substantial adverse effect on the local coolant temperatures, which could, in turn, have a severe impact on the structural behavior of the cold fingers. The potential for a flow instability exists in gases, such as helium and carbon dioxide, in which fluid viscosity increases with temperature. A flow instability is possible because a small decrease in flow, due to a slight perturbation, can cause an increase in fluid temperature,

which in turn can cause an increase in fluid viscosity and hence a further decrease in flow. If this chain of events could somehow feed on itself, a significant decrease in flow is possible. Conversely, one can postulate a small increase in flow eventually driving a significant increase in flow. In mathematical terms this would imply that a single value of pressure drop can correspond to both a relatively high flow (with a relatively low value of viscosity) and a relatively low flow (with a relatively high value of viscosity). Under these circumstances a self-initiating oscillation or flow instability could occur at a fixed pressure drop as the flow varies between these two extremes or the flow in each region could go to one of the extremes and remain there. Reference 7, describes an analogous phenomenon, laminar instability, which can occur among a series of parallel channels when the flow in some of the channels is at or near the transition Reynolds number that divides laminar and turbulent flow. References 8-10 analyzes flow instability in a heated channel.

Reference 11 provides the following relationship for pebble bed pressure drop, ΔP :

$$\Delta P = \frac{f}{1 - \epsilon} \frac{H}{d} \frac{1}{2} \rho u^2$$

$$f = \frac{320}{Re_h} + \frac{6}{Re_h^{0.1}} \quad (16)$$

$$Re_h = \frac{Re}{1 - \epsilon} \quad \text{if } Re_h < 10^5, \quad = 10^5 \text{ otherwise}$$

$$Re = \frac{\rho u d}{\mu}$$

where ϵ is the (coolant) void fraction, H is the height of the pebble bed, d is the pebble diameter, ρ is the density of the gas, u is the mean velocity, and μ is the viscosity of the gas. The mean velocity, u , is determined by dividing the volumetric flow rate of the coolant by the flow area that in this instance is determined as if there were no pebbles. For example, if the pebbles are contained in a round tube of radius r , the flow area would be πr^2 .

Because ρ and μ are functions of coolant temperature and coolant temperature varies with distance from the pebble bed inlet, x , $d(\Delta P)/dx$ is a function of x . Therefore, $d(\Delta P)/dx$ can be integrated from $x = 0$ to $x = H$ to obtain the pressure drop from pebble bed inlet to the pebble bed outlet. The quantity $d(\Delta P)/dx$ can be obtained from equation 2 by dividing both sides of the first relationship by H and evaluating the result at the appropriate temperature, i.e., value of x . The velocity, u , can be eliminated from equation 2 by using the continuity equation, which requires that the flow rate, \dot{m} , be the product of ρ , u , and the flow area, A . The idea gas law provides a relationship for ρ as follows:

$$\rho = \frac{P_s}{RT} \quad (17)$$

where P_s is the system pressure, R is the idea gas constant for the gas being considered, and T is the absolute temperature of the gas. The viscosity, μ , can be represented as:

$$\mu = a T^b \quad (18)$$

where a and b are constants. For helium, for example, $a = 3.953 \times 10^{-7}$, $b = 0.687$, T is in Kelvin, and μ is in units of Pa·s.¹⁰ Hence, equation 2 can used to obtain the following:

$$\frac{d(\Delta P)}{dx} = \frac{1}{\frac{\varepsilon^3}{1-\varepsilon}} \frac{1}{d} \frac{1}{2} \frac{\dot{m}^2}{A^2} \frac{f}{\rho} \quad (19)$$

$$Re = \frac{\dot{m} d}{A \mu}$$

In the first relationship of equation 5, f/ρ is a function only of the coolant temperature, T , and T is a function only of x .

For the current analysis it will be assumed that the power per unit length is a constant. Therefore, for constant specific heat capacity at constant pressure, c_p , the coolant temperature rises linearly with distance from the inlet and it can be shown that the coolant temperature, $T(x)$ is given by:

$$T(x) = T_{in} \left(1 + \frac{Q}{\dot{m} c_p T_{in} H} x \right) \quad (20)$$

where Q is the pebble bed channel power and T_{in} is the coolant inlet temperature, $T(0)$.

Now, $d(\Delta P)/dx$ in equation 5 can be integrated over the height of the pebble bed, or from the coolant inlet temperature to the coolant outlet temperature, T_{out} , $T(H)$, to obtain ΔP as follows:

$$\Delta P = C \bar{f} \dot{m}^2$$

$$C = \frac{1-\varepsilon}{2} \frac{H}{\varepsilon^3} \frac{1}{d} \frac{1}{A^2} \frac{1}{\rho_{in}}$$

$$\bar{f} = \frac{X}{\theta - 1} \quad (7)$$

$$\theta = \frac{T_{out}}{T_{in}} = 1 + \frac{Q}{\dot{m} c_p T_{in}}$$

$$X = \frac{320}{Re_h(T_{in})} \frac{1}{b+2} (\theta^{(b+2)} - 1) + \frac{6}{(Re_h(T_{in}))^{0.1}} \frac{1}{0.1b+2} (\theta^{(0.1b+2)} - 1)$$

where ρ_{in} is the coolant density at the inlet to the coolant channel. In the derivation of equation 7 it was assumed that $Re_h < 10^5$. If this were not true then Re_h would be a constant and a flow instability would be impossible here. This assumption will be examined further later.

From a conceptual perspective one could think of picking values for the viscosity exponent, b , and the temperature ratio, θ , and then plotting ΔP as a function of \dot{m} . Then one could observe if in some ranges of ΔP , ΔP versus \dot{m} has two values of \dot{m} for each value of ΔP . A more mathematical approach is to determine if there is a point on the curve where the slope is zero. All points to one side of this point would have a negative slope, which corresponds to an instability – since stable flow is only possible if increasing flow rate results in increasing pressure drop – and all points to the other side would have a positive slope and correspond to stable flow. The slope of the ΔP versus \dot{m} is determined by differentiating equation 7 and is as follows:

Figure 4 indicates that for a helium-cooled reactor, a flow instability could occur if the ratio of reactor outlet to inlet absolute temperature is at least 3.57. This allowed ratio is for very low Reynolds numbers and increases with Reynolds number; it is 29.3 at very high Reynolds numbers. For the current pebble bed application, at rated power the temperature ratio is about 1.5, which is clearly in the stable region for all conceivable flows. For planned operation at powers less than rated power, the temperature ratio would be no greater than that at rated power. For reactor loss-of-flow and overpower accidents, the temperature ratio could temporarily increase to values above 1.5. However, even if the outlet temperature increased by 200° C to 1050° C, the temperature ratio would not exceed 1.8. Although there are dynamic effects that accompany these anticipated accidents that are being ignored here, the temperature ratio is so far from the stability limit that a flow instability is not expected. Moreover, these dynamic effects typically do not last more than the first few minutes of the accident.

The only difference between the choice of helium and carbon dioxide gases, assuming the both behave like ideal gases and both have the same form of viscosity versus temperature relationship, is the viscosity exponent. Thus, for example, if the carbon dioxide exponent were also 0.687, then Figure 4 would apply equally well to carbon dioxide. The carbon dioxide exponent should be investigated or Figure 4 should be redone to include a reasonable range of parametric values of the exponent. However, drastically different results are not expected for carbon dioxide.

Another detail is that the channel pressure drop also has inlet and outlet form pressure losses. However, these are essentially independent of viscosity and inversely proportional to density. If the inlet temperature is constant, then the inlet density is also constant. As the flow rate decreases, it causes the outlet temperature to increase and the density at the outlet to decrease. The exit form-loss pressure drop is proportional to the square of the flow rate divided by the density. It can be shown that the decrease in density is more than offset by the decrease in flow squared. Thus, the exit form loss should have a stabilizing effect. Thus, if Figure 4 shows that the flow is stable, when the form losses are considered the flow will still be stable.

Equation 7 represents a useful byproduct of the current stability analysis. In the past, equation 2 was used to evaluate core pressure drop and all properties were evaluated at the average of the inlet and the outlet temperatures. Equation 7 should be a superior relationship for determining core pressure drop, although large discrepancies are not anticipated at rate conditions. It should be noted, however, that initially the potential for flow instability was investigated by using equation 2 with viscosity and density evaluated at the average of the inlet and outlet temperatures. This less accurate method of determining pressure drop incorrectly indicated that there was no potential for flow instability.

In conclusion, while flow instability has been shown to be theoretically possible under some extreme conditions of temperature ratio, nothing approaching those conditions can be expected for the current gas-cooled fast reactor designs.

5.0 FLOW-INDUCED VIBRATION

Each cold finger is about 24 cm in outer diameter and extends from the top of the reactor vessel head to the bottom of the pebble bed. Although the reactor vessel dimensions are not accurately known, it is anticipated that the unsupported span of the cold fingers from the vessel head to the top of the pebble bed will be about 6.5 m. Since the cold fingers are supported at the top of the vessel head and not at the bottom of the head, the cold finger length along the thickness of the head is part of the 6.5-m span subject to vibration. The reactor coolant must flow across the cold fingers regardless of whether they are in the inlet plenum – which implies a downflow core design –

or they are in the outlet plenum – which implies an upflow core design. In either case, the cold fingers are long slender members that are subject to a cross flow that could cause them to vibrate. In addition, there can be axial flow along the cold fingers that can also contribute to flow-induced vibrations. Reference 12 was consulted for advice in addressing this potential problem of flow-induced vibration.

Reference 12 stated that although some experiments may be needed for a first of a kind reactor, calculations may enable minor or easy adjustments to be made in the design phase that would be very difficult and expensive after the reactor is built. Reference 12 provides an elaborate analytical prescription based on specific parts of Reference 13. According to Reference 12, the cross flow is the most important mode of flow-induced vibration. For this initial preliminary investigation, only this mode will be investigated.

In a downflow reactor design the cold fingers will be in the inlet plenum and in a upflow design they will be in the outlet plenum. Since the inlet temperature is 370° C colder than the outlet temperature, 480 versus 850° C, the downflow design could be the better option from the perspective of the structural integrity of the cold fingers. Since the cold fingers are immersed in the pebble bed and therefore will be subjected to the most severe temperatures, both designs could be equally limiting. The current analysis, however, will focus only on the downflow option.

First, the fundamental natural frequency of the cold finger must be determined. Then the vortex shedding frequency caused by the cross flow must be calculated. Flow-induced vibration can occur if these two frequencies are close together. When there are multiple rods in a cross flow, as there are here, the flow field around each rod can be influenced by the others. However, this should not be a major effect when the rods are relatively far apart, as they are for the cold fingers, and will not be considered at this time.

The relationship for natural frequency of a beam is provided on p. 461 of Reference 13 and is:

$$\omega_n = A \sqrt{\frac{EI}{mL^4}} \quad (22)$$

where ω_n is the angular natural frequency, A is a coefficient provided with the equation in a table on the same page, E is Young's modulus, I is the area moment of inertia, m is the mass per unit length of the beam, and L is the length of the beam. The upper end of the cold finger is fixed to the top of the vessel head and the lower end is imbedded in the pebble bed and is therefore neither totally fixed or totally free. Reference 12 recommended using the fixed-hinged case in the table and to consider only the fundamental mode of vibration, which is the one that produces the lowest frequency. The value of A for this case is 15.4. For the length of beam, Reference 12 recommended using the unsupported length of the cold finger plus half of the pebble bed height.

Because the pebble bed height is assumed to be 2.0 m, L was taken to be 7.5 m. For E, I, and m, only the characteristics of the pressure tube were considered.

Based on the table provided in Chapter 2.0 above, E is taken to be 200 GPa and the density of the tube, ρ , is taken to be 3.0 g/cc. If d_i and d_o are the inner and outer diameter of the pressure tube, respectively, it can be shown that I is one sixteenth of the product of the annular cross sectional area of the tube and the quantity $(d_o^2 + d_i^2)$. It is easy to show that m is the product of the annular cross sectional area of the tube and the density. Hence, equation 9 can be written as:

$$\omega_n = A \sqrt{\frac{E(d_o^2 + d_i^2)}{16\rho L^4}} \quad (23)$$

As equation 10 shows, while l and m in equation 9 are strongly dependent on the tube thickness, i.e., the difference between the tube inner and outer diameters, the ratio of l to m is only a weak function. The outer diameter is taken to be 24 cm. The wall thickness will be assumed be 0.8 cm, which implies that the inner diameter is 22.4 cm. A better understanding of the material properties and an analysis of the structure of the pressure tube is needed to determine accurately an optimal value for the wall thickness. However, as can be seen from equation 10, a relative large change in the wall thickness will have only a small impact on ω_n . Thus, equation 10 is evaluated and ω_n is found to be 183 radian/s, which is divided by 2π radians/cycle to obtain a frequency of 29.2 Hz.

The other half of this analysis is to determine the vortex shedding frequency. For a single cylinder in a uniform cross flow, this is given by equation (7.1) on p. 252 of Reference 11 and is:

$$St = \frac{f_s D}{U} \quad (24)$$

where St is the Strouhal number, f_s is the vortex shedding frequency that is being sought, D is the diameter of the cylinder, d_o for the current case, and U is the cross flow velocity. Values of the Strouhal number are determined experimentally and are plotted as a function of Reynolds number, Re , on p. 255 of Reference 11. Reynolds number is defined as:

$$Re = \frac{\rho_f U D}{\mu} \quad (25)$$

where ρ_f and μ are the density and the viscosity of the fluid, respectively.

The fluid is assumed to be at 7 MPa and 480° C and to behave as an idea gas. Therefore, for helium ρ_f is 4.48 kg/m³ and μ is 37.2×10^{-6} Pa s. The corresponding values for carbon dioxide are 49.2 kg/m³ and 32.3×10^{-6} Pa s. One of the most difficult to determine quantities is the cross flow velocity, U . First the reactor flow rate in kg/s will be determined, second this will be divided by the local fluid density, ρ_f , in order to determine to volumetric flow rate, m³/s, then judgment will be used in determining the effective flow area, and finally the volumetric flow rate will be divided by the effective flow area to determine the flow velocity, U .

The product of the reactor flow rate, \dot{m} , specific heat capacity at constant pressure, c_p , and the coolant temperature rise, ΔT , is equal to the reactor power Q . The power is 300 MWt, ΔT is, 370° C, i.e., the difference between the 850° outlet temperature and the 480° C inlet, and c_p is evaluated at the average of the inlet and outlet temperatures, 665° C. For helium c_p is independent of temperature and is 5193 J/kg-K and for carbon dioxide it is estimated to be 1200 J/kg-K. Therefore, \dot{m} is 156 kg/s for helium and 676 kg/s for carbon dioxide. The corresponding volumetric flow rates are 34.9 m³/s for helium and 13.7 m³/s for carbon dioxide.

The difficult part is to determine a value for the effective flow area. If the flow entering the inlet plenum of the reactor is first evenly distributed around the periphery of the vessel, then the velocity will be uniform and the peak velocity will be low. Thus, one could imagine that all of the flow enters uniformly through the lateral surface of a cylinder whose diameter of 2.5 m approximates that of the region that contains all of the cold fingers. The height of this cylinder could be 2 m or more. The corresponding flow area for a cylinder height of 2 m is 5π m². A much less favorable situation is one in which there are no flow baffles in the upper plenum to distribute the incoming flow and a stream perhaps 1 m in diameter flows across one of the cold fingers. For this case the effective flow area would be 0.25π m². The two corresponding values of U would be 2.2 and 44 m/s for helium and 0.87 and 17 m/s for carbon dioxide.

Table 2 provides the four combinations of velocity for the two gases along with the corresponding Reynolds numbers obtained with the aid of equation 12. Page 255 of Reference 13 provides a graph of Strouhal number versus Reynolds. Pages 252-253 of Reference 13, describe this graph and state that Strouhal number remains nearly constant with a value of 0.2 within the range of Reynolds numbers from 300 to 2×10^5 and that this range is defined as a subcritical range. They further stated that as the Reynolds number is further increased to about 3.5×10^5 , the Strouhal number seems to increase depending on the turbulence intensity of the incoming flow. They continue: "However, the vortex shedding in this region is much weaker and defining an accurate shedding frequency is sometimes difficult. Beyond a Reynolds number of about 3.5×10^6 , the Strouhal number again seems to remain constant, with $St \approx 0.27$, with a strengthening of vortex shedding. The limits of the regions and the figures quoted are modified by cylinder roughness, turbulence in the incoming flow, cylinder aspect ratio, and the proximity of structures such as walls or adjacent cylinders." Near and within the 3.5×10^5 to 3.5×10^6 Reynolds number range there are several curves for Strouhal number for parametric levels of turbulence intensity. In the table, for Reynolds numbers of 3.2×10^5 and 6.4×10^6 , the curve corresponding to the lowest turbulence intensity and yielding the highest Strouhal number was selected. The maximum Strouhal number indicated anywhere on the graph is about 0.46. Table 2 shows the four values of Strouhal number read from the graph and their corresponding vortex shedding frequencies obtained with the aid of equation 11.

Table 2. Vortex Shedding Frequencies.

Gas	Velocity, m/s	Reynolds Number	Strouhal Number	Vortex Shedding Freq., Hz
Helium	2.2	6.4×10^4	0.20	1.8
	44	1.2×10^6	0.46	84
Carbon Dioxide	0.87	3.2×10^5	0.45	1.6
	17	6.4×10^6	0.27	20

The four vortex shedding frequencies in the table are to be compared with the natural frequency of 29.2 Hz calculated above. For obvious reasons, there is considerable uncertainty in the vortex shedding frequency for either coolant and also in the natural frequency of the cold fingers. However, there is enough information here to conclude that flow-induced vibration of the cold fingers is a possibility that should continue to be addressed in parallel with the hardware design. Additional types of flow-induced vibration analyses will also need to be made, as prescribed by Reference 12, and this probably should be followed by definitive experimental testing of the final design.

6.0 DISCUSSION AND CONCLUSIONS

As Chapters 2 and 3 demonstrate, finding a material that could meet all of the structural, thermal, and neutronic requirements could be a daunting task. The analysis in Chapter 4 clearly demonstrates that while a flow instability is theoretically possible under some extreme conditions, none of those conditions are anticipated in a gas-cooled power reactor of the type being considered. These conditions can occur in nuclear reactors for rocket propulsion that have ratios of absolute coolant outlet temperature to absolute coolant inlet temperature of

about 3.5 or more. For the current application, this ratio is only 1.5. The initial preliminary analysis of flow-induced vibration, Chapter 5, indicates that it is too early in the design phase to be able to provide a definitive answer, but there is a potential problem here. Hence, there is a need to do analysis of flow-induced vibration in parallel with the development of the design, so that the problem can be avoided.

References

1. Private communication with Edward Hoffman of ANL on December 5, 2002.
2. Private communication with Todd Allen of ANL-West in December 2002.
3. S. J. Zinkle and L. L. Snead, "Thermophysical and Mechanical Properties of SiC/SiC Composites (5/28/98 draft)," Oak Ridge National Laboratory.
4. S. J. Zinkle and N. M. Ghoniem, "Operating Temperature Windows for Fusion Reactor Structural Materials," *Fusion Engineering and Design* 51-52 (2000) pp. 55-71.
5. S. Timoshenko, *Strength of Materials, Part II, Advanced Theory and Problems*, Third Edition, D. Van Nostrand Company, Inc., Princeton, New Jersey, 1966, p. 135.
6. E. E. Feldman and T. Y. Wei, "Thermal-Hydraulic and Safety Evaluation of the PB-GCFR Core Design," Nuclear Energy Research Initiative Project #01-022: Particle-Bed-Gas-Cooled Fast Reactor (PB-GCFR) Design, Task 2.1 Milestone/Deliverable, Nuclear Engineering Division, Argonne National Laboratory, February 28, 2003.
7. Gilbert Melese and Robert Katz, *Thermal and Flow Design of Helium-Cooled Reactors*, American Nuclear Society, La Grange Park, Illinois, p. 230.
8. D. L. Black, G. E. Klinzing, and J. W. Tierney, "Temperature-Viscosity Induced Laminar Instabilities," *Nuclear Engineering and Design*, Volume 40, 1977, pp. 225-233.
9. R. W. Bussard and R. D. DeLauer, *Nuclear Rocket Propulsion*, McGraw-Hill Book Company, Inc., New York, 1958, pp. 128-129.
10. R. W. Bussard and R. D. DeLauer, *Fundamentals of Nuclear Flight*, McGraw-Hill Book Company, Inc., New York, 1965, pp. 140-148.
11. E. Achenbach, "Heat and Flow Characteristics of Packed Beds," *Experimental Thermal and Fluid Science*, Vol. 10, 1995, pp. 17-27.
12. Private communication with Shoei-Sheng Chen, December 11, 2002.
13. Shoei-Sheng Chen, *Flow-Induced Vibration of Circular Cylindrical Structures*, Hemisphere Publishing Corporation, Washington, DC, 1987.

Task 4: Fuel/Structural Materials Irradiation Performance

4.1 Fuel/Structural Materials Irradiation Performance (J. W. Holland, I. G. Prokofiev)

This project was focused on developing a PB-GCFR with design features that mutually ensure the key Generation IV system goals: passive safety, improved fuel proliferation resistance, enhanced plant efficiency and reduced fuel-cycle waste. A new advanced fuel form is an essential element of the required core-design innovations needed to achieve the Gen IV goals. At least during the early stages of the conceptual design, fuel and structural materials selection is proceeding along three parallel paths because multiple basic core configurations are being considered – particle bed, pin and plate/block (fuel dispersed within a matrix). At this time, the particle-bed concept is considered the reference configuration. Property data found in the open literature pertaining to fuels and structural materials were collected and assessed to identify candidate fuels and structural materials for the ongoing PB-GCFR design activities.

Although significantly more work has been done on carbide fuels compared to nitride fuels, they each have advantages and disadvantages. Nitrides operate at roughly the same temperatures as carbides, but possessing higher melting temperatures and thermal conductivities, nitrides are relatively colder than carbides during normal in-pile operation. It was found, that with a high degree of quality control in their manufacture, nitride fuels will swell less during service and possess higher fracture strength than carbide fuels. Based on a thorough evaluation of the available data and performance information, the following recommendations are made:

- The preferential fuel for additional consideration for all three fuel types is (U,Pu)N with (U,Pu)C as the alternative,
- TiN is the preferred compatible material for use with the nitride fuel and ZrC with the carbide fuel,
- It should be determined if ZrC is also compatible with nitride fuel as a coating, and
- A determination should be made whether Ti, Zr or one of their alloys can be used as the matrix material for the plate/block fuel concept.

During the extensive literature search and subsequent fuels and materials assessment, it became apparent that additional high-temperature mechanical properties are needed for TiN, ZrC, and the alloys of Ti and Zr. In addition, their response to fast-spectrum irradiation must be characterized.

In a similar manner, property data for industrially available structural materials with well-established manufacturing technologies were collected and assessed to identify candidate materials for various key components of the PB-GCFR. Detailed design information about these components do not presently exist; therefore, as a starting point, materials and materials systems that were considered in other reactor development projects were considered first.

A variety of engineered materials were ranked according to their material type and the temperature range over which they are effective based upon information published in the open literature in numerous property guides. Austenitic and ferritic steels perform well in a reactor environment up to 650°C. Nickel-based superalloys extend service to 850-900°C, but they experience some fast-spectrum irradiation damage. Refractory metals and alloys provide reasonable behavior to temperatures beyond 1000°C, and finally, ceramics extend the service temperature even higher. The experience base for the ceramics, refractory metals and some of the nickel-based superalloys mentioned above is very small, particularly with respect to irradiation

performance, and consequently, their use necessitates that a considerable R&D effort will be required.

The following structural-material recommendations are made:

- Ceramics such as SiC, ZrC, TiC, MgO, Zr(Y)O₂, TiN, Si₃N₄, etc., are required for structures within or immediately adjacent to the fuel zone if temperatures as high as 1600°C must be withstood (expected during a depressurization accident). Otherwise, refractory metals and alloys will easily withstand steady-state service at 900°C.
- 2 ¼ Cr-1Mo and 9-12Cr steel are recommended for the pressure vessel.
- Inconel 718, Inconel 800 and Hastelloy X are acceptable candidates for cooling-system components.
- Borated Type 304 and 316 stainless steel, ferritic HT9 and various vanadium alloys are reasonable choices for shielding and thermal barriers, but final selection must await completion of neutronic and thermal-hydraulic analyses.
- High-density materials such as uranium, tungsten, iron, stainless steel, Nb-1Zr are all acceptable initial candidates for use as a reflector; however, final consideration must follow completion of neutronic and thermal-hydraulic analyses.

Similarly as for the fuel, additional high-temperature mechanical property data coupled with irradiation performance information are needed for many of the structural materials that were considered. This fact is particularly true of the low-alloy steels, nickel-based superalloys, refractory alloys and ceramics. Nearly all of the mechanical properties are detrimentally affected by irradiation at high temperature.

This preliminary assessment of candidate fuels and structural materials was based upon information available in the open literature and serves as a starting point for the ongoing design and continuing development of the PB-GCFR. Of course, the selection of materials will be refined as additional design criteria and property data become available.

The FY2003 activities for this area were mainly focused on consultations with fuel/structural materials experts and continuing to gain insights into materials that are applicable at the high operating temperature and fluence of the PB-GCFR design. The project also kept cognizant with ongoing activities on GFR under an INERI project led by ANL and French CEA. As example, this information was used in selecting materials for the cold fingers as discussed under Task 3.

Table 1. Typical Physical Properties of Structural Materials ^a

Structural Material	Density (g/cm ³)	Thermal Conductivity (W/mK)		Specific Heat (J/kgK)	Young's Modulus (GPa)	Melting Range (°C)
		100°C	500°C			
Type 304 SS	8.0	16.2	21.5	500	193	1400 - 1450
Type 316 SS	8.0	16.2	21.5	500	193	1375 - 1400
Inconel 617	8.36	6.4	—	419	—	1330 - 1380
Inconel 718	8.19	7.2	—	435	—	1260 - 1336
Inconel 800H	7.94	7.9	—	460	—	1357 - 1385
Niobium	8.57	52.7	63.2	268	103	2468
Tantalum	16.6	54.4	66.6	139	185	2996
Molybdenum	10.22	142	123	276	324	2610
Tungsten	19.25	155	130	138	400	3410

^a Excerpted from "GEM 2001, Guide to Engineered Materials," *Advanced Materials & Processes*, Vol. 158, No. 6. Dec. 2000.

Task 5: Engineering Assessment of Selected Core Design

The following paragraphs are highlights of activities conducted in the Engineering Assessment area, in the second year of the project.

5.1 *Design Approach for a Small Modular Pebble Bed Gas-Cooled Fast Reactor Optimized for Decay Heat Removal (E. E. Feldman, T. Y. C. Wei)*

1.0 INTRODUCTION

Twenty five years ago when gas-cooling was being considered as the alternative to liquid metal (sodium) cooling, the key decision taken was to utilize the technology developed for the latter in gas-cooled systems to the extent possible. The accepted rationale was that this would reduce research and development costs, accelerate the introduction of gas-cooled fast reactors into the nuclear mix and increase the acceptability by this leveraged arrangement of U.S. national funding for the program as a possible alternative to the liquid metal fast breeder reactor (LMFBR). At that time in the U. S., the gas-cooled fast reactor (GCFR) was an initiative of a private consortium. This approach was accepted by the U.S. AEC and also in Europe, particularly in the European Economic Community (EEC) and also in the Federal Republic of Germany. As a result the GCFR design of Gulf General Atomic (GGA) in the U. S., the GBRs (1 of 4) of the EEC and the KFK GCFR in Germany eventually all converged on LMFBR fuel technology.

There was some initial effort to attempt to convert the emerging particle fuel technology of the thermal gas reactor (helium cooled HTGRs) but that was eventually terminated. The challenging task of providing durable coatings for the fast reactor application turned out to be too daunting. LMFBR fuel technology was that of solid solution ceramic fuel pellets clad in metallic tubes with a fission gas plenum. GCFR fuel therefore became solid solution ceramic pellets clad in metallic tubes. It was realized even at that time that this fuel type was not necessarily the optimum type for the thermal-hydraulic characteristics of gas coolant. Variations were investigated such as clad surface roughening and vented pins. However, it was recognized that the major differences in the thermal-hydraulic (T-H) attributes of gas coolant vis a vis liquid metal coolant, namely, poor heat transfer properties at low pressure and low coolant thermal and mass inertia may not be adequately served by the pin technology. In particular, the safety case for decay heat removal during depressurization accidents combined with total loss of electric power could not avoid the spectrum of severe accidents with whole core melt.

Before the issue of fuel technology and its role in accident space could be addressed, the U.S. national program on the GGA GCFR was terminated. This was soon followed by the cancellation in Western Europe of their respective national programs on the gas-cooled fast reactors. In the meantime, effort continued on the thermal gas cooled reactor technology area to improve the safety for that reactor type. The focus was on walk-away safety and led to the emphasis on incorporating passive decay heat removal (DHR) mechanisms to complement the active DHR systems in the safe removal of core heat. The industry position is now that the safety case for the avoidance of core disruption for the highly improbable accident of depressurization with total loss of electric power can now be made for small modular gas cooled thermal reactor through entirely passive mechanisms. The fuel technology utilized in these reactors is not pin-pellet technology but is entirely different and based upon coated particles. In particular the pebble bed modular reactor (PBMR) being developed in South Africa is based upon Jülich-derived technology. Fuel pebbles composed of fuel particles are the fuel elements. Advocates of the PBMR technology have

asserted that this fuel form has particular advantages for the safety case and decay heat removal accidents.

This NERI project has focused on this assertion and has investigated utilization of the potential pebble fuel form in gas-cooled fast reactors as a means of enhancing the possibilities for decay heat removal through passive means. This is in combination with and as a complement to ultra reliable active DHR systems. The NERI effort is concentrated on issues involving core design optimized for mechanisms for passive decay removal. Follow-on NERI work is recommended for investigating the implications of the proposed core designs on the primary-systems/vessel design and the balance-of-plant (BOP) configuration. This report documents the results on the core design study and furthermore provides proposals for future work on primary system/BOP design to implement fully the possibilities for passive DHR given by these core designs.

2.0 PASSIVE SAFETY PERSPECTIVE

When the reactor is shutdown, the decay heat that is not removed from the fuel must be stored in it. This extra heat energy results in a rise in fuel temperature. Thus, after the reactor is shutdown, if the decay heat generation rate exceeds the decay heat removal capability, the core temperatures will increase until the generation rate has decreased to that of the removal capability. As the decay heat rate continues to decrease with time the core temperatures will continue to decrease. Thus, for a given decay heat removal rate, the amount of extra heat energy that the fuel must absorb is finite. Hence, for a given fuel heat capacity (i.e., the product of the mass of the fuel and its specific heat capacity) and decay heat removal rate, there is a corresponding peak fuel temperature.

The amount of excess energy that must be absorbed by the fuel can be represented graphically, as area under the curve in Fig. 1. This curve is for uranium-fueled reactors. For example, if the steady-state decay heat removal capability is 1% full power, then the excess decay heat energy is all the area bounded by the horizontal line for decay powers of 0.01, the vertical line of time equals 0, and the decay heat curve itself. A linear rather than a log-log graph would be more suitable for a pictorial representation but would not properly represent the time scale. The decay heat curve was numerically integrated to produce Fig. 2. The numbers shown along the curve represent values of the ordinate. For example, if the decay-heat removal system has a steady-state capability of 1% full power, then 35.938 full-power seconds (fps) of energy will be stored in the core when the peak temperature is reached. The time of this peak can be determined from Fig. 1, where 0.01 is seen to correspond to about 2.5 hours.

Figure 2 therefore shows the required decay heat removal capability to stay below the peak stored energy criteria. This can be done by first determining how much the fuel temperature would be allowed to rise during an upset condition. This amount would be based on the difference between the maximum temperature the fuel can withstand without unacceptable damage and its maximum temperature during normal full-power operation. This temperature difference, the heat capacity of the fuel, and the fuel peaking factors would enable one to determine the maximum amount of additional energy in full-power seconds that the fuel can absorb during an upset, without sustaining unacceptable damage. Figure 2 then directly correlates this value of full power seconds to a steady-state decay-heat removal capability. Typically passive decay-heat removal systems in thermal gas cooled reactors are normally capable of removing less than 1% power. This means that ~35 fps needs to be absorbed by some other mechanism. This is fairly demanding as it would for example require tens of seconds of full flow. There is a need to raise this capability to the 1 to 2% range as it would be difficult to find fuel materials, which could absorb this extra heat without derating the core power density significantly.

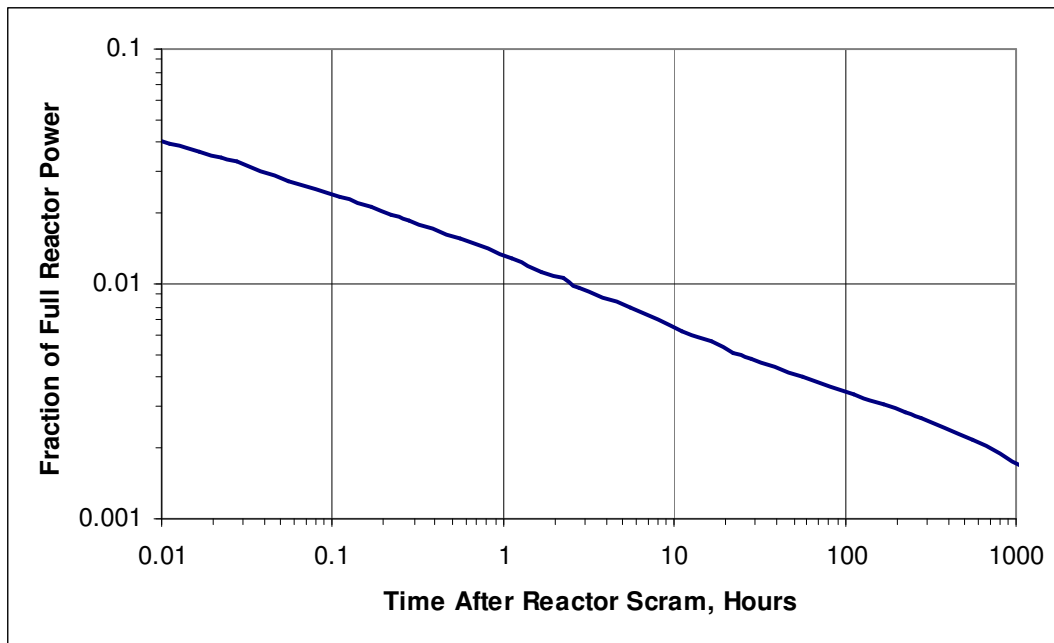


Fig. 1. Decay Heat Curve for Uranium-Fueled Reactors.

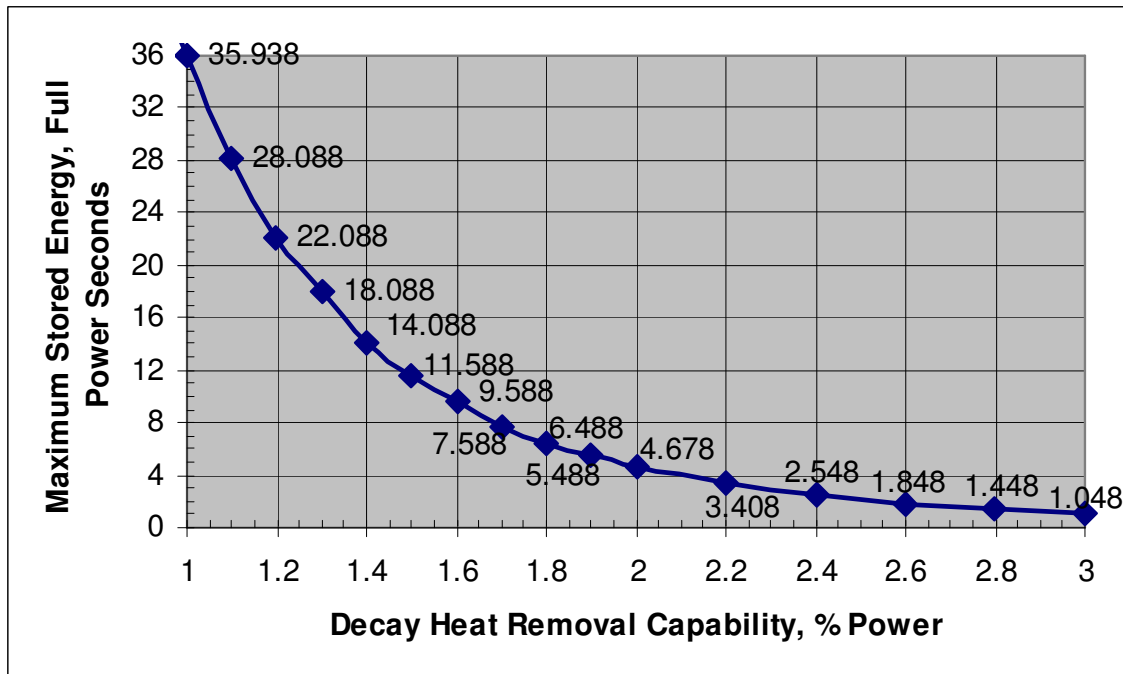


Fig. 2. Maximum Stored Energy.

In the initial exploratory work of this NERI project, several methods for removing decay heat during depressurization accidents with concurrent loss of site power were investigated. These included 1) conducting and radiating the heat from the core and through the reactor vessel walls, 2) the use of in-core heat exchangers, i.e., cold fingers, and 3) natural convection between the reactor core and a heat sink. Item (1) was found to be inadequate for core power densities in the range of 25 W/cc and above, item (2), cold fingers, were extensively studied and found to be a potential solution but with many design issues. Natural convection, item (3), was found to be totally ineffective for helium at atmospheric pressure or even at a few atmospheres. However, it was observed that natural convection may work for helium above 10 atmospheres or carbon dioxide at several atmospheres. These pressurized options would require some form of pressurized containment around the reactor vessel during the accident. The previous analyses of natural convection used core hydraulic models for straight coolant channels such as those found in block or pin cores. It was assumed that natural convection would be more effective in pin and block cores than in pebble-bed cores, since pebble-bed cores tend to have higher hydraulic resistances.

Recently, it was decided to take a fresh look at natural convection in pebble bed cores since natural convection with a pressurized containment appeared to be the most promising concept. The pebble-bed core hydraulic resistance may be manageable if the core diameter were maximized so as to keep the flow velocity and core pressure drop low. If the minimum required system pressure could be guaranteed through the use of a guard vessel, i.e., a larger secondary containment around the primary pressure boundary, then the system could truly be passive. Several core designs need to be addressed (essentially a combination of pebble size, core diameter, and core height) and a design proposed to minimize core pressure drop and maximize natural convection. Scoping analytical results for these core designs need to be produced initially with first-order one-dimension steady-state models. There would then be the need to perform transient simulations of more complex situations. Although conduction and radiation from the core and through the vessel wall does not adequately remove decay heat, they could be of significant assistance and credit for this could be taken through an integrated transient model that includes conduction and radiation along with natural convection.

It was also decided to revisit semi-passive/semi-active approaches in the form of autonomous systems and the use of autonomous systems was added to the list of concepts being explored. These systems use the decay heat from the shutdown reactor core to provide the pumping power to force the loop flows that remove the decay heat. These will need to be discussed because they impact the layout of the major hydraulic loops of the plant in ways that are similar to those for the deployment of natural convection loops for decay heat removal. Interactions between these two approaches need to be assessed at an early design stage.

The remaining sections in this report therefore address the impact of natural convection on the system design and the effect that the use of autonomous systems may have on the design optimized for natural convection conditions. Natural convection has been selected as the passive safety approach and autonomous systems have been selected for the semi-active/semi-passive approach.

3.0 PASSIVE SAFETY SYSTEMS DESIGN

Several core designs with different combinations of pebble size, core diameter, and core height, have been considered. The results of this study were used to derive a design that minimizes core pressure drop and maximizes natural convection. To take a fresh look at natural convection in a pebble-bed core design, model improvements, including one to better account for natural

convection in pebble-bed cores, were developed. These models are first-order, one-dimensional steady-state models. It would be highly desirable to have the capability to perform transient simulations of more complex situations. This capability is given by the RELAP5/ATHENA code and the steps to incorporate the RELAP5/ATHENA code in the modeling work for the PB-GCFR have been identified and discussed.

3.1 Selection of Pebble-Bed Core Design

Three pebble-bed core designs were earlier proposed for use with the cold-finger decay-heat removal system. [1] Since natural circulation was not being considered for decay heat removal at the time, core hydraulic resistance was less of a constraint in the optimization process. Accordingly, a core with a friction pressure drop of about 3 bar was assumed and any additional pressure drop that could be produced by an upper or a lower axial reflector was ignored. All of three cores were sized to have a power density of 50 W/cc in the pebble regions excluding the core regions occupied by the cold fingers.

During iteration between safety and neutronics design activities, it was observed that the presence of cold fingers makes maintaining criticality over the core residence time difficult in a long life core design. Hence, it was necessary to reduce the power density and designs of 25 W/cc were considered. If the power density were to be reduced to 25 W/cc, however, perhaps the cold fingers, which introduce new challenges for the reactor design would not be needed. Therefore, it was decided to take a fresh approach. In the past the use of natural convection for decay heat removal in pebble-bed cores was thought to be impractical because pebble-bed cores tend to have large hydraulic resistances. However, it may be possible to overcome this problem by minimizing hydraulic resistance by maximizing the core diameter. Pressure drop is approximately proportional to coolant velocity squared, which, in turn, is inversely proportional to flow area squared. Flow area is proportional to core diameter squared. Therefore, pressure drop is approximately inversely proportional to the fourth power of diameter. An added relatively small benefit of increasing the core diameter is that the core height gets shorter for a given power density.

A related issue is the diameter of the pebble. Larger diameter pebbles results in a smaller core pressure drop and in a greater effective thermal conductivity for the pebble bed. However, larger pebbles have higher center temperatures, due to the larger internal pebble temperature rise. For the current effort, it is assumed that the entire volume of each spherical pebble is filled with a homogeneous mixture of uranium carbide particles distributed throughout in a silicon carbide matrix. In the past it was assumed the thermal conductivity of these pebbles would be about 30 W/m-K. Closer examination indicates that under irradiated conditions, 20 W/m-K would be a more representative value.

Based on the above considerations, a core diameter of 3.0 m and a pebble diameter of 4.0 cm were selected. This core diameter is about the largest that can fit into a reactor vessel of about 7 m in diameter and allow enough room for the radial reflector and shielding and any needed coolant inlet flow paths. The 3.0-m core diameter results in a 1.70 m core height for a 25 W/cc core and a height-to-diameter ratio of 0.566. Although this ratio is much less than 1.0, it is believed that criticality will be maintained over the entire life cycle of the core. The friction pressure drop across this core at full power conditions is only 0.65 bar, which is much less than the 3 bar of the earlier core designs that employed cold fingers.

The 4 cm pebble diameter results in a nominal temperature rise, i.e., without power peaking factors included, from the free stream of the coolant in the core to the pebble center of 211°C, of which

136° C is temperature rise in the pebble and the other 75° C is the film temperature rise. Since a maximum local power peaking factor of 2.0 is anticipated, the 211° C average core rise results in a 422° C maximum temperature rise at full-power steady-state conditions. The reactor coolant is 850° C at the exit, but the peak fuel temperature will occur between the core mid-plane and the exit where the coolant temperature will be considerably less than 850° C. Since the sum of 850° C and 422° C is 1272° C, peak fuel temperatures significantly less than this and of about 1200° C are expected. A 1200° C maximum fuel temperature would allow a 400° C margin if the maximum allowed fuel temperature under upset conditions is 1600° C. This margin would allow the fuel to absorb a considerable amount of the excess decay heat during the earlier part of an accident in which the decay power exceeds the decay heat removal capability. It should be noted that the use of advanced fuel and structural materials might allow raising the temperature limit above 1600° C.

In some instances the average temperature of the hottest pebble is of greater concern than the peak temperature of this pebble. For a sphere with uniform thermal properties and heat generation rate throughout its volume, the steady-state average temperature increase relative to the surface temperature is 40% of the increase from the surface to the peak (which occurs at the center). Thus, in these instances the 136° C pebble temperature rise would be replaced by 40% of this value, or 54° C, and hence the 211° C value would be replaced by 129° C, i.e., 75° C + 54° C, and when the 2.0 power peaking factor is included, the largest temperature rise from the coolant free stream value to the pebble average is only 258° C, instead of $2.0 \times 211^\circ$, or 422° C. This implies that the margin is considerably larger than that obtained above where peak pebble temperatures were assumed.

Another consideration is the upper and lower axial reflectors. These must be close to the core for them to be effective in reflecting neutrons back into the core and to provide neutron shielding for the structures above and below the core. Therefore, in the design it is assumed that there is a 0.5-m layer of non-fueled-bearing 4-cm diameter pebbles below the core and one above it. This lower axial reflector has a friction pressure drop of 0.15 bar at rated conditions and the upper one has a friction pressure drop of 0.23 bar, for a combined pressure drop for all three regions of 1.03 bar. The upper axial reflector has a significantly higher pressure drop than the lower axial reflector because the exit coolant temperature is much higher than the inlet coolant temperature.

3.2 Analytical Natural Convection Model

A schematic of a natural circulation loop is shown in Fig. 3. In the current application, the entire fueled region is assumed composed of pebbles of the same size. The regions above and below the core are assumed to be axial reflector pebbles that do not generate heat. A new pressure drop model is used for the heated core region. This model becomes indeterminate and cannot be used directly when the inlet and outlet temperatures are the same, as occurs in the axial reflector regions above and below the core. In this case this asymptotic limit of the new model should be the same as the isothermal pebble-bed model used to derive the new model and provided by Reference 3. Therefore, the isothermal model was used for these isothermal regions.

In the modeling of flow through core with straight channels, the entrance and exit form-losses, or K-losses, were based on the coolant velocity in the fueled region. For these cases an entrance loss of 0.5 and an exit one of 1.0 were typically used. For pebble-bed application, the determination of a representative coolant velocity for the fueled region requires refined models. A possible method is to assume the effective flow cross sectional area is the cross sectional area of the core multiplied by the coolant void fraction of 0.387. Another issue is the value of the entrance K-loss. For a rounded entrance, this value can be very small, such as 0.05. The exit loss is insensitive to exit

shape and is a function of the ratio of the change in cross sectional area at the exit, with a maximum value for straight duct of 1.0. The entrance and the exit loss were not included in the current model and therefore each was in effect set to zero. This is a very optimistic assumption, which must be revisited later. Similarly, in the current modeling, the pebble-bed pressure losses are assumed the only losses around the flow loop. This is optimistic and should also be revisited.

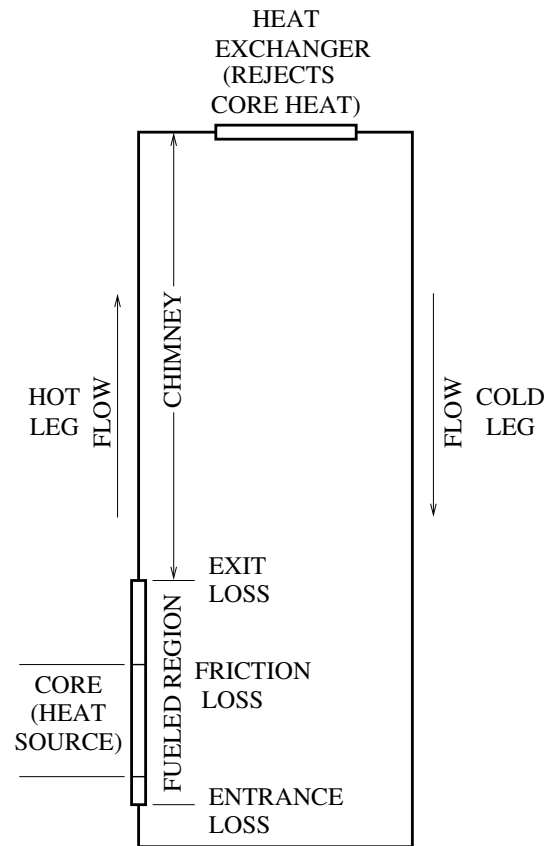


Fig. 3. Natural Convection Loop.

3.3 Natural Convection Results

The loop natural convection model was used to determine the required system pressure, i.e., containment back-pressure, for a series of parametric cases. In this steady-state model the sum of the friction pressure drops is equated with the buoyancy pressure rise. The only friction pressure drops in the loop are assumed to be those across the core and the upper and lower axial reflectors. Thus, all entrance and exit form losses and all hydraulic resistances in the piping and the external heat exchanger were ignored. Hence, this is a very optimistic model and less favorable results are expected when all resistances are included. The chimney height as defined in Fig. 3 was assumed 10 m in all cases. It may be possible to increase this a few meters to provide more favorable results when calculations are made with less optimistic assumptions. However, the chimney height is limited by the vessel height, which is assumed to be about 24 m, if the heat exchanger is to go inside the vessel, as is being proposed (see Section 4).

The primary-side exit coolant temperature from the heat exchanger at the top of the loop is governed in part by the conditions on its secondary side. Therefore, during upset conditions, it was assumed that the temperature exiting the heat exchanger and entering the reactor core is 250° rather than 480°. In the analysis the reactor exit temperature was fixed at either 850° C or 1600° C. The latter temperature is representative of the maximum allowed fuel temperature and the former is representative of a lower bound of the maximum allowed structural temperature. The lower value is the more reasonable choice since it is essential to keep the structures intact during an upset condition. However, the 850° C value, perhaps, could be raised 50 or 100° C, depending on the structural materials. A series of parametric cases were analyzed in which the system pressure needed to sustain a given steady-state power was obtained.

All of the parametric results are shown in Fig. 4. Both the helium and carbon dioxide coolant options were considered, with the former indicated on the graph without symbols (and in red) and the latter with symbols. For each choice of coolant, the solid curve represents the 850° C temperature limit and the dashed curve represents the 1600° C limit.

In order to use Fig. 4 to determine the required system pressure, i.e., the guard containment back-pressure, one must first determine the decay heat removal capability that the decay heat removal system must provide. This is determined with the aid of Figure 2. The maximum energy the fuel is allowed to store is essentially proportional to the rise in fuel temperature from the normal operating conditions until the highest allowed fuel temperature is reached during the upset condition. Here we are concerned with the pebble mass-averaged temperature at normal operating conditions and the peak mass-averaged value during the upset. During shutdown conditions, the power is sufficiently low that, to a reasonable approximation, each pebble has a uniform temperature.

As explained in Section 3.1, a representative value for the margin between the peak fuel temperature in the core at normal operation conditions and the allowed fuel maximum temperature, assumed to be 1600°, is 400° C. This peak temperature is at the center of the hottest pebble. It can be shown analytically that the volume-averaged temperature of a sphere with both uniform volumetric heat generation rate and thermal conductivity is the surface temperature plus 40% of the pebble temperature rise from the surface to the center. Thus, the remaining 60% represents increased temperature margin. For the 4-cm pebble design proposed in Section 3.1, the temperature rise from the surface to the center of the pebble was 136° C for 25 W/cc and twice this value, i.e., 272° C, when the 2.0 power peaking factor was included. Thus, if there is a 400° C margin between the peak pebble temperature and the assumed 1600° C limit, then 60% of 272° C, or 163° C, can be added to the 400° C margin, for a total margin of 563° C. For now we will take an overly conservative approach and assume that 400° C, rather than 563° C, is the amount that the volume-averaged temperature of the hottest pebble can rise without exceeding the 1600° C limit.

From elementary physics it is known that the stored energy, E , in a given volume of fuel is equal to the product of the mass of the fuel, its specific heat capacity (c_p), and its temperature rise (ΔT). The mass of the fuel is the product of the volume of the fuel and the density of the fuel pebbles (ρ). The volume of pebbles in a given volume, V , is the product of V and the fraction of V that the pebbles occupy. The fuel fraction is 1 minus the void fraction (vf) and the void fraction is taken to be 0.387. Hence:

$$E = V \times (1 - vf) \times \rho \times c_p \times \Delta T$$

The decay energy is also the integral of the decay power from time equals zero until the peak temperature is reached. This integral, expressed in full power seconds (Inte) is provided by Fig. 2 and can be expressed in joules by multiplying the full power seconds by the normal operation power of the volume (Pow). Hence:

$$E = Pow \times Inte$$

Combining these two equations, one obtains:

$$Inte = \frac{(\rho \times c_p) \times (1 - vf) \times \Delta T}{\frac{Pow}{V}}$$

Pow/V is the (local) power density of the volume. The average power density of the core is taken to be 25 W/cc (25 MW/m³). However, the power peaking factor where the hottest pebble occurs is assumed 2.0. Thus, the power density at the hottest pebble is 50 MW/m³. The product of density and specific heat capacity for the fuel pebbles is taken to be 3.8 × 10⁶ J/m³-K. Thus, with vf taken to be 0.387 and ΔT taken to be 400° C, one can evaluate Inte and find it to be 18.6 s. Figure 2 shows that the required steady-state decay heat removal capability is about 1.3% of full power. Figure 4 indicates that if the 850° C limit applies, then the system pressure must be about 13 bar for helium and 4 bar for carbon dioxide. For the 1600° C limit, the corresponding pressures are about 7 bar and 2 bar for helium and carbon dioxide, respectively.

Employing a guard containment that can withstand 13 bar may not be practical, although a 7 bar guard containment may be doable. This analysis does not take advantage of heat transfer within the core and heat transfer from the core to the radial reflector and shielding and ultimately through the reactor vessel wall. Also, had it been assumed that ΔT is 563° C, instead of 400° C, then Inte would be 26.2 s, the required steady-state decay heat removal capability would be about 1.1%, and the required values of system pressure would be about 11 bar instead of 13 bar for helium with an 850° C outlet temperature.

As previously discussed, these results are based on the analytical steady state natural convection loop model of Fig. 3. A number of assumptions have been made and simplifications regarding the modeling of the physical phenomena are inherent. Key among these are the absence of the heat exchanger hydraulic friction pressure drop, dynamic effects of the core thermal inertia and the decay curve history. A RELAP5/ATHENA model that was developed as part of this project includes these phenomena. As this is a high-level model without the design details, which are currently not available, boundary condition parameters are utilized to scope the envelope of the response. Two phenomena, which are simulated through these boundary conditions, are the forcing primary flow due to the response of the turbomachinery and heat removal on the secondary side of the emergency decay heat exchanger. In addition, the pressure history is simulated by essentially tripping valves, which quickly force the pressure to the asymptotic target design pressure of the guard containment atmosphere. Whenever a satisfactory system response is obtained necessary design details such as the sizing of the guard containment could be performed.

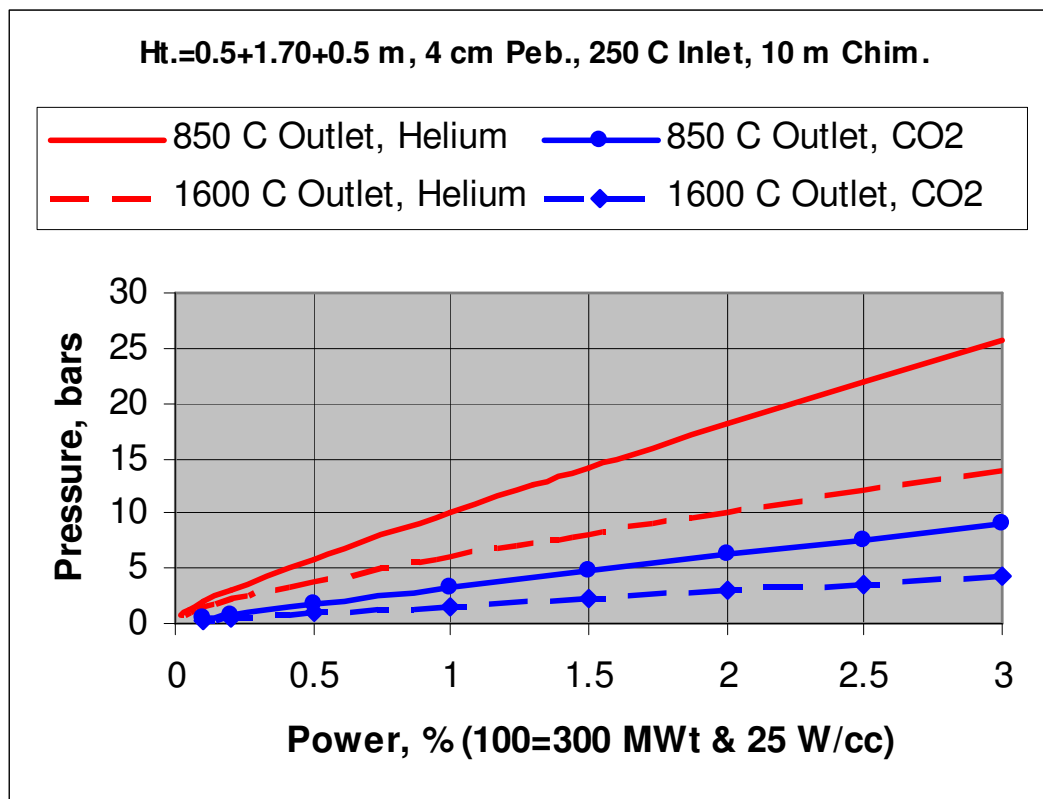


Fig. 4. System Pressure to Sustain a Required Decay Heat Removal Capability.

4.0 REACTOR VESSEL LAYOUT CONSIDERATIONS

Prior analysis of natural convection with helium or carbon dioxide indicated that natural convection would not adequately be able to remove decay-heat after the primary system pressure has depressurized to 1 atmosphere. Therefore, other methods of decay heat removal, such as cold fingers and direct heat radiation and conduction from the core through the vessel wall, were considered. Because these alternatives also have difficulties, it was decided to examine methods that can result in convective primary coolant flow during loss-of-site power. Methods that potentially could enable adequate convection under these conditions include the autonomous systems (Section 5), the use of heavy-gas accumulators, and natural convection with adequate containment pressure.

The heavy-gas accumulators would store a heavy gas, such carbon dioxide or nitrogen. During a severe depressurization accident with concurrent loss of site power, these accumulators could inject a heavy gas into the primary system and would drive the heavy gas through the core during the early part of the depressurization accident and cool the core for as long as the supply of gas lasted. This would cause core behavior analogous to that of an extended coastdown. The injected gas would also pressurize the containment around the reactor vessel and could thereby maintain the pressure inside the reactor vessel at least several atmospheres. This could greatly help natural convection. The heavy gas could displace the helium coolant in the primary circuit and thereby enhance natural convection. However, a heavy-gas injection scheme introduces several problems and issues. Among them are being able to inject the gas at the correct point in the primary system without knowing in advance where the breach in the primary pressure boundary will

occur. Injecting the gas in the inlet plenum, for example, when the breach is close to the inlet plenum, will cause the heavy gas to escape through the breach. The heavy gas would still pressurize the containment, but a significant concentration of the heavy gas may not circulate in the primary system. Other issues, include guaranteeing that the gas injection will activate when it is needed and not at other times when it could be seriously detrimental to a reactor plant that is otherwise functioning properly. These issues are being investigated by Brookhaven National Laboratory as part of an I-NERI project.

Because of issues and problems associated with the employment of autonomous systems and also with heavy-gas accumulators, natural convection by itself was reconsidered. Of course, some means would be needed to ensure that there would be sufficient containment pressure. This could take the form of a pressurized containment building. However, an extra "guard" containment vessel around the primary system boundary that could be pressurized appears to be a better option. This concept is the same as the "proximity" containment suggested by CEA as part of an I-NERI project and is in some ways analogous to the "machinery dome" used in other reactor plant designs. This guard containment in some respects would take on the same role as a guard vessel in a sodium-cooled reactor, in that it could contain the primary coolant in the event that the main primary vessel failed.

The presence of a pressurized containment makes the maintenance of the plant more difficult largely because it makes the boundary of the primary system less accessible. In addition, maintaining pressure within this system is another issue. These issues could be mitigated by using a gas-injection system to pressurize the containment at the initiation of the accident. This option, however, appears to be less acceptable since the system could not be considered fully passive and there is also the issue of guaranteeing that it will trigger when and only when it is needed and perform properly. Thus, a guard containment system that is always pressurized while the reactor is operating may be the better choice.

The guard containment boundary would have to be cooled during normal reactor operation. This is because during normal reactor operation heat is always being removed through the reactor vessel wall. If the flow of this heat were impeded, the vessel wall could exceed its operating temperature limit. This is a serious issue because the vessel wall is a pressure boundary that must withstand a pressure differential of 7 MPa. Cooling the guard containment does not appear to be a major problem and a temporary loss of cooling during a severe reactor depressurization accident should be tolerable.

In order to promote natural circulation between the reactor core and the heat exchanger in the primary circuit, the heat exchanger would have to be at a considerably higher elevation than the reactor core. Natural convection can only be maintained when the column of gas in the downward-flow path (i.e., the cold leg, which includes the heat exchanger and the path below it) is heavier than that of the column of gas in the upward-flow path (i.e., the hot leg, which includes the reactor core and the path above it). The means of initiating and maintaining adequate natural convective flow in the primary circuit deserves careful consideration. For example, if the reactor were scrammed and full primary flow were maintained long enough to equalize the temperatures around the natural convective primary loop, excessive temperatures within the core could occur before sufficient natural convective flow is established. In this initiating scenario, the upper axial reflector would remain relatively cold as the core heated up and this reflector would absorb heat from the core exit coolant and further impede the establishment of a hot leg that is capable of sustaining adequate natural convection.

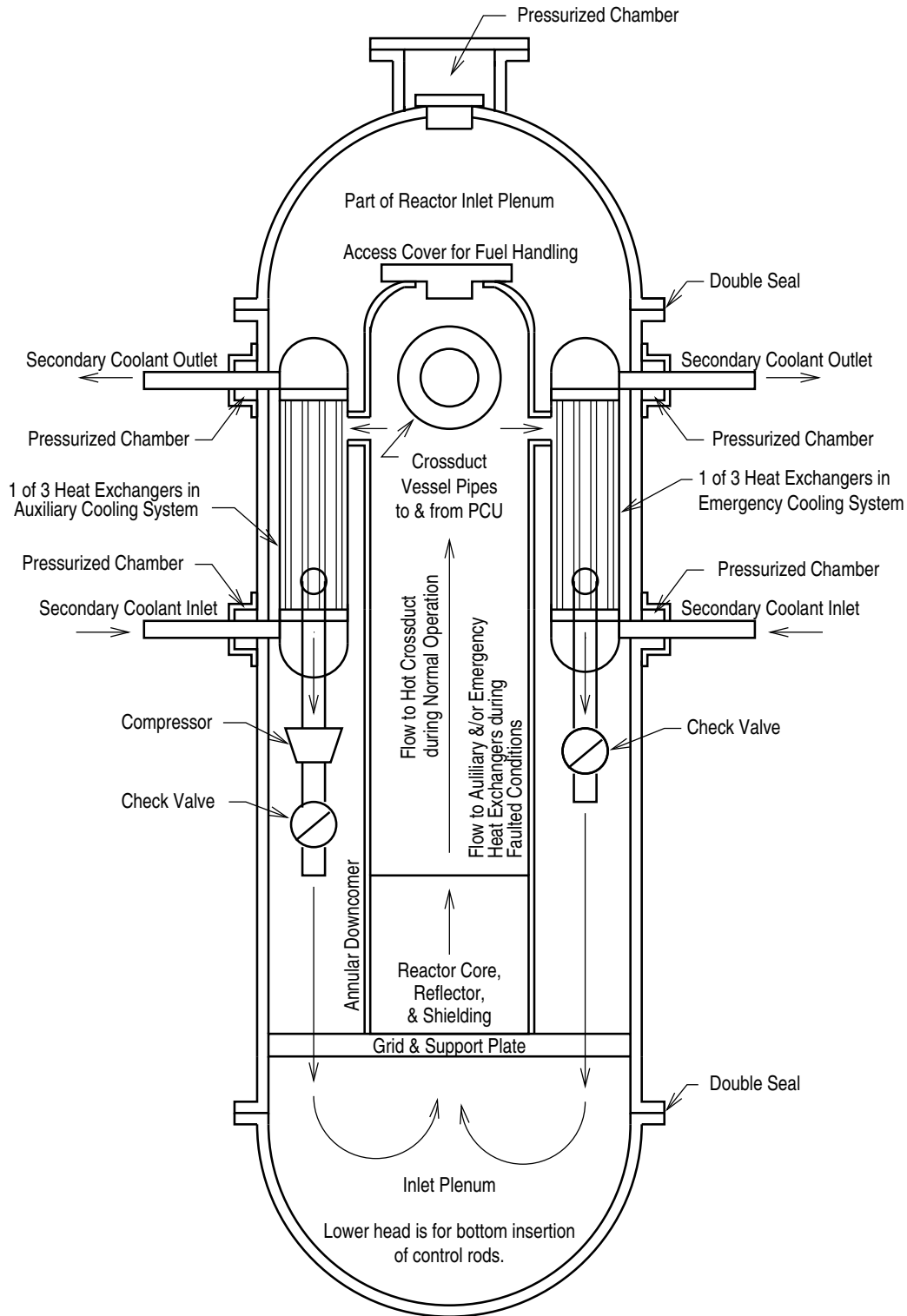
Another issue to be addressed with regard to natural circulation is the location of the primary system breach. If the breach occurred near the top of the hot leg of the primary circuit, such as in the upper part of the reactor outlet plenum, then cooler gases (or the heavier guard containment gas) could enter and fill much of the hot leg of the natural circulation loop. This could prevent the establishment of sufficient natural circulation around the loop. The ingress of large amounts of cooler gases would probably not occur until the depressurization was essentially complete. Then the cooler gases could enter and displace some of the warmer gas in the hot leg. One of the ways that may be effective in avoiding this problem is to place the heat exchanger needed for natural convection inside the primary reactor vessel, as shown in Figure 5, rather than place it on the outside and have long connecting pipes.

In Fig. 5, the heat exchangers indicated on the upper right and labeled "1 of 3 Heat Exchangers in Emergency Cooling System" are the ones of interest here. The ones on the left and labeled "1 of 3 Heat Exchangers in Auxiliary Cooling System" are the equivalent of the shutdown cooling system that is used during refueling in typical gas-cooled reactor plants. These systems are powered and would be effective during pressurization accidents as long as there is power to drive their compressors and pumps. As the figure indicates, the emergency and auxiliary heat exchangers are inside the primary vessel so that the chance of a serious breach between the reactor outlet plenum and any of these heat exchangers is minimized. In Section 5, an analogous issue is raised with regard to autonomous systems. In addition, potential weak points in the vessel pressure boundary are each protected by an extra barrier. For example, the plug at the top of the vessel cover, which is a refueling port, has a sealed chamber around it, which would be kept at a specific pressure between the vessel pressure of 7 MPa and the pressure outside the containment. By monitoring this chamber pressure, one could detect a leak around the refueling plug or one between the chamber and the region above the chamber. Similarly, there are pressurized chambers where the secondary coolant pipes from the heat exchangers pass through the primary vessel wall. In addition, there are double seals with a pressurized chamber (not shown) between each pair of seals where the top and bottom hemispherical heads join the rest of the primary.

Placing the heat exchangers used for natural convection inside the vessel rather than outside requires that the vessel be tall enough to accommodate them. In addition, a significant amount of space inside the vessel will be needed for the heat exchanger, their piping and valves, and primary-circuit compressors used with them. This complicates assembly and maintenance. Another concern is the control-rod drive penetrations. Top entry control rod drives would complicate the upper head design, possibly interfere with the refueling port, and double sealing their penetrations could prove difficult. Therefore, bottom entry control rod drives are being considered here. It may be better to use a weld to attach the bottom hemisphere of the reactor vessel rather than use a bolted joint with a double seal, as indicated in Fig. 5. A concern in any design is internal leaks. If, for example, the access cover for fuel handling, had a large leak or were dislodged, the inlet reactor flow could go directly to the outlet plenum without passing through the core.

5.0 AUTONOMOUS SYSTEMS

In a revisitation of semi-passive/semi-active approaches, the use of autonomous systems has been included in the list of concepts being explored. These systems use the decay heat from the shutdown reactor core to provide the pumping power to force the loop flows that remove the decay heat. Figure 6 shows a schematic diagram for a direct-cycle plant with an autonomous shutdown decay-heat removal system (inside the dotted perimeter) in parallel with the main power conversion unit.



Argonne National Laboratory
May 16, 2003 (EEF)

Fig. 5. Reactor Vessel Layout for Natural Convection in Direct-Cycle Plant.

If the main power conversion unit (on the left side of the figure) were not present and all of the primary flow went to the autonomous system, the plant layout would essentially be that of a reactor plant with an indirect cycle; i.e., there is an intermediate heat exchanger between the reactor and the power cycle part of the plant, or heat engine. This heat engine rejects heat to the atmosphere and produces electric power, via a generator (not shown). The autonomous system is designed to run all of the time, except when the decay power is extremely low. The electricity generated by this system is separate from the main (site) power grid and is therefore available even when the plant becomes disconnected from the main power grid.

When there is a loss of site power, the power from the autonomous system continues to power the compressor/circulator shown in the figure that drives flow through the core and the heat exchanger. There is an electric power storage device, which could be an electric storage battery, in the circuit between the generator and the compressor. This would be needed in the event that there is a temporary interruption in power produced by the autonomous system and also for situations when the decay power gets too low to keep the system running. In the latter case, the electric storage device would enable the autonomous system to keep running longer and the plant to continue removing decay heat longer.

In the event the autonomous system fails during normal operation, it may be necessary to shut the plant down. During normal operation of the reactor plant, the compressors in the power conversion unit keep the pressure at the reactor inlet higher than that at the outlet and thereby drive the flow through the reactor core. If the compressor in the autonomous system were eliminated from the design, then the pressure differential across the reactor core would cause most of the main primary flow to bypass the reactor core and go backwards through the primary side of the heat exchanger that is connected to the auxiliary heat engine. Therefore, a check valve is needed to prevent backward flow should the compressor for the autonomous system fail.

Plant layouts for two indirect-cycle plants were also devised. In one, the power conversion unit and the autonomous system were in parallel, and in the other, they were in series. Figure 7 shows a schematic diagram for an indirect-cycle plant with an autonomous decay-heat removal system in parallel with the main power conversion unit. The autonomous heat removal system in Fig. 7 is the same as in Fig. 6. The rest of the system layout is that of a typical indirect cycle plant except for the check valve that is included along the main primary flow path between the power conversion unit and the reactor. This check valve is needed to prevent backward flow through the main heat exchanger, i.e., the one on the left side of the reactor in the figure, when the power to the main primary compressor is lost and the autonomous system is driving coolant through the reactor core. This bypass flow would allow much of the primary flow to bypass the reactor. There could be some difficulties in obtaining a design with the proper flow balance between the main power-conversion unit loop and the primary flow in the autonomous loop.

Figure 8 shows a schematic diagram for an indirect-cycle plant with the main power conversion unit and the autonomous decay-heat removal system in series in the primary loop. This arrangement does not require any check valves. Electric power to drive the primary flow comes for both the main power conversion unit and the autonomous one. If the power from the main power conversion unit is lost, then electric power produced by the autonomous system continues to maintain sufficient primary flow to remove decay heat.

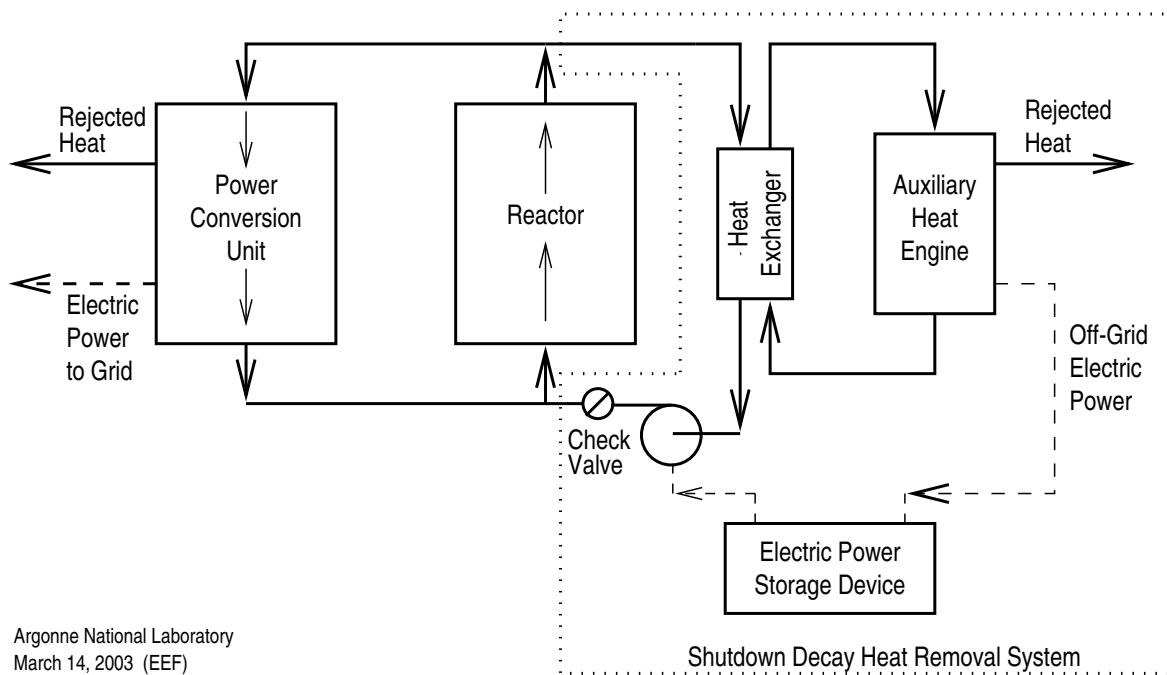
In all three arrangements, Figures 6 through 8, the autonomous system would be running all of the time, including normal operation of the reactor plant, so that it would always be available and not need to be started during an emergency. Therefore, the system would be removing heat all of the time and would affect plant efficiency. In addition, the system would have to be designed to

insure that it ran properly at both full system pressure and at depressurized conditions, which in some plant designs could be as low as one atmosphere. The autonomous system potentially could be usable for normal decay heat removal while the plant is shutdown and during fuel handling.

The choices for heat engines for the autonomous system are a gas turbine (Brayton cycle), a steam turbine (Rankine cycle), Stirling engine (Stirling cycle), solid-state devices, such as thermal photovoltaic, thermal electric, and thermionic ones, thermosiphon Rankine engine, and ThermoAcoustic Heat Engine (TASHE). The choices for electric storage devices include electric storage battery, fuel cell, and flywheel.

During a depressurization accident there would probably be only outflow through the break from the pressurized primary circuit to the reactor containment and no concurrent ingress of cold containment gases. After the depressurization, however, it may be possible for cold gases to enter through the break. This represents a potential problem. If cooled gases from the containment entered the primary system through the break and prevented hot coolant from the reactor core from reaching the heat exchanger that is connect to the autonomous system, the auxiliary heat engine would stop running. This could be the result of a large break in or near the reactor-vessel outlet plenum, for example. Therefore, it may be highly desirable to put the heat exchanger inside the primary vessel so that there is no external primary piping between the vessel and the primary-side of the heat exchanger.

An important safety issue regarding the direct-cycle and indirect-cycle parallel arrangements is the potential for check valve failures. If during normal full reactor power operation, the compressor that is powered by the auxiliary heat engine were to stop and the check valves failed to prevent backflow through the primary side of the auxiliary engine heat exchanger, a significant part of the primary flow could bypass the reactor core.



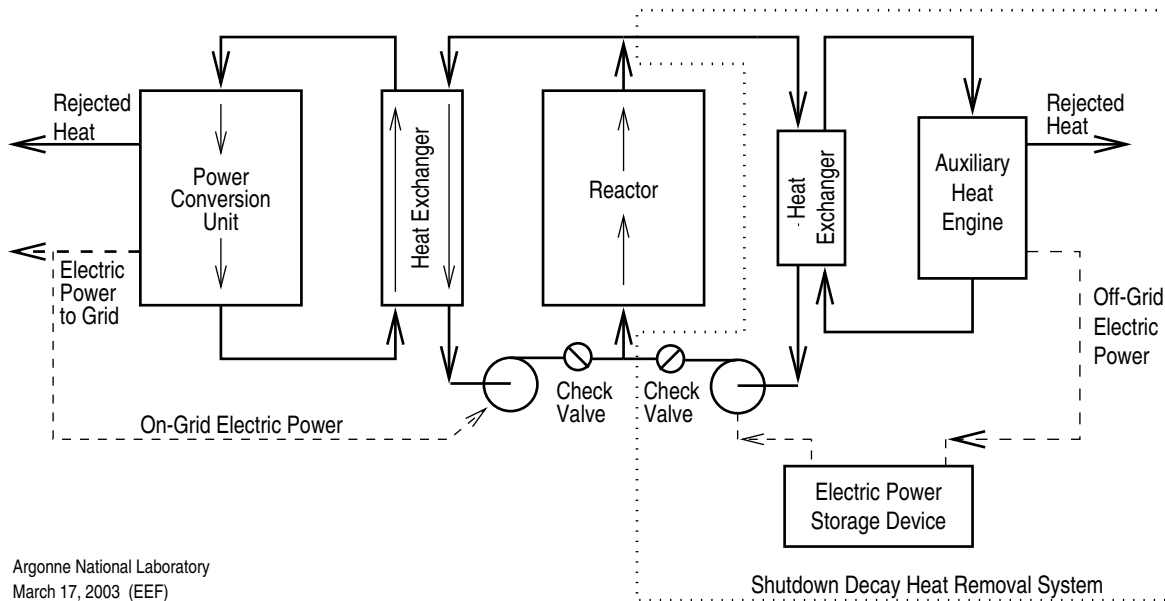
Argonne National Laboratory
March 14, 2003 (EEF)

Fig. 6. Direct-Cycle Layout with an Autonomous Shutdown Decay Heat Removal System.

A final issue is that autonomous systems have a very large amount of moving parts and therefore cannot be considered to be passive systems. They may be classified as "semi-passive", as opposed to "active", because they do not need to be started up in an emergency, as one would need to do with a backup diesel-powered electric generator. A related issue is that the primary coolant flow that provides the energy for the autonomous system must undergo a very large reduction in pressure and density just at the instant the system is needed and thus there is always the potential that the auxiliary heat engine will stop when it is needed most.

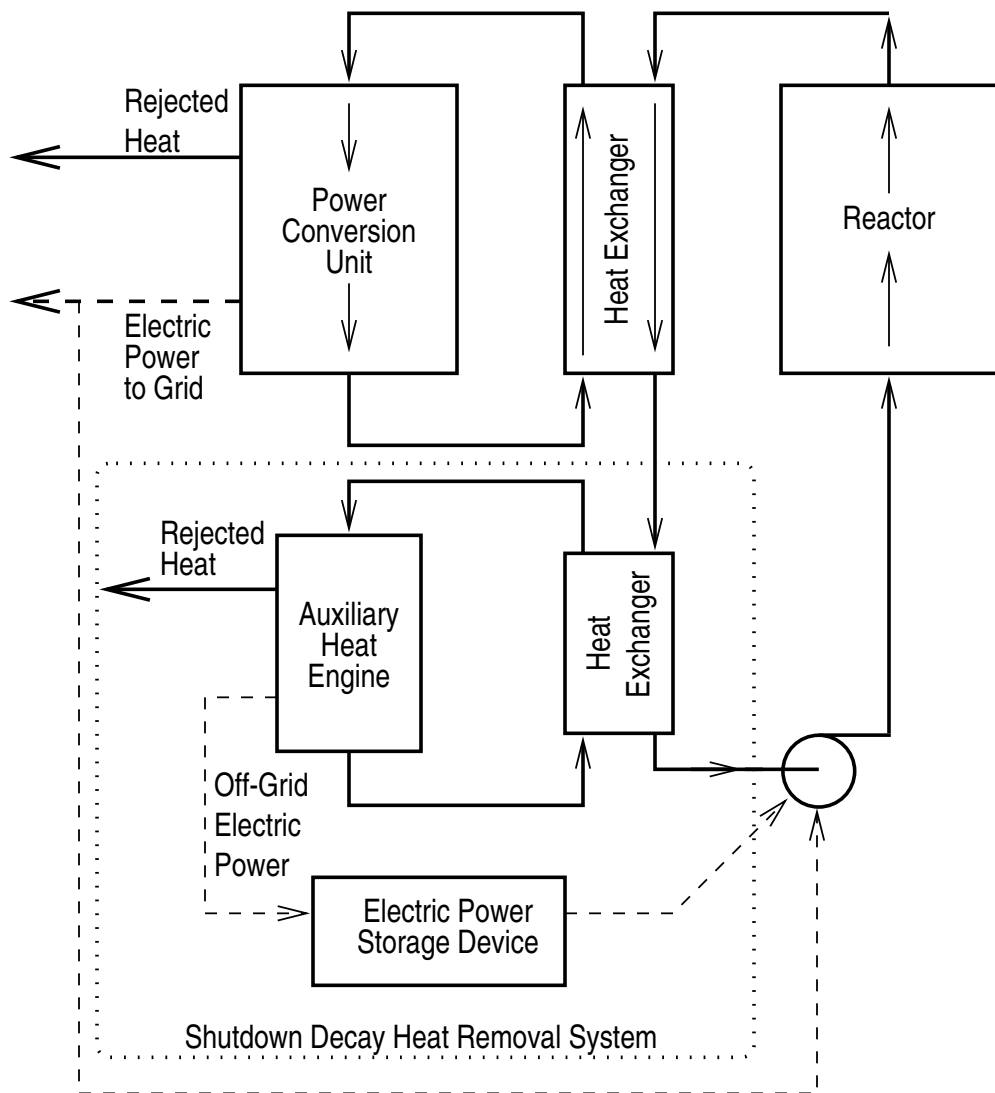
6.0 CONCLUSIONS FOR FOLLOW-ON WORK

Two approaches to decay heat removal, autonomous systems and natural convection in a pebble bed core, have been selected. For direct-cycle plants, both concepts require that one or more additional primary flow loops be added to the plant. These loops have heat exchangers that either power the autonomous systems or merely dump decay heat, in the cases of natural convection. These extra loops require check valves to help prevent reverse flow that could cause a significant portion of the main coolant flow to bypass the reactor core. Since this issue can be avoided in indirect-cycle plants, they should be given further consideration. An issue that is common to the use of either autonomous or natural convective systems is a break in the primary system boundary that would allow cold containment gas to enter the reactor vessel between the reactor outlet plenum and the inlet to the autonomous system. This could be detrimental for an autonomous system, since it is powered by the heated coolant from the reactor core. This would also be detrimental for a natural convection system, since it would diminish the buoyancy that drives the primary flow around the natural convective circuit. In order to avoid this problem, or minimize its likelihood of occurrence, it was suggested that the heat exchangers that are added to the primary circuit to enable natural convection be placed inside the primary vessel. To bolster the safety case for natural convection, the primary vessel will be enclosed within a guard containment (secondary containment) to maintain the coolant pressure at some significant level.



Argonne National Laboratory
March 17, 2003 (EEF)

Fig. 7. Indirect-Cycle Layout with an Autonomous Shutdown Decay Heat Removal System in Parallel.



Argonne National Laboratory
March 14, 2003 (EEF)

Fig. 8. Indirect-Cycle Layout with an Autonomous Shutdown Decay Heat Removal System in Series.

Since autonomous systems add complex machinery to the plant, they cannot be considered to be passive, but may be considered to be semi-passive. Natural convective systems do not work at atmospheric conditions and therefore require some form of pressurized confinement, but if this pressurized confinement is provided, the system can be passive. Natural convective systems are less complex than autonomous ones, but providing a confinement/guard containment with sufficient pressure capability could be a challenge.

This NERI project proposes a pebble-bed core design that has minimal hydraulic resistance through the core so that it would be most conducive to natural convection. This core is the largest diameter 300 MWt core that fits into the allowed diameter, 3 m, and has essentially the largest pebble diameter that steady-state thermal considerations will allow. These considerations must

include evaluations of upset conditions that are initiated from normal operating conditions since there must be a sufficient thermal margin between the normal operating temperature and the maximum temperature the fuel can withstand without sustaining damage. This margin would be used to absorb the initial excess decay energy, when the reactor is generating between about 7% decay power and the smaller amount that the decay-heat removal system is capable of removing. Based on these considerations, a pebble diameter of 4 cm was selected. The core power density is 25 W/cc and the total core power is 300 MWt.

The decay power immediately after scram from full power is close to 7% of full power. Since natural convective decay-heat removal systems typically can remove no more than only about 1 or 2% of decay power, the excess decay energy must be temporarily stored in the reactor until the decay power has declined sufficiently. The decay heat curve was used to determine the amount of energy that would have to be stored as a function of decay-heat removal capability. In addition, first-order models that could be used to analyze natural convection were identified. The first-order models were used to assess natural convection in a direct-cycle plant in which the natural convection heat exchanger was assumed to be 10 m about the reactor fueled region, which includes the upper axial reflector. The results showed that for helium coolant the guard containment pressure would have to be about 13 bar if the primary system temperature were not to exceed about 850° C. Lower pressures would be needed if the temperature limit were 1600° C instead of 850° C or if the coolant were carbon dioxide instead of helium. Although the first-order models allow the basic governing phenomena to be understood and evaluated, they have limitations. They do not include heat transfer by conduction and radiation within the core, for example, and they require that the modeling be done piecemeal and that transient behavior be approximated by a series of steady-state models. Therefore, the deployment of a more powerful transient system-modeling capability, RELAP5/ATHENA, was initiated and complementary calculations were performed.

In conclusion, a design for a pebble-bed core that employs a natural convective heat removal system has been selected and the modeling capability to better analyze it and other reactor systems has been assembled. It is recommended that follow-on NERI project work be performed to consider the implications of this core design and safety approach for the primary vessel design, the balance-of-plant layout and the containment considerations.

REFERENCES

1. E. E. Feldman and T. Y. C. Wei, "Thermal-Hydraulic and Safety Evaluation of the PB-GCFR Core Design," Nuclear Engineering Research Initiative Project #01-022: Particle-Bed-Gas-Cooled Fast Reactor (PB-GCFR) Design Task 2.2 Milestone/Deliverable, Argonne National Laboratory, February 2003.
2. E. E. Feldman and T. Y. C. Wei, "Core Key Mechanical Design Evaluation for a Pebble-Bed Gas-Cooled Fast Reactor," Nuclear Engineering Research Initiative Project #01-022: Particle-Bed-Gas-Cooled Fast Reactor (PB-GCFR) Design Task3 Milestone/Deliverable, Argonne National Laboratory, February 2003.
3. E. Achenbach, "Heat and Flow Characteristics of Packed Beds," *Experimental Thermal and Fluid Science*, Vol. 10, 1995, pp. 17-27.
4. R. Span and W. Wagner, "An Equation of State for Carbon Dioxide Covering the Fluid Region from the Triple-Point Temperature to 1100 K at Pressures up to 800 MPa," *J. Phys. Chem. Ref. Data*, Vol. 25, No. 6, 1996, pp. 1509-1595.
5. A. Fenghour, W. A. Wakeham, and V. Vesovic, "The Viscosity of Carbon Dioxide," *J. Phys. Chem. Ref. Data*, Vol. 27, No. 1, 1998, pp. 31-41.

Publication List and Presentations

Reports

Deliverables

T. Taiwo, M. Fatone, and G. Palmiotti, *Preliminary Evaluation of a Reference Compact Core Using Pebble-Bed Reactor Design*, Deliverable Report for Task 1.1, NERI#010-022, January 25, 2002.

E. E. Feldman and T. Y. Wei, *Point Design Concepts for a Gas-Cooled Fast Reactor*, Deliverable Report for Task 2.1, NERI#01-022, February 2002.

J. W. Holland and I. G. Prokofiev, *Assessment of Candidate Fuel and Structural Materials for Use in a Particle-Bed Gas-Cooled Fast Reactor*, Deliverable Report for Task 4.0, NERI#01-022, February 2002.

M. Fatone and T. Taiwo, *Neutronic Studies of Long-Life Pebble-Bed Gas-Cooled Fast Reactor Cores*, Deliverable Report for Task 1.2, NERI#010-022, August 2002.

E. A. Hoffman, T. A. Taiwo, W. S. Yang, and M. Fatone, *Investigation of Transuranics Breakeven and Burner Cores for Particle-Bed Gas-Cooled Fast Reactor*, Deliverable Report for Task 1.3, NERI#010-022, February 2003.

E. E. Feldman and T. Y. C. Wei, *Thermal-Hydraulic and Safety Evaluation of the PB-GCFR Design*, Deliverable Report for Task 2.2, NERI#010-022, February 2003.

E. E. Feldman and T. Y. C. Wei, *Core Key Mechanical Design for a Pebble-Bed Gas-Cooled Fast Reactor*, Deliverable Report for Task 2.2, NERI#010-022, February 2003.

E. E. Feldman and T. Y. C. Wei, *Design Approach for a Small Modular Pebble Bed Gas-Cooled Fast Reactor Optimized for Decay Heat Removal*, Deliverable Report for Task 5, NERI#010-022, August 2003.

Quarterly Reports

"Nuclear Energy Research Initiative #01-022, Particle-Bed Gas-Cooled Fast Reactor (PB-GCFR) Design, Technical Quarterly Report (Sept – Nov 2001)," December 2002.

"Nuclear Energy Research Initiative #01-022, Particle-Bed Gas-Cooled Fast Reactor (PB-GCFR) Design, Technical Quarterly Report (Dec 2001 – Feb 2002)," March 2002.

"Nuclear Energy Research Initiative #01-022, Particle-Bed Gas-Cooled Fast Reactor (PB-GCFR) Design, Technical Quarterly Report (March 2002 – May 2002)," June 2002.

"Nuclear Energy Research Initiative #01-022, Particle-Bed Gas-Cooled Fast Reactor (PB-GCFR) Design, Technical Quarterly Report (June 2002 – Aug 2002)," September 2002.

"Pebble-Bed Gas-Cooled Fast Reactor (PB-GCFR) Design," Contribution to the NERI Program Annual Report, submitted to US-DOE Office of Nuclear Energy, Science and Technology, June 21, 2002.

"Nuclear Energy Research Initiative #01-022, Particle-Bed Gas-Cooled Fast Reactor (PB-GCFR) Design, Technical Quarterly Report (Sept – Nov 2002)," December 2003.

"Nuclear Energy Research Initiative #01-022, Particle-Bed Gas-Cooled Fast Reactor (PB-GCFR) Design, Technical Quarterly Report (Dec 2002 –Feb 2003)," March 2003.

"Nuclear Energy Research Initiative #01-022, Particle-Bed Gas-Cooled Fast Reactor (PB-GCFR) Design, Technical Quarterly Report (March 2003 – May 2003)," June 2003.

Intra-Laboratory Memorandum

E. E. Feldman, *A Series of Scoping Decay Heat Removal Calculations to Better Understand Depressurization Accidents in Gas-Cooled Reactors and Better Evaluate Fuel Design Options*, Intra-Laboratory Memo, Argonne National Laboratory, November 14, 2001.

J. Holland, *Strategies for Selection of Fuel and Materials for Gen IV GCFR*", Intra-Laboratory Memo, Argonne National Laboratory, November 30, 2001.

T. Wei, *Milestone Report on Fuel/Structural Materials for PB-GCFR NERI Project*, Intra-Laboratory Memo, Argonne National Laboratory, December 21, 2001.

M. Fatone, *Studies of the Design of a Pebble-Bed Gas Cooled Fast Reactor System*, Argonne National Laboratory Intra-Laboratory Memo, February 12, 2002.

M. Fatone, *Periodic Report on the Physics Studies for the PB-GCFR*, Intra-Laboratory Memo, Argonne National Laboratory, April 30, 2002.

M. Fatone, *Physics Studies for the PB-GCFR on the Use of Graphite as Matrix*, Argonne National Laboratory, Intra-Laboratory Memo, Argonne National Laboratory, July 20, 2002.

M. Fatone, *Physics studies of the Pebble-Bed Gas cooled Fast Reactor Design using the Cold Finger Concept for Decay Heat Removal*, Intra-Laboratory Memo, Argonne National Laboratory September 2002.

E. E. Feldman, *A Design Concept and an Analytical Model for a Condenser and Natural Draft Cooling Tower Combination to Be Used for Decay Heat Removal for a Gas-Cooled Pebble-Bed Fast Reactor*, Intra-Laboratory Memo, Argonne National Laboratory, August 1, 2002.

E. E. Feldman, *The Cold Finger Concept for Decay Heat Removal in Generation IV Helium-Cooled Fast Pebble-Bed Reactors*", Intra-Laboratory Memo, Argonne National Laboratory, 2002.

E. E. Feldman, *Initial Thermal Design of a Generation IV 300 MWt Gas-Cooled Pebble-Bed Reactor Utilizing Cold Fingers*, Intra-Laboratory Memo, Argonne National Laboratory, 2002.

Presentations

Particle-Bed Gas-Cooled Fast Reactor (PB-GCFR) NERI Project, presentation by T. Taiwo at CEA-Cadarache, France, March 13, 2002.

Particle-Bed Gas-Cooled Fast Reactor (PB-GCFR) NERI Project, presentation by T. Taiwo at the USDOE Special Session on NERI Projects, held during the June 2002 ANS National Meeting, in Hollywood, FL, June 12, 2002.

Particle-Bed Gas-Cooled Fast Reactor (PB-GCFR) Design, presentation by T. Taiwo at USDOE NERI Review Meeting, Rockville, May 21 2003.

Papers

T. A. Taiwo, M. Fatone, G. Palmiotti, R. N. Hill, *Physics Studies for a Particle-Bed Gas Cooled Fast Reactor Core Design*, Proceedings of the 1st International Topical Meeting on High Temperature Reactor Technology, Petten, Netherlands, April 22-24, 2002.

John W. Holland, Iouri G. Prokofiev, and Amy B. Hull, *High-Temperature, Helium-Cooled Fuel and Perspective for Development*, Proceedings of the Fifteenth International Conference on Physics of Radiation Phenomena and Radiation Materials Science, Alushta, Crimea, Ukraine, June 10-15, 2002.

E. A. Hoffman, T. A. Taiwo, W. S. Yang, and M. Fatone, *A Particle-Bed Gas Cooled Fast Reactor Core Design For Waste Minimization*, Proc. 7th Information Exchange Meeting on Actinide and Fission Product Partitioning and Transmutation, Jeju, Korea, October 14-16, 2002.

E. A. Hoffman, T. A. Taiwo, and W. S. Yang, *Long-Lived Transuranic-Fueled Pebble-Bed Gas-Cooled Fast Reactor Designs*, GLOBAL 2003: Advanced Nuclear Energy and Fuel Cycle Systems, New Orleans, November 16-20, 2003. (pending)

Acknowledgment

This material is based upon work supported by the U. S. Department of Energy under the NERI program Award No. MSF 01-0022 and NERI Project Number 01-022.